COMPUTATION OF REYNOLDS STRESSES IN AXISYMMETRIC VORTICES AND JETS USING A SECOND ORDER CLOSURE MODEL

by

Min Jiang

Thesis submitted to the faculty of the
Virginia Polytechnic Institute and State University
in partial fulfillment of the requirements for the degree of

MASTER OF SCIENCE

in

Engineering Science and Mechanics

APPROVED:

Dr. Saad A. Ragab, Chairman

Dr. Dean T. Mook

Dr. William J. Devenport

August, 1994

Blacksburg, Virginia

LD
5055
V855
1994
J536
c.2

COMPUTATION OF REYNOLDS STRESSES IN AXISYMMETRIC VORTICES AND JETS USING A SECOND ORDER CLOSURE MODEL

by

Min Jiang

Committee Chairman: Dr. Saad A. Ragab

Department of Engineering Science and Mechanics

(ABSTRACT)

Donaldson's single-point second-order model[13] is used to close the Reynolds stress transport equations in cylindrical coordinates. A reduced set of equations are then solved for the decay of axisymmetric vortices and jets. A self-similar solution to the axisymmetric vortices is obtained numerically. The characteristics of the mean flow variables as well as the Reynolds stresses in this solution are discussed. Comparisons of the current results with Donaldson[13] and Donaldson and Sullivan[16] are also presented.

The results show that the vortex core is free from turbulent shear stresses. The turbulent kinetic energy is also found to be relatively weak within the core region. The overshoot of the circulation is found to be 5% of the circulation at infinity over a wide range of Reynolds numbers.

The effects of Reynolds number on the decay of the vortices are computed and discussed. Some of the quantities, such as mean flow circulation and turbulent kinetic energy, are found to be sensitive to the Reynolds number. However, the overshoot is found to be insensitive to the Reynolds number but its location does.

A set of suitable model constants for the axisymmetric jets is also found and a self-similar solution for the jet case is obtained. Comparisons of the computed results with some recent experimental data are presented.

ACKNOWLEDGEMENTS

I would like to take this oppertunity to thank Dr. Saad A. Ragab, my major advisor, for his step-by-step guidance with great patience, and his constant encouragement throughout the duration of my research work and graduate studies here in the ESM Department, Virginia Tech. Without this invaluable help, any part of this research or this thesis could not have been possible.

I would like to thank Dr. Dean T. Mook and Dr. William J. Devenport for serving on my advisory committee.

I would like to thank Prof. Gendi Ma, my undergraduate advisor, for her sincere care and encouragement on my studies and research in the USA.

I would like to thank all my teachers at Virginia Tech and the University of Science and Technology of China.

I would like to thank Mr. Duane Taylor and Mr. Tim Tomlin, who run the ESM computer lab, for helping me out with the computers on which most of this work was done.

I would like to thank all my friends and colleagues for their friendship, moral support and help, of them I name a few: Dr. Madhu K. Sreedhar, Mr. Reza Karkehabadi, Mr. Alan Luton, Mr. Michael P. Smith, Mr. Khaled S. Youssef, Mr. Weiqing Lin, Mr. Frederick A. Just, Mr. Yannick Fierling.

I would like to thank the Office of Naval Research, specifically Dr. L. P. Purtell, for continued financial support through Grant No. N00014-92-J-4087.

Finally, a very special appreciation goes to my wife and my parents, for their continuous support, understanding, encouragement and sacrifice without which this goal could never have been achieved.

TABLE OF CONTENTS

1 INTRODUCTION 1

2 THE BASIC EQUATIONS 7

2.1 Introduction 7

2.2 The RANS and RST equations 7

2.2.1 The quasi-cylindrical approximation 8

2.2.2 The mean flow equations 8

2.2.3 The Reynolds-stress transport equations 9

2.3 Donaldson second-order closure model and the closed equations 11

3 DECAY OF TWO-DIMENSIONAL TURBULENT VORTICES 14

3.1 The governing gquations 14

3.2 The initial and boundary conditions 16

3.3 The computational scheme and grid 18

3.4 Results and discussion 19

3.4.1 The results for a vortex at $Re = 10^4$ 19

3.4.2 The effects of Reynolds number 24

4 A SELF-SIMILAR SOLUTION FOR AXISYMMETRIC JETS 27

4.1 Introduction 27

4.2 The governing equations, the boundary and initial conditions 28

4.3 Results and discussion 34

5 CONCLUSIONS 36

A RANS AND RST EQUATIONS IN CYLINDRICAL COORDINATES 72

A.1 Definitions of the variables 72

A.2 The Reynolds-averaged Navier-Stokes equations (RANS) 72

A.3 The Reynolds-stress transport equations (RST) 73

LIST OF FIGURES

2.1 The cylindrical coordinate system (r, θ, z) 43

3.1 The computational grid for 4-point backward differencing in axial direction and 3-point central differencing in Radial Direction 44

3.2 Behavior of the core radius and core velocity from the current computation and comparison with Donaldson's results ($Re = 10^4$, $t^* = (\frac{V_{10}}{r_{10}})t$) [DS: Donaldson[8] and Donaldson & Sullivan[11]] 45

3.3 Behavior of the circulation at the core radius, in comparison with Donaldson's results ($Re = 10^4$, $t^* = (\frac{V_{10}}{r_{10}})t$) [DS: Donaldson[8] and Donaldson & Sullivan[11]] 46

3.4 Behavior of the maximum turbulent kinetic energy, in comparison with Donaldson's results ($Re = 10^4$, $t^* = (\frac{V_{10}}{r_{10}})t$, $k_{max} = (\overline{u_i' u_i'})_{max}$) [DS: Donaldson[8] and Donaldson & Sullivan[11]] 47

3.5 Radial distribution of the circulation for the self-similar solution, in comparison with Donaldson's results ($Re = 10^4$) [DS: Donaldson[8] and Donaldson & Sullivan[11]] 48

3.6 Radial distribution of the normalized turbulent kinetic energy for the self-similar solution, in comparison with Donaldson's results ($Re = 10^4$) [DS: Donaldson[8] and Donaldson & Sullivan[11]] 49

3.7 Radial distribution of the normalized turbulent shear stress for the self-similar solution, in comparison with Donaldson's results ($Re = 10^4$) [DS: Donaldson[8] and Donaldson & Sullivan[11]] 50

3.8 Comparison of computations with the measurements for the mean flow velocity in the inner region [DS: Donaldson[8] and Donaldson & Sullivan[11]; H&J measured: Hoffmann and Joubert[23]] 51

3.9 Radial distribution of the turbulent shear stress for the self-similar solution ($Re = 10^4$) 52

3.10 Radial distribution of the turbulent radial normal stress component for the self-similar solution ($Re = 10^4$) 53

3.11 Radial distribution of the turbulent circumferential normal stress component for the self-similar solution ($Re = 10^4$) 54

3.12 Radial distribution of the turbulent axial normal stress component for the self-similar solution ($Re = 10^4$) 55

3.13 Radial profiles of the circulation at different times in comparison with the laminar case ($Re = 10^4$, $t^* = (\frac{V_{10}}{r_{10}})t$) 56

3.14 Radial profiles of the turbulent kinetic energy at different times ($Re = 10^4$, $t^* = (\frac{V_{10}}{r_{10}})t$) 57

3.15 Sensitivity of k_{max}/V_1^2 to the initial magnitude of the turbulent fluctuations 58

3.16 Effect of the initial magnitude of fluctuation on the behavior of maximum turbulent kinetic energy ($Re = 10^4$, $t^* = (\frac{V_{10}}{r_{10}})t$) 59

3.17 Effect of the initial distribution of fluctuation on the behavior of maximum turbulent kinetic energy ($Re = 10^4$, $t^* = (\frac{V_{10}}{r_{10}})t$) [A: initial distributions of turbulent intensities follow Eq(3.8) through (3.10)] [B: initial distributions of turbulent intensities follow Eq(3.26)] 60

3.18 Dependence of maximum turbulent kinetic energy on Reynolds number . . 61

3.19 Effect of the Reynolds number on the radial profiles of the turbulent shear stress 62

3.20 Effect of the Reynolds number on the radial profiles of the turbulent kinetic energy 63

3.21 Effect of the Reynolds number on the circulation profiles 64

3.22 **Behavior** of the core radius and velocity for different Reynolds number after accounting for time origins 65

4.1 Comparison of self-similar solution of computed mean axial velocity with experimental results for an axisymmetric jet 66

4.2 Comparison of self-similar solution of computed mean radial velocity with experimental results 67

4.3 Comparison of self-similar solution of computed turbulent shear stress with experimental results 68

4.4 Comparison of computational results with experimental data: magnitude of axial velocity fluctuations 69

4.5 Comparison of computational results with experimental data: magnitude of radial velocity fluctuations 70

4.6 Comparison of computational results with experimental data: magnitude of circumferential velocity fluctuations 71

Chapter 1

INTRODUCTION

Turbulent vortices are of considerable engineering and technological concern. In aviation, the wakes of lifting bodies such as aircraft often contain strong streamwise vortices. Those vortices generated in the wake of large aircraft present a serious threat to small airplanes following or crossing the wake within a certain distance. They also pose strong potential hazards in heavy air-traffic areas, such as low-altitude space near the runway, and thus limit the capacities of airports. Powerful vortices can be shed by submarines as well, leading to undesired pressure forces. They also persist for a long distance downstream and make the submarines more detectable.

On the other hand, however, vortices provide some beneficial characteristics and hence have many engineering applications. Trapped vortices on delta wings, for instance, contribute significantly to the lift. In combustion chamber, they can be used to enhance the mixing.

Since the laminar diffusion of a line vortex was studied by Lamb[34], many advances in theory, experiment and computation have been published. Squire[59] proposed a theory considering the diffusion of a turbulent vortex. In his theory, the eddy-viscosity is assumed to be proportional to the circulation. It results that the solution to the turbulent vortex is similar to its laminar analogue. However, Newman[42] found that the assumed constant eddy viscosity did not match well with the measurements. Dosanjh et al.[15] concluded

that, for turbulent vortices, the decay rates of velocity and other geometry parameters were eight to ten times larger than laminar vortices. Owen[44] pointed out that the turbulent viscosity depends on the the Reynolds number defined with respect to the instantaneous circulation rather than on the initial circulation as Squire proposed.

In 1963, Hoffmann and Joubert[30] presented a concept of triple layer structure based on the radial distribution of circulation which consists of a power-law region, an inner layer where the circulation has a logarithmic distribution, and an outer layer. They also found that the vortices were completely independent of viscous effects above a certain Reynolds number. Nielsen and Schwind[46] set forth a theory for the different stages in the evolution of trailing vortices. They compared the three layered structure in a turbulent vortex to that of a turbulent boundary layer which also possesses a similar structure.

Govindaraju and Saffman[19] first proposed the existence of the overshoot in the circulation profile of a turbulent vortex. This conclusion is strongly supported by Uberoi[61] who stated that turbulence in a vortex can be generated and maintained only if the circulation has a non-monotonic variation. He also stated that a vortex is stable while a combination of a vortex and a swirl is unstable. This nonuniform variation of circulation leads to the argument that a vortex has multilayered structure.

Saffman[54] also considered a triple layer structure. He showed the dependence of the decay of a trailing line vortex on the Reynolds number.

There has been quite a lot of experimental work on turbulence decay and vortex wakes. Among them, Newman[42] reported the earliest measurements in a turbulent vortex. Corsigilia et al.[8] measured the velocity profiles of wing tip vortices over a rectangular wing and found that the circumferential velocity distributions had the same functional form as those determined by Hoffman and Joubert[30].

Singh[56] measured components of the Reynolds-stress tensor in his experimental investigation of structure and stability of vortices. Phillips and Graham[50] obtained Reynolds-stress measurements for a variety of axial flows ranging from a strong wake-like to a strong jet-like profile.

Devenport et al.[11] and Zsoldos and Devenport[64] discuss vortex core meandering effects due to low frequency waves. They also measured Reynolds-stresses and other turbulence quantities. Devenport et al.[12] developed a theoretical approach to account for the effects of vortex core meandering.

Numerical simulations of turbulent flows have been undertaken for several decades. Remarkable progress in the understanding of the physics and structure of incompressible turbulent flows has been achieved using direct numerical simulation(DNS) (Reynolds[52]). Direct numerical simulations have been successfully used in the analysis of isotropic turbulence (Orszag and Patterson[45]), homogeneous shear flows (Rogers and Moin[53]), fully developed channel flow (Kim, Moin and Moser[33]), and zero-pressure-gradient boundary-layer flow (Spalart[57]).

Due to the limitations on computer capacities, DNS is limited to low Reynolds numbers and simple geometries. Turbulence modeling, as another route to the analysis of turbulent flows, has shown its capabilities and has been widely used in research and prediction of turbulent flows. Speziale[58], Ha[21] and Taubee[60] have provided good review in this area.

In the early 70's, attempts on turbulence modeling were focused mainly on getting invariant one-point closure models, which were thought to be universally valid. Those attempts seemed to be unsuccessful, and it followed that the disappointment on the prediction of the axisymmetric round jet became a classic example to depreciate the applications of the one-

point closure models. However, some one-point closure models, because of the simplicity of their structure, still have many advantages in applications.

In recent years, there have been two major groups developing and promoting second-order models, they are Launder's group at Imperial College and Lumley's group at Cornell University. The primary structures of the models by these two groups are promoted from the works of Launder, Reece and Rodi[35] and Lumley[38], respectively, though some of their earlier papers such as Hanjalic and Launder[24] and Lumley and Khajek-Nouri[39] set some roots for the recent ones. Launder et al. attempt to simplify the formulations by using constant parameters and neglecting some formulations which they argue to be unimportant. On the contrary, Lumley uses rational principles, trying to get a general second-order model. Consequently, some of the formulations proposed by Lumley are hard to apply due to their complexity.

In spite of the differences and debates between these philosophies, a lot of common concepts used in these second-order models come from earlier work, among which are Chou[5, 6, 7], Davidov[9, 10] and Donaldson[13].

Various models have been used in the computations of vortices since 70's. Donaldson[13] and Donaldson and Sullivan[16] presented an invariant model which solves for the Reynolds-stresses along with the mean flow quantities. Later on, Donaldson and Bilanin[14] applied the model in the computation of the vortex wake of a low speed aircraft. Bilanin et al[4] used a second order closure model to study the effect of background turbulence, wind shear and the proximity to the ground on the rate of decay of vortex pairs. And they found that the decay rate increased with increasing background turbulence. Hecht et al.[26, 27] used the same technique to investigate the decay of turbulent vortices in stratified fluids. Hogg and Leschiner[31] used a finite-volume formulation for comparing the performance

of a two-equation eddy-viscosity model to a Reynolds-stress transport closure model for highly swirling confined flow. Abid and Speziale[1] used a Reynolds stress closure model in channel flow and homogeneous shear flow. Zheng and Ash[63] compared Reynolds-stress transport model with zero-equation, one-equation and two-equation eddy-viscosity models. They found that all of the eddy-viscosity models showed excessive dissipation. Hence they used Donaldson's model[13] in the computation of near-ground vortex case.

Besides vortex flows, axisymmetric jets are another important type of flows. It is often considered as a case to test turbulence models and other prediction theories of turbulent flows.

A lot of experimental results on jets have been reported. Here we just mention a few of them. In 1969, Wygnanski and Fiedler[62] performed a comprehensive study of the self-similar region of the round jet and reported moments, energy balance, etc. Lumley[38] reported some measurements in a turbulent air jet in 1978.

Recently, Panchapakesan and Lumley[48, 49] published their new experimental results on axisymmetric jets of air and helium. Hussein et al.[32] reported their measurements obtained from similar experiments. These results have actually contributed to data basis to evaluate turbulence models.

Motivation of Current Research

It is worth emphasizing that the explicit formulation and clear concepts in Donaldson's second-order closure model[13] provide an efficient way to compute of Reynolds-stresses as well as the mean flow variables. However, the studies of decay of two-dimensional vortices by Donaldson[13] and Donaldson and Sullivan[16] are still incomplete in some important

aspects which need to be understood. For instance, the effects of Reynolds number on the similarity solutions were not considered by those authors. Secondly, the application of this model to other types of turbulent flows has not been studied. The axisymmetric jet case, which used to be a difficult example of prediction by one-point closure models has not been found in the literature using this model. Yet there is no strong evidence that denies the possibility of getting reasonable results by using this model with suitable model constants.

Therefore the objectives of this research are:

1. To improve Donaldson's results for the two-dimensional vortex cases, using Donaldson's second-order closure model, specifically, to determine the effects of the Reynolds number on the self-similarity of axisymmetric vortices.

2. To apply the model to the axisymmetric jet case, and to find out a suitable set of model parameters by comparing numerical and experimental data.

The work, of course, begins with the derivation of the governing equations, which are listed in Chapter 2. The general form of them is also derived, and listed in Appendix A. Also in Chapter 2, Donaldson's second-order closure model is introduced and the closed equations are presented.

In Chapter 3, The computational scheme and study of decay of a two-dimensional vortex are described and discussed in detail.

In Chapter 4, an investigation of axisymmetric jets through computation is reported. The new parameters of the model as well as the comparisons of the computational results with the experimental data are presented.

Chapter 2

THE BASIC EQUATIONS

2.1 Introduction

Two problems are considered in this thesis. The first problem is the decay of a turbulent axisymmetric vortex with zero mean axial and radial velocities. This is an unsteady problem in which the mean velocity profile and four of the six Reynolds-stress components are determined as functions of time and the radial distance. There are no variations in the circumferential or axial direction.

The second problem is the spatially developing axisymmetric turbulent jet. Only the mean circumferential velocity is zero. As in the first problem, there are four non-zero Reynolds-stress components. All flow variables are functions of the axial and radial coordinates.

2.2 The RANS and RST equations

The appropriate equations for each problem can be derived from the Reynolds-averaged Navier-Stokes(RANS) equations and the Reynolds-stress transport(RST) equations in cylindrical coordinates (r, θ, z). The coordinate system is sketched in figure 2.1.

The RANS and RST equations in cylindrical coordinates are derived for incompressible flows. The procedure for deriving these equations is straightforward (e.g. Hinze[28]) but the algebra is lengthy. In deriving these equations, the author started with the Navier-Stokes

equations in cylindrical coordinates (e.g. Panton[47]). An independent derivation of the same equations is by Ragab[51] who derived the equations in general curvilinear tensors first and then reduced them to cylindrical coordinates by substituting appropriate expressions for the metric tensor. These two independent derivations provide identical equations. It seems that the RST equations in cylindrical coordinates without the assumptions of axial symmetry are not available in the open literature. For completeness and future reference, the RANS and RST equations are documented in Appendix A.

2.2.1 The quasi-cylindrical approximation

The equations for axisymmetric flows follow directly from the general equations given in appendix A by dropping all the derivatives with respect to θ. In the present applications to jets and vortices it is customary to introduce the quasi-cylindrical approximation, which is a boundary-layer type approximation. It is assumed that the variation of the flow variables in the radial direction is much faster than that in the axial direction (streamwise), and that the mean radial velocity component is much smaller than the axial or circumferential component. The major simplification that results from this approximation is the absence of the diffusion terms (second-order derivatives) in the axial direction. Thus, the problem becomes parabolic which allows the use of marching techniques to advance the solution in space or time starting with appropriate initial profiles. For detailed derivation of the quasi-cylindrical approximation, the reader is referred to the article by Hall[23].

2.2.2 The mean flow equations

Let U, V, and W denote the mean velocity components in the radial (r), circumferential (θ), and axial (z) directions, respectively. And let u', v' and w' denote the corresponding

turbulent fluctuations. The governing equations are:

Continuity:

$$\frac{\partial U}{\partial r} + \frac{U}{r} + \frac{\partial W}{\partial z} = 0 \tag{2.1}$$

θ-momentum:

$$\frac{\partial G}{\partial t} + U\frac{\partial G}{\partial r} + W\frac{\partial G}{\partial z} = \frac{1}{Re}(\frac{\partial^2 G}{\partial r^2} - \frac{1}{r}\frac{\partial G}{\partial r}) - 2\overline{u'v'} - r\frac{\partial \overline{u'v'}}{\partial r} \tag{2.2}$$

z-momentum:

$$\frac{\partial W}{\partial t} + U\frac{\partial W}{\partial r} + W\frac{\partial W}{\partial z} = -\frac{\partial P}{\partial z} + \frac{1}{Re}(\frac{\partial^2 W}{\partial r^2} + \frac{1}{r}\frac{\partial W}{\partial r}) - \frac{\overline{u'w'}}{r} - \frac{\partial \overline{u'w'}}{\partial r} \tag{2.3}$$

r-momentum:

$$\frac{\partial U}{\partial t} - \frac{G^2}{r^3} = -\frac{\partial P}{\partial r} \tag{2.4}$$

where $G = Vr$, and P is the mean pressure. Note that the circulation Γ is $2\pi G$.

2.2.3 The Reynolds-stress transport equations

Since one of the objectives of this research is to understand the behavior of the Reynolds-stresses during the decay of vortices and axisymmetric jets, the Reynolds-stress transport equations have to be considered. For axisymmetric flows under the quasi-cylindrical approximation, the Reynolds-stress transport equations can be simplified as

$$\begin{aligned}
&\frac{\partial \overline{u'^2}}{\partial t} + W\frac{\partial \overline{u'^2}}{\partial z} + U\frac{\partial \overline{u'^2}}{\partial r} - 4G\frac{\overline{u'^2}}{r^2} + 2\frac{\partial U}{\partial r}\overline{u'^2} + \frac{\partial \overline{u'^3}}{\partial r} + \frac{\overline{u'^3}}{r} \\
&-2\frac{\overline{u'v'^2}}{r} - 2\overline{u'\frac{\partial p'}{\partial r}} - \frac{1}{Re}\{\frac{\partial^2 \overline{u'^2}}{\partial r^2} + \frac{1}{r}\frac{\partial \overline{u'^2}}{\partial r} - 2\frac{\overline{u'^2} - \overline{v'^2}}{r^2} \\
&-2[\overline{(\frac{\partial u}{\partial r})^2} + \frac{1}{r^2}\overline{(\frac{\partial u'}{\partial \theta} + v')^2} + \overline{(\frac{\partial u'}{\partial z})^2}]\} = 0
\end{aligned} \tag{2.5}$$

$$\frac{\partial\overline{v'^2}}{\partial t}+W\frac{\partial\overline{v'^2}}{\partial z}+U\frac{\partial\overline{v'^2}}{\partial r}+2U\frac{\overline{v'^2}}{r}+\frac{2}{r}\frac{\partial G}{\partial r}\overline{u'v'}$$
$$+\frac{\partial\overline{u'v'^2}}{\partial r}+3\frac{\overline{u'v'^2}}{r}-\frac{2}{r}\overline{p'\frac{\partial v'}{\partial\theta}}-\frac{1}{Re}\{\frac{\partial^2\overline{v'^2}}{\partial r^2}+\frac{1}{r}\frac{\partial\overline{v'^2}}{\partial r}+2\frac{\overline{u'^2}-\overline{v'^2}}{r^2}$$
$$-2[\overline{(\frac{\partial u}{\partial r})^2}+\frac{1}{r^2}\overline{(\frac{\partial v'}{\partial\theta}+u')^2}+\overline{(\frac{\partial v'}{\partial z})^2}]\}=0 \tag{2.6}$$

$$\frac{\partial\overline{w'^2}}{\partial t}+W\frac{\partial\overline{w'^2}}{\partial z}+2\frac{\partial W}{\partial r}\overline{u'w'}+U\frac{\partial\overline{w'^2}}{\partial r}+\frac{\partial\overline{u'w'^2}}{\partial r}+\frac{\overline{u'w'^2}}{r}-2\overline{(p'\frac{\partial w'}{\partial z})}$$
$$-\frac{1}{Re}\{\frac{\partial^2\overline{w'^2}}{\partial r^2}+\frac{1}{r}\frac{\partial\overline{w'^2}}{\partial r}-2[\overline{(\frac{\partial w'}{\partial r})^2}+\frac{1}{r^2}\overline{(\frac{\partial w'}{\partial\theta})^2}+\overline{(\frac{\partial w'}{\partial z})^2}]\}=0 \tag{2.7}$$

$$\frac{\partial\overline{u'v'}}{\partial t}+W\frac{\partial\overline{u'v'}}{\partial z}+U\frac{\partial\overline{u'v'}}{\partial r}+U\frac{\overline{u'v'}}{r}-2G\frac{\overline{v'^2}}{r^2}+\frac{\overline{u'^2}}{r}\frac{\partial G}{\partial r}+\frac{\partial U}{\partial r}\overline{u'v'}$$
$$+\frac{\partial\overline{u'^2v'}}{\partial r}+2\frac{\overline{u'^2v'}}{r}-\frac{\overline{v'^3}}{r}-\frac{\partial\overline{v'p'}}{\partial r}-(\frac{1}{r}\overline{p'\frac{\partial u'}{\partial\theta}}+\overline{p'\frac{\partial v'}{\partial r}})$$
$$-\frac{1}{Re}\{\frac{\partial^2\overline{u'v'}}{\partial r^2}+\frac{1}{r}\frac{\partial\overline{u'v'}}{\partial r}-4\frac{\overline{u'v'}}{r^2}-2[\overline{(\frac{\partial u'}{\partial r})(\frac{\partial v'}{\partial r})}$$
$$+\frac{1}{r^2}\overline{(\frac{\partial u'}{\partial\theta}-v')(\frac{\partial v'}{\partial\theta}+u')}+\overline{(\frac{\partial u'}{\partial z})(\frac{\partial v'}{\partial z})}]\}=0 \tag{2.8}$$

$$\frac{\partial\overline{u'w'}}{\partial t}+W\frac{\partial\overline{u'w'}}{\partial z}+U\frac{\partial\overline{u'w'}}{\partial r}+\frac{\partial U}{\partial r}\overline{u'w'}-2G\frac{\overline{v'w'}}{r^2}+\frac{\partial W}{\partial r}\overline{u'^2}$$
$$+\frac{\partial\overline{u'^2w'}}{\partial r}+\frac{\overline{u'^2w'}}{r}-\frac{\overline{v'^2w}}{r}+\frac{\partial\overline{w'p'}}{\partial r}-(\overline{p'\frac{\partial w'}{\partial r}}+\overline{p'\frac{\partial u'}{\partial z}})$$
$$-\frac{1}{Re}\{\frac{\partial^2\overline{u'w'}}{\partial r^2}+\frac{1}{r}\frac{\partial\overline{u'w'}}{\partial r}-\frac{\overline{u'w'}}{r^2}-2[\overline{(\frac{\partial u'}{\partial r})(\frac{\partial w'}{\partial r})}+\frac{1}{r^2}\overline{(\frac{\partial u'}{\partial\theta}-v')\frac{\partial w'}{\partial\theta}}$$
$$+\overline{(\frac{\partial u'}{\partial z})(\frac{\partial z'}{\partial z})}]\}=0 \tag{2.9}$$

$$\frac{\partial\overline{v'w'}}{\partial t}+W\frac{\partial\overline{v'w'}}{\partial z}+U\frac{\partial\overline{v'w'}}{\partial r}+\frac{U}{r}\overline{v'w'}-\frac{\partial G}{\partial r}\frac{\overline{v'w'}}{r}+\frac{\partial W}{\partial r}\overline{u'v'}$$
$$+\frac{\partial\overline{u'v'w'}}{\partial r}+\frac{\overline{u'v'w'}}{r}-(\frac{1}{r}\overline{p'\frac{\partial w'}{\partial\theta}}+\overline{p'\frac{\partial v'}{\partial z}})-\frac{1}{Re}\{\frac{\partial^2\overline{v'w'}}{\partial r^2}+\frac{1}{r}\frac{\partial\overline{v'w'}}{\partial r}$$
$$-\frac{\overline{v'w'}}{r^2}-2[\overline{(\frac{\partial v'}{\partial r})(\frac{\partial w'}{\partial r})}+\frac{1}{r^2}\overline{(\frac{\partial v'}{\partial\theta}-u')\frac{\partial w'}{\partial\theta}}+\overline{(\frac{\partial v'}{\partial z})(\frac{\partial z'}{\partial z})}]\}=0 \tag{2.10}$$

2.3 Donaldson second-order closure model and the closed equations

The equations (2.1) through (2.10) are set for the mean flow quantities U, G, W, P and the Reynolds-stress components $\overline{u'^2}$, $\overline{v'^2}$, $\overline{w'^2}$, $\overline{u'v'}$, $\overline{u'w'}$ and $\overline{v'w'}$. However, the Reynolds-stress transport equations (2.5) through (2.10) introduce extra unknown correlations: the triple-velocity correlations, pressure-velocity correlations, pressure-strain correlations, and also viscous dissipation terms. To close the system at this level, a turbulence model is needed for the extra unknowns. In this thesis, a Reynolds-stress turbulence model developed by Donaldson[13] is used to close these equations. For incompressible flow, the general tensor form of this model is

$$\overline{u_i' u_j' u_k'} = -v_c \Lambda q[(\overline{u_i' u_j'})_{,k} + (\overline{u_j' u_k'})_{,i} + (\overline{u_k' u_i'})_{,j}] \tag{2.11}$$

$$\overline{u_i' p'} = -p_c \rho \Lambda q(\overline{u'^l u_i'})_{,l} \tag{2.12}$$

$$\overline{p' u_{i,j}'} + \overline{p' u_{j,i}'} = -\rho \frac{q}{\Lambda}(\overline{u_i' u_j'} - \frac{1}{3} g_{ij} q^2) \tag{2.13}$$

$$g^{lm}\overline{u_{i,l}' u_{j,m}'} = a\frac{\overline{u_i' u_j'}}{\Lambda^2} + b\frac{q}{\nu\Lambda}(\beta\overline{u_i' u_j'} + \frac{1-\beta}{3} g_{ij} q^2) \tag{2.14}$$

where $q^2 = \overline{u'^m u_m'}$, and a, b, β, p_c, v_c are constants to be specified. Λ represents a local integral length scale of turbulence.

After the model has been expressed in cylindrical coordinates and substituted for the triple-velocity, pressure-velocity, pressure-strain, and dissipation correlations, the system is closed at the second-order level. The Reynolds-stress transport equations are then written as:

$$\begin{aligned}\frac{\partial\overline{u'^2}}{\partial t}+W\frac{\partial\overline{u'^2}}{\partial z} &= -U\frac{\partial\overline{u'^2}}{\partial r}+4\overline{u'v'}\frac{G}{r^2}+(3v_c+2p_c)\frac{\partial}{\partial r}(M\frac{\partial\overline{u'^2}}{\partial r})+\frac{v_cM}{r}(3\frac{\partial\overline{u'^2}}{\partial r}-2\frac{\partial\overline{v'^2}}{\partial r})\\ &+2\frac{p_c}{r}\frac{\partial}{\partial r}[M(\overline{u'^2}-\overline{v'^2})]-2(2v_c+p_c)\frac{M}{r^2}(\overline{u'^2}-\overline{v'^2})\\ &-\frac{M}{\Lambda^2}\{\overline{u'^2}(1+2b\beta)-\frac{q^2}{3}[1+2b(\beta-1)]\}\\ &+\frac{1}{Re}[\frac{\partial^2\overline{u'^2}}{\partial r^2}+\frac{1}{r}\frac{\partial\overline{u'^2}}{\partial r}-\frac{2}{r^2}(\overline{u'^2}-\overline{v'^2})-2\frac{a}{\Lambda^2}\overline{u'^2}] \qquad (2.15)\end{aligned}$$

$$\begin{aligned}\frac{\partial\overline{v'^2}}{\partial t}+W\frac{\partial\overline{v'^2}}{\partial z} &= -U\frac{\partial\overline{v'^2}}{\partial r}-2\frac{U}{r}\overline{v'^2}-\frac{2}{r}\frac{\partial G}{\partial r}\overline{u'v'}+v_c\frac{\partial}{\partial r}[M(\frac{\partial\overline{v'^2}}{\partial r})]\\ &+\frac{M}{r}(3v_c\frac{\partial\overline{v'^2}}{\partial r}+2p_c\frac{\partial\overline{u'^2}}{\partial r})+2\frac{v_c}{r}\frac{\partial}{\partial r}[M(\overline{u'^2}-\overline{v'^2})]\\ &+2(p_c+2v_c)\frac{M}{r^2}(\overline{u'^2}-\overline{v'^2})-\frac{M}{\Lambda^2}\{\overline{v'^2}(1+2b\beta)-\frac{q^2}{3}[1+2b(\beta-1)]\}\\ &+\frac{1}{Re}[\frac{\partial^2\overline{v'^2}}{\partial r^2}+\frac{1}{r}\frac{\partial\overline{v'^2}}{\partial r}+\frac{2}{r^2}(\overline{u'^2}-\overline{v'^2})-2\frac{a}{\Lambda^2}\overline{v'^2}] \qquad (2.16)\end{aligned}$$

$$\begin{aligned}\frac{\partial\overline{w'^2}}{\partial t}+W\frac{\partial\overline{w'^2}}{\partial z} &= -U\frac{\partial\overline{w'^2}}{\partial r}-2\frac{\partial W}{\partial r}\overline{u'w'}+v_c\frac{\partial}{\partial r}[M(\frac{\partial\overline{w'^2}}{\partial r})]+\frac{v_cM}{r}\frac{\partial\overline{w'^2}}{\partial r}\\ &-\frac{M}{\Lambda^2}\{\overline{w'^2}(1+2b\beta)-\frac{q^2}{3}[1+2b(\beta-1)]\}\\ &+\frac{1}{Re}[\frac{\partial^2\overline{w'^2}}{\partial r^2}+\frac{1}{r}\frac{\partial\overline{w'^2}}{\partial r}-2\frac{a}{\Lambda^2}\overline{w'^2}] \qquad (2.17)\end{aligned}$$

$$\begin{aligned}\frac{\partial\overline{u'v'}}{\partial t}+W\frac{\partial\overline{u'v'}}{\partial z} &= -U\frac{\partial\overline{u'v'}}{\partial r}-\frac{U}{r}\overline{u'v'}-\frac{\partial U}{\partial r}\overline{u'v'}+2\frac{G}{r^2}\overline{v'^2}-\frac{1}{r}\frac{\partial G}{\partial r}\overline{u'^2}\\ &+(2v_c+p_c)\frac{\partial}{\partial r}[M(\frac{\partial\overline{u'v'}}{\partial r})]-2(v_c-p_c)\frac{1}{r}\frac{\partial}{\partial r}(M\frac{\partial\overline{u'v'}}{\partial r})\\ &+(4v_c-p_c)\frac{M}{r}\frac{\partial\overline{u'v'}}{\partial r}-4(p_c+2v_c)\frac{M}{r^2}\overline{u'v'}-\frac{M}{\Lambda^2}\overline{u'v'}(1+2b\beta)\\ &+\frac{1}{Re}[\frac{\partial^2\overline{u'v'}}{\partial r^2}+\frac{1}{r}\frac{\partial\overline{u'v'}}{\partial r}-\frac{4\overline{u'v'}}{r^2}-2\frac{a}{\Lambda^2}\overline{u'v'}] \qquad (2.18)\end{aligned}$$

$$\begin{aligned}\frac{\partial\overline{u'w'}}{\partial t}+W\frac{\partial\overline{u'w'}}{\partial z} &= -U\frac{\partial\overline{u'w'}}{\partial r}-\frac{\partial U}{\partial r}\overline{u'w'}+2\frac{G}{r^2}\overline{v'w'}-\frac{\partial W}{\partial r}\overline{u'^2}\\ &+(2v_c+p_c)\frac{\partial}{\partial r}[M(\frac{\partial\overline{u'w'}}{\partial r})]+\frac{p_c}{r}\frac{\partial}{\partial r}(M\overline{u'w'})\\ &+2\frac{v_cM}{r}\frac{\partial\overline{u'w'}}{\partial r}-(p_c+2v_c)M\frac{\overline{u'w'}}{r^2}-\frac{M}{\Lambda^2}\overline{u'w'}(1+2b\beta)\\ &+\frac{1}{Re}[\frac{\partial^2\overline{u'w'}}{\partial r^2}+\frac{1}{r}\frac{\partial\overline{u'w'}}{\partial r}-\frac{\overline{u'w'}}{r^2}-2\frac{a}{\Lambda^2}\overline{u'w'}] \qquad (2.19)\end{aligned}$$

$$\begin{aligned}\frac{\partial\overline{v'w'}}{\partial t}+W\frac{\partial\overline{v'w'}}{\partial z} &= -U\frac{\partial\overline{v'w'}}{\partial r}-\frac{U}{r}\overline{u'w'}-\frac{1}{r}\frac{\partial G}{\partial r}\overline{u'w'}-\frac{\partial W}{\partial r}\overline{u'v'}\\ &+v_c\frac{\partial}{\partial r}[M(\frac{\partial\overline{v'w'}}{\partial r})]+2\frac{v_cM}{r}\frac{\partial\overline{v'w'}}{\partial r}-\frac{v_c}{r}\frac{\partial}{\partial r}(M\overline{v'w'})\\ &-2v_cM\frac{\overline{v'w'}}{r^2}-\frac{M}{\Lambda^2}\overline{v'w'}(1+2b\beta)\\ &+\frac{1}{Re}[\frac{\partial^2\overline{v'w'}}{\partial r^2}+\frac{1}{r}\frac{\partial\overline{v'w'}}{\partial r}-\frac{\overline{v'w'}}{r^2}-2\frac{a}{\Lambda^2}\overline{v'w'}] \qquad (2.20)\end{aligned}$$

where $q=\sqrt{\overline{u'^2}+\overline{v'^2}+\overline{w'^2}}$ and $M=\Lambda q$.

Hence, the new system formed by equations (2.1) through (2.4) and (2.15) through (2.20) are closed for the mean pressure, mean flow velocity and Reynolds-stress components. The specific values of the model constants and the length scale Λ will be given for each application in the next two chapters.

Chapter 3

DECAY OF TWO-DIMENSIONAL TURBULENT VORTICES

3.1 The governing gquations

A simplified model of trailing vortices is obtained by neglecting the mean axial flow component, W. The continuity equation shows that the mean radial velocity, U, must also vanish. Thus, the mean streamlines are concentric circles, and the problem reduces to the determination of the decay of the circulation profile and Reynolds-stresses, which are now functions of t and r only. The only mean flow equation that needs to be considered is the θ-momentum equation. Because this equation contains the turbulent shear stress $\overline{u'v'}$, the equations for $\overline{u'^2}$, $\overline{v'^2}$, $\overline{w'^2}$ and $\overline{u'v'}$ must also be solved simultaneously with the mean flow equation. Thus, the governing equations for this case are:

θ-momentum:

$$\frac{\partial G}{\partial t} = \frac{1}{Re}\left(\frac{\partial^2 G}{\partial r^2} - \frac{1}{r}\frac{\partial G}{\partial r}\right) - 2\overline{u'v'} - r\frac{\partial \overline{u'v'}}{\partial r} \tag{3.1}$$

Equation for $\overline{u'^2}$:

$$\begin{aligned}\frac{\partial \overline{u'^2}}{\partial t} &= 4\overline{u'v'}\frac{G}{r^2} + (3v_c + 2p_c)\frac{\partial}{\partial r}\left(M\frac{\partial \overline{u'^2}}{\partial r}\right) + \frac{v_c M}{r}\left(3\frac{\partial \overline{u'^2}}{\partial r} - 2\frac{\partial \overline{v'^2}}{\partial r}\right) \\ &+ 2\frac{p_c}{r}\frac{\partial}{\partial r}[M(\overline{u'^2} - \overline{v'^2})] - 2(2v_c + p_c)\frac{M}{r^2}(\overline{u'^2} - \overline{v'^2}) \\ &- \frac{M}{\Lambda^2}\{\overline{u'^2}(1 + 2b\beta) - \frac{q^2}{3}[1 + 2b(\beta - 1)]\} \\ &+ \frac{1}{Re}\left[\frac{\partial^2 \overline{u'^2}}{\partial r^2} + \frac{1}{r}\frac{\partial \overline{u'^2}}{\partial r} - \frac{2}{r^2}(\overline{u'^2} - \overline{v'^2}) - 2\frac{a}{\Lambda^2}\overline{u'^2}\right]\end{aligned} \tag{3.2}$$

Equation for $\overline{v'^2}$:

$$\begin{aligned}\frac{\partial\overline{v'^2}}{\partial t} &= -\frac{2}{r}\frac{\partial G}{\partial r}\overline{u'v'} + v_c\frac{\partial}{\partial r}[M(\frac{\partial\overline{v'^2}}{\partial r})] + \frac{M}{r}(3v_c\frac{\partial\overline{v'^2}}{\partial r} + 2p_c\frac{\partial\overline{u'^2}}{\partial r}) \\ &+2\frac{v_c}{r}\frac{\partial}{\partial r}[M(\overline{u'^2} - \overline{v'^2})] + 2(p_c + 2v_c)\frac{M}{r^2}(\overline{u'^2} - \overline{v'^2}) \\ &-\frac{M}{\Lambda^2}\{\overline{v'^2}(1 + 2b\beta) - \frac{q^2}{3}[1 + 2b(\beta - 1)]\} \\ &+\frac{1}{Re}[\frac{\partial^2\overline{v'^2}}{\partial r^2} + \frac{1}{r}\frac{\partial\overline{v'^2}}{\partial r} + \frac{2}{r^2}(\overline{u'^2} - \overline{v'^2}) - 2\frac{a}{\Lambda^2}\overline{v'^2}] \end{aligned} \tag{3.3}$$

Equation for $\overline{w'^2}$:

$$\begin{aligned}\frac{\partial\overline{w'^2}}{\partial t} &= v_c\frac{\partial}{\partial r}[M(\frac{\partial\overline{w'^2}}{\partial r})] - \frac{M}{\Lambda^2}\{\overline{w'^2}(1 + 2b\beta) - \frac{q^2}{3}[1 + 2b(\beta - 1)]\} \\ &+\frac{v_c M}{r}\frac{\partial\overline{w'^2}}{\partial r} + \frac{1}{Re}[\frac{\partial^2\overline{w'^2}}{\partial r^2} + \frac{1}{r}\frac{\partial\overline{w'^2}}{\partial r} - 2\frac{a}{\Lambda^2}\overline{w'^2}] \end{aligned} \tag{3.4}$$

Equation for $\overline{u'v'}$:

$$\begin{aligned}\frac{\partial\overline{u'v'}}{\partial t} &= 2\frac{G}{r^2}\overline{v'^2} - \frac{1}{r}\frac{\partial G}{\partial r}\overline{u'^2} \\ &+(2v_c + p_c)\frac{\partial}{\partial r}[M(\frac{\partial\overline{u'v'}}{\partial r})] - 2(v_c - p_c)\frac{1}{r}\frac{\partial}{\partial r}(M\frac{\partial\overline{u'v'}}{\partial r}) \\ &+(4v_c - p_c)\frac{M}{r}\frac{\partial\overline{u'v'}}{\partial r} - 4(p_c + 2v_c)\frac{M}{r^2}\overline{u'v'} - \frac{M}{\Lambda^2}\overline{u'v'}(1 + 2b\beta) \\ &+\frac{1}{Re}[\frac{\partial^2\overline{u'v'}}{\partial r^2} + \frac{1}{r}\frac{\partial\overline{u'v'}}{\partial r} - \frac{4\overline{u'v'}}{r^2} - 2\frac{a}{\Lambda^2}\overline{u'v'}] \end{aligned} \tag{3.5}$$

The above equations have been nondimensionalized by using the initial core radius, r_{10}, as a reference length, and the initial core velocity V_{10} as a reference velocity. The Reynolds number is then given by $Re = V_{10}r_{10}/\nu$, where ν is the kinematic viscosity. Note that this Renolds number is different from Re_{Γ_∞} which is defined as $Re = \Gamma_\infty/\nu$. The relation between them is

$$\begin{aligned} Re_{\Gamma_\infty} &= 2\Pi\frac{1 + 2x_0}{2x_0}Re \\ &= 8.783595Re. \end{aligned}$$

3.2 The initial and boundary conditions

The five coupled equations (3.1) through (3.5) are to be solved for G, $\overline{u'^2}$, $\overline{v'^2}$, $\overline{w'^2}$ and $\overline{u'v'}$. The initial conditions (at $t = 0$) and boundary conditions (at $r = 0$ and $r = \infty$) must be specified. Following Donaldson and Sullivan[16], we use the Oseen laminar solution for the initial distribution of circulation,

$$G(r,0) = \frac{1+2x_0}{2x_0}(1 - e^{-x_0 r^2}) \tag{3.6}$$

where $x_0 = 1.256431209$ is the non-zero solution of the equation

$$e^{x_0} = 1 + 2x_0. \tag{3.7}$$

Note that (3.6) is an exact solution to Eq.(3.1) in the absence of turbulent stresses and with x_0 replaced by $Re/4t$ in the exponential term. Note also that the circulation at infinity normalized by the core circulation is $G(\infty,t) = 1 + 1/2x_0 = 1.39795$. The inverse of this quantity is 0.71533, which gives the initial core circulation normalized by that at infinity.

The initial conditions for the turbulent stresses are assumed in the form

$$\overline{u'^2}(r,0) = k_{ini}\frac{e^{-x_0 r^2}}{x_0 r^2}\frac{(1 - e^{-x_0 r^2})}{2} \tag{3.8}$$

$$\overline{v'^2}(r,0) = k_{ini}e^{-2x_0 r^2} \tag{3.9}$$

$$\overline{w'^2}(r,0) = \frac{\overline{u'^2}(r,0) + \overline{v'^2}(r,0)}{2} \tag{3.10}$$

$$\overline{u'v'}(r,0) = 0 \tag{3.11}$$

where k_{ini} is a constant that sets up the initial strength of the fluctuations. These form are taken as the same as Donaldson[14] without justification at this stage. But it will be shown shortly that the forms of initial conditions have no effect on the final solutions.

Because of symmetry, the turbulent shear stress $\overline{u'v'}$ must vanish at $r = 0$, thus we set

$$\overline{u'v'}(0,t) = 0 \tag{3.12}$$

However, the normal stresses need not vanish at $r = 0$. The appropriate boundary condition for $\overline{w'^2}$ is

$$\left.\frac{\partial \overline{w'^2}}{\partial r}\right|_{r=0} = 0 \tag{3.13}$$

and those for $\overline{u'^2}$ and $\overline{v'^2}$ are

$$\overline{u'^2}(0,t) = \overline{v'^2}(0,t) \tag{3.14}$$

and

$$\left.\frac{\partial \overline{u'^2}}{\partial r}\right|_{r=0} = \left.\frac{\partial \overline{v'^2}}{\partial r}\right|_{r=0} \tag{3.15}$$

The last two boundary conditions follow from the fact that the differential equations for $\overline{u'^2}$ and $\overline{v'^2}$ are identical in the limit $r \to 0$.

A second set of boundary conditions as $r \to \infty$ is given by

$$\overline{u'^2}(r,t) \to 0 \tag{3.16}$$

$$\overline{v'^2}(r,t) \to 0 \tag{3.17}$$

$$\overline{w'^2}(r,t) \to 0 \tag{3.18}$$

$$\overline{u'v'}(r,t) \to 0 \tag{3.19}$$

$$G(r,t) = Const \tag{3.20}$$

where the constant is the value of $G(\infty, 0)$, which is given by the initial conditions.

3.3 The computational scheme and grid

A finite-difference code is developed for the computation of the decay of two-dimensional unsteady vortices. The above equations and conditions are solved as a coupled system of five equations using a marching technique. The finite-difference mesh is shown in figure 3.1. The grid used is uniform both in the radial direction and along the time axis.

In the procedure of discretization of the governing equations, a 4-point backward differencing is applied along the t axis,

$$\left(\frac{\partial f}{\partial t}\right)_{i,j} = \frac{(a_0 f_{i,j} + a_1 f_{i-1,j} + a_2 f_{i-2,j} + a_3 f_{i-3,j})}{\Delta t} \tag{3.21}$$

where $a_0 = \frac{11}{6}$, $a_1 = -3$, $a_2 = \frac{3}{2}$, $a_3 = \frac{-1}{3}$. This formula gives a third-order accurate scheme. It is used at the stations of $i \geq 4$, where $i = 1$ corresponds to the initial conditions at $t = 0$. For $i = 2$, we use $a_0 = 1$, $a_1 = -1$, $a_2 = a_3 = 0$, which gives a first-order scheme. And for $i = 3$, we use $a_0 = \frac{3}{2}$, $a_1 = -2$, $a_2 = -\frac{1}{2}$, $a_3 = 0$, which gives a second-order scheme.

The spatial derivatives are approximated by a 3-point central difference formulae:

$$\left(\frac{\partial f}{\partial r}\right)_{i,j} = \frac{f_{i,j+1} - f_{i,j-1}}{2\Delta r} \tag{3.22}$$

and

$$\left(\frac{\partial^2 f}{\partial r^2}\right)_{i,j} = \frac{f_{i,j+1} - 2f_{i,j} + f_{i,j-1}}{\Delta r^2} \tag{3.23}$$

Upon replacing the partial derivatives in Eqs.(3.1) to (3.5) with finite-difference expressions, we obtain a system of nonlinear algebraic equations. A Newton-Raphson quasi-linearization process is used to the linearized the system before solving it. For example, a nonlinear term $(fg)_{i,j}$ is written as

$$(fg)_{i,j}^{\{k\}} = f_{i,j}^{\{k\}} g_{i,j}^{\{k-1\}} + f_{i,j}^{\{k-1\}} g_{i,j}^{\{k\}} - f_{i,j}^{\{k-1\}} g_{i,j}^{\{k-1\}} \tag{3.24}$$

where the superscript k indicates an unknown quantity and $k-1$ refers to a value from previous iteration or a guessed value.

Discretized by this way, the governing equations are replaced by a linear block tri-diagonal system:

$$\begin{pmatrix} B_1 & C_1 & & & & & & \\ A_2 & B_2 & C_2 & & & & & \\ & \ddots & \ddots & \ddots & & & & \\ & & A_j & B_j & C_j & & & \\ & & & \ddots & \ddots & \ddots & & \\ & & & & A_{n-1} & B_{n-1} & C_{n-1} & \\ & & & & & A_n & B_n & \end{pmatrix} \begin{pmatrix} \zeta_1 \\ \zeta_2 \\ \vdots \\ \zeta_j \\ \vdots \\ \zeta_{n-1} \\ \zeta_n \end{pmatrix} = \begin{pmatrix} D_1 \\ D_2 \\ \vdots \\ D_j \\ \vdots \\ D_{n-1} \\ D_n \end{pmatrix} \tag{3.25}$$

in which A_j, B_j, C_j are 5×5 matrices. For $j = 2, 3, \ldots, n-1$, they consist of the coefficients in the j-th equation set which involves the variables at points $j-1$, j, and $j+1$. ζ_j is the vector of unknowns, and D_j is the vector containing known values or guessed values. The first and the last lines in the system (3.25) correspond to the boundary conditions at $r = 0$ and $r = r_\infty$, respectively. In the computation, the outer boundary conditions are applied at a large but finite radius. At each time step, the system is solved repeatedly until a convergence criterion is met. The second-order accuracy in Δr and third-order accuracy in Δt have been established by grid refinements.

3.4 Results and discussion

3.4.1 The results for a vortex at $Re = 10^4$

The decay of a vortex at $Re = 10^4$ is first computed and the results are compared with the published results of Donaldson and Sullivan[16] and Donaldson[13] (hereafter, DS) who used the same turbulence model. The initial conditions and model constants are identical

to those of DS. The initial level of turbulent intensity, k_{ini} is 10^{-2}. The model constants are:

$$a = 2.5$$

$$b = 0.125$$

$$p_c = v_c = \beta = 1$$

and the length scale Λ is set equal to $0.16r_1$ where r_1 is the core radius at time t.

It is realized that there is another set of model constants used by Donaldson and Bilanin[14]. However, since there are no detailed experimental results for axisymmetric vortices, it is hard to conclude which set, among all the possible combinations, is the best for the two-dimensional vortex case. Numerical tests show no qualitative differences when varying these parameters. Therefore, the computational results presented in this chapter are based on the model constants listed above.

As shall be discussed shortly, significant quantitative differences have been found between the present results and those published in DS. In an effort to explain these differences, we found that the equation for $\overline{u'v'}$ listed in DS is in error. The correlation term $\overline{u'v'}(\frac{\partial V}{\partial r}+\frac{V}{r})$ in equation (41) of Donaldson[13] and equation (13) in Donaldson and Sullivan[16] should be $\overline{u'^2}(\frac{\partial V}{\partial r}+\frac{V}{r})$. When the incorrect equation is used in our code, the obtained results are found to be in good agreement with, but not identical to, the published results in DS. Therefore, the error mentioned above may only be a misprint rather than an error that was carried throughout the computations in DS. The differences could be due to numerical problems. Incidentally, no details about the numerical method are given in DS. To avoid confusion, the results based on the incorrect equation will not be presented or referenced in this thesis.

The core radius r_1/r_{10} and core velocity V_1/V_{10} are shown as functions of time in figure 3.2. After a period of adjustment, in which the core radius actually decreases with time, the slope of radius and velocity curves gradually approach $1/2$ and $-1/2$, respectively. Donaldson's results show that these slopes are reached at a much earlier time. The initial decrease in the radius implies that the laminar Oseen solution is inconsistent with the self-similar profile that the turbulent vortex eventually approaches.

The time development of the core circulation $\Gamma_1(= 2\pi r_1 V_1)$ is shown in figure 3.3, along with the results of DS. Note that Γ_1/Γ_∞ approaches value of 0.5 at long times. This value is in the range of 0.322 to 0.552 which is experimentally reported by Hoffman and Joubert[30].

The maximum turbulent kinetic energy $k_{max} = (\overline{u_i' u_i'})_{max}$ (k is actually twice the kinetic energy) is normalized with the square of the core velocity $V_1^2(t)$ and is plotted against time in figure 3.4. Again a transitional period prevails during which the arbitrary initial disturbances adjust to a dynamically realizable state, then k_{max}/V_1^2 approaches a steady level. The fact that the turbulent kinetic energy scales with the maximum tangential velocity indicates the existence of a self-similar solution to the turbulent axisymmetric vortex. Note that the results of DS also indicate the existence of a self-similar solution except that the level of k_{max}/V_1^2 is at least one order of magnitude higher than what the current calculations show.

Figure 3.5 compares the current computed circulation profile with that obtained by DS. The current result shows that the location of the overshoot is at $\eta \approx 5.5$, while DS shows that it is at $\eta \approx 3$.

The radial distribution of the turbulent kinetic energy k/k_{max} is shown in figure 3.6 against $\eta = r/r_1$. Whereas results of DS show that the turbulent kinetic energy is maximum and almost uniform within the core, the current results show that the kinetic energy has a

local minimum on the centerline and attain its maximum around $\eta = 2.2$.

The turbulent shear stress $\tau = \overline{u'v'}$ normalized with its maximum is shown against η in figure 3.7. We note that the core region ($\eta < 1$) is practically free from turbulent shear stresses. Only viscous shear stresses are present. The results of DS shown in figure 3.7 are qualitatively different because they show large turbulent shear stress in the core.

The circumferential velocity profile V/V_1 in the inner region is plotted in figure 3.8, along with the results of DS and the measurements of Hoffmann and Joubert[30]. It is clear that the current computed profile is in better agreement with the measured profile than the one computed by DS.

The main conclusion of DS is that a self-similar solution exists for the turbulent axisymmetric vortex. Although the results presented by these authors are inaccurate, their main conclusion is still valid. To further substantiate the existence of a self-similar solution, we obtained results for a very long time, $t^* = 5000$. The profiles of the four Reynolds-stress $\overline{u'v'}/V_1^2$, $\overline{u'^2}/V_1^2$, $\overline{v'^2}/V_1^2$ and $\overline{w'^2}/V_1^2$ are plotted in figures 3.9, 3.10, 3.11 and 3.12, against η. Although one curve is shown in each figure, the respective results at t^* =2000, 3000, 4000, and 5000 all collapse on the shown curve. This establishes a numerical evidence that a self-similar solution exists. In this solution the turbulent stresses scale with the square of the maximum circumferential velocity, and the core radius and core velocity vary with time like $t^{1/2}$ and $t^{-1/2}$, respectively.

The self-similar solution shows that the core is basically free from turbulent shear stress, as evident in figure 3.9. Also the maximum turbulent shear occurs at about $\eta = 3.5$. The turbulent intensities $\overline{u'^2}$, $\overline{v'^2}$ and $\overline{w'^2}$ are maximum at a radius of about $2.2r_1$ and they have local minimum on the centerline. Note also that the radial component $\overline{u'^2}$ is the strongest component while the circumferential $\overline{v'^2}$ and the axial $\overline{w'^2}$ components are of comparable

strength. The radial distribution of the sum of the turbulent intensities is shown in figure 3.14 at different times. Again the approach to a self-similar solution is clearly demonstrated for $t^* > 1000$.

The circulation profile Γ/Γ_∞ is plotted in figure 3.13 as a function of η at different times. The most significant characteristics of this profile is the existence of an overshoot in the circulation. The overshoot is only 5% of the circulation at infinity and it occurs at $\eta \approx 5.5$. Note that the initial profile ($t = 0$) does not possess an overshoot and that the overshoot develops in time as the self-similar solution is approached. Govindaraju and Saffman[19] obtained a self-similar solution using an eddy viscosity model. They predicted a circulation profile with a much stronger overshoot of 30%. However, experimental results don't support such a strong overshoot.

It is important to show that the self-similar solution is independent of the initial conditions. The effects of the initial level of the turbulent intensities and their locations have been investigated. The initial level of the turbulent intensities is given by k_{ini} in Eq.(3.8). The maximum kinetic energy k_{max}/V_1^2 against time is shown in figure 3.15 for three values of k_{ini}, 10^{-4}, 10^{-3}, and 10^{-2}. It is clear that for the strong levels of 10^{-2} and 10^{-3}, the vortex goes through a transition process and a steady level of k_{max}/V_1^2 is sustained. But for the weak level of 10^{-4} the vortex remains laminar and the initial disturbances are quenched. No attempt is made to determine the exact critical level of k_{ini}, for which a turbulent vortex is obtained. That level may also depend on the Reynolds number. It is interesting to note that the maximum level of k_{max}/V_1^2 attained during transition as well as its level in the self-similar solution are independent of k_{ini}. This independence is clearly demonstrated in figure 3.16 which is the same as figure 3.15 except that the time origin is shifted by 90 units for the case of $k_{ini} = 10^{-2}$. Furthermore, it has been checked that the self-similar profiles

depicted in figures 3.9 through 3.14 are also independent of k_{ini}.

In the above computation, the initial distributions of $\overline{u'^2}$, $\overline{v'^2}$ and $\overline{w'^2}$ are given by Eqs.(3.8) through (3.10), which place the maxima of $\overline{u'^2}$, $\overline{v'^2}$ and $\overline{w'^2}$ at the origin. To investigate the sensitivity of the self-similar solution to the location of these maxima, new distributions given by

$$\overline{u'^2} = \overline{v'^2} = \overline{w'^2} = k_{ini} e^{-2(r-2)^2} \tag{3.26}$$

with $k_{ini} = 10^{-2}$ are used. These distributions place the maxima at $r = 2$. The variation of k_{max}/V_1^2 with time is shown in figure 3.17 for the two different initial distributions. It is clear that the final level of k_{max}/V_1^2 is independent of initial location of the maximum turbulent intensities. It has also been checked that the self-similar profiles are independent of that location.

3.4.2 The effects of Reynolds number

The investigation in the previous section has been motivated by the case studied by DS which was conducted at a Reynolds number of 10^4. It is important to study the characteristics of the turbulent vortex at higher Reynolds numbers, and to establish the effects of Reynolds number on the self-similar solution.

The variations of k_{max}/V_1^2 vs time for $Re = 10^4$, 10^5 and 10^6 are shown in figure 3.18. Firstly, we note that the time needed to reach a self-similar solution, as indicated by the leveling-off of k_{max}/V_1^2, increases rapidly with Reynolds number. This is only an indication that the initial laminar profile is far from the self-similar solution that the vortex wants to approach. Secondly, we observe that the level of maximum turbulent kinetic energy normalized by the square of the core velocity decreases very rapidly with the increase in the Reynolds number.

The Reynolds number has also significant effects on the turbulent stress profiles as well as the mean circulation profile. The effect of Reynolds number on the shear stress profile is shown in figure 3.19. The profiles for k/V_1^2 are shown in figure 3.20. At $Re = 10^4$ the turbulent energy is concentrated near $\eta = 2.2$. As the Reynolds number is increased, the maximum of normalized turbulent energy decreases but the region over which the energy significantly extends farther out. We also note that the position of the maximum turbulent kinetic energy is insensitive to Reynolds number. It is always around $r = 2.2r_1$.

The effects of Reynolds number on the self-similar mean circulation profile are shown in figure 3.21. The circulation overshoot is almost independent if Re. Its value is roughly 5% of Γ_∞. However, the location of that overshoot is highly dependent on Re. It shifts to a higher radius as Re is increased. Accordingly, the core circulation Γ_1/Γ_∞ decreases as Re increases. This trend of Γ_1 is basically consistant with the experimental measurements summarized by Govindaraju and Saffman[19].

It has been noted that the time needed for 1/2-power law to emerge for r_1 and V_1 increases quite rapidly with Re. To shed some light on this behavior, let's reconsider the initial mean velocity profile given by Eq.(3.6). This solution is actually a self-similar solution to the laminar diffusion of a point vortex of circulation Γ_∞. The circulation at any r and t is given by

$$\Gamma = \Gamma_\infty \left(1 - e^{-\frac{Re}{4t}r^2}\right) \tag{3.27}$$

where Re is Reynolds number. The comparison of Eq.(3.6) with Eq.(3.27) shows that the initial solution ($t = 0$) used in this study is a laminar vortex with an age equal to

$$\begin{aligned} t_0^* &= \frac{Re}{4x_0} \\ &= 0.1989762736Re. \end{aligned}$$

Therefore, when plotting the variation of r_1/r_{10} and V_1/V_{10} with time one should shift the time origin by t_0^*. This has been done for the three Reynolds numbers $Re = 10^4$, 10^5 and 10^6, and the results are shown in figure 3.22. Note that both r_1 and V_1 decreases initially very rapidly then r_1 asymptotically approaches $t^{\frac{1}{2}}$ and V_1 behaves like $t^{-\frac{1}{2}}$. The decrease of r_1 seems to be unphysical. However this is unimportant because it only implies that the initial core circulation is too high in comparison with the value dictated by the self-similar solution.

Chapter 4

A SELF-SIMILAR SOLUTION FOR AXISYMMETRIC JETS

4.1 Introduction

In addition to their many technological applications, axisymmetric jets have been used by many investigators to validate new turbulence models. Two comprehensive experimental studies of axisymmetric air jets have recently been published by Panchapakesan and Lumley[48] and Hussein, Capp and George[32], hereafter referred to as PL and HCG, respectively. Mean velocity profiles and turbulent intensity profiles as well as several higher-order correlations have been presented by those authors. The objective of this chapter is to investigate the performance of Donaldson and Bilanin[14] second-order closure model for axisymmetric jets using the recent experimental data of PL and HCG. It has been found that the turbulence model constants suggested by Donaldson and Bilanin[14] produced totally unacceptable results in comparison with the experimental data. Therefore, the model constants have to be tuned for better agreement with the experiments. As we shall see later, the new model constants result in excellent agreement between the computed and experimental mean velocity and turbulent shear stress $\overline{u'v'}$ profiles, but only a fair agreement for the turbulent intensities $\overline{u'^2}$, $\overline{v'^2}$ and $\overline{w'^2}$ profiles.

4.2 The governing equations, the boundary and initial conditions

Free, non-swirling axisymmetric jets are considered in this chapter. Thus, the mean tangential velocity is identically zero and the θ-momentum equation drops out. Furthermore, in the quasi-cylindrical approximation, the mean pressure is uniform throughout the flow field. We need to solve the continuity and z-momentum equations for the mean radial velocity U and axial velocity W. However, the momentum equation contains the shear stress component $\overline{u'w'}$, and hence we have to solve the transport equations for the four Reynolds-stress components $\overline{u'w'}$, $\overline{u'^2}$, $\overline{v'^2}$ and $\overline{w'^2}$.

With Donaldson and Bilanin[14] second-order closure model incorporated in the transport equations, the governing equations for the jet are

Continuity:

$$\frac{\partial U}{\partial r} + \frac{U}{r} + \frac{\partial W}{\partial z} = 0 \tag{4.1}$$

z-momentum:

$$U\frac{\partial W}{\partial r} + W\frac{\partial W}{\partial z} = \frac{1}{Re}(\frac{\partial^2 W}{\partial r^2} + \frac{1}{r}\frac{\partial W}{\partial r}) - \frac{\overline{u'w'}}{r} - \frac{\partial \overline{u'w'}}{\partial r} \tag{4.2}$$

The Reynolds-stress transport equations:

$$\begin{aligned} W\frac{\partial \overline{u'^2}}{\partial z} &= -U\frac{\partial \overline{u'^2}}{\partial r} + (3v_c + 2p_c)\frac{\partial}{\partial r}(M\frac{\partial \overline{u'^2}}{\partial r}) + \frac{v_c M}{r}(3\frac{\partial \overline{u'^2}}{\partial r} - 2\frac{\partial \overline{v'^2}}{\partial r}) \\ &\quad +2\frac{p_c}{r}\frac{\partial}{\partial r}[M(\overline{u'^2} - \overline{v'^2})] - 2(2v_c + p_c)\frac{M}{r^2}(\overline{u'^2} - \overline{v'^2}) \\ &\quad -\frac{M}{\Lambda^2}\{\overline{u'^2}(1 + 2b\beta) - \frac{q^2}{3}[1 + 2b(\beta - 1)]\} \\ &\quad +\frac{1}{Re}[\frac{\partial^2 \overline{u'^2}}{\partial r^2} + \frac{1}{r}\frac{\partial \overline{u'^2}}{\partial r} - \frac{2}{r^2}(\overline{u'^2} - \overline{v'^2}) - 2\frac{a}{\Lambda^2}\overline{u'^2}] \end{aligned} \tag{4.3}$$

$$
\begin{aligned}
W\frac{\partial\overline{v'^2}}{\partial z} &= -U\frac{\partial\overline{v'^2}}{\partial r} - 2\frac{U}{r}\overline{v'^2} + v_c\frac{\partial}{\partial r}[M(\frac{\partial\overline{v'^2}}{\partial r})] \\
&+\frac{M}{r}(3v_c\frac{\partial\overline{v'^2}}{\partial r} + 2p_c\frac{\partial\overline{u'^2}}{\partial r}) + 2\frac{v_c}{r}\frac{\partial}{\partial r}[M(\overline{u'^2} - \overline{v'^2})] \\
&+2(p_c + 2v_c)\frac{M}{r^2}(\overline{u'^2} - \overline{v'^2}) - \frac{M}{\Lambda^2}\{\overline{v'^2}(1 + 2b\beta) - \frac{q^2}{3}[1 + 2b(\beta - 1)]\} \\
&+\frac{1}{Re}[\frac{\partial^2\overline{v'^2}}{\partial r^2} + \frac{1}{r}\frac{\partial\overline{v'^2}}{\partial r} + \frac{2}{r^2}(\overline{u'^2} - \overline{v'^2}) - 2\frac{a}{\Lambda^2}\overline{v'^2}] \qquad (4.4)
\end{aligned}
$$

$$
\begin{aligned}
W\frac{\partial\overline{w'^2}}{\partial z} &= -U\frac{\partial\overline{w'^2}}{\partial r} - 2\frac{\partial W}{\partial r}\overline{u'w'} + v_c\frac{\partial}{\partial r}[M(\frac{\partial\overline{w'^2}}{\partial r})] + \frac{v_c M}{r}\frac{\partial\overline{w'^2}}{\partial r} \\
&-\frac{M}{\Lambda^2}\{\overline{w'^2}(1 + 2b\beta) - \frac{q^2}{3}[1 + 2b(\beta - 1)]\} \\
&+\frac{1}{Re}[\frac{\partial^2\overline{w'^2}}{\partial r^2} + \frac{1}{r}\frac{\partial\overline{w'^2}}{\partial r} - 2\frac{a}{\Lambda^2}\overline{w'^2}] \qquad (4.5)
\end{aligned}
$$

$$
\begin{aligned}
W\frac{\partial\overline{u'w'}}{\partial z} &= -U\frac{\partial\overline{u'w'}}{\partial r} - \frac{\partial U}{\partial r}\overline{u'w'} - \frac{\partial W}{\partial r}\overline{u'^2} \\
&+(2v_c + p_c)\frac{\partial}{\partial r}[M(\frac{\partial\overline{u'w'}}{\partial r})] + \frac{p_c}{r}\frac{\partial}{\partial r}(M\overline{u'w'}) \\
&+2\frac{v_c M}{r}\frac{\partial\overline{u'w'}}{\partial r} - (p_c + 2v_c)M\frac{\overline{u'w'}}{r^2} - \frac{M}{\Lambda^2}\overline{u'w'}(1 + 2b\beta) \\
&+\frac{1}{Re}[\frac{\partial^2\overline{u'w'}}{\partial r^2} + \frac{1}{r}\frac{\partial\overline{u'w'}}{\partial r} - \frac{\overline{u'w'}}{r^2} - 2\frac{a}{\Lambda^2}\overline{u'w'}] \qquad (4.6)
\end{aligned}
$$

The above equations are parabolic partial differential equations that can be solved by a marching technique starting with some initial profiles at a given station z_0. However, because of the rapid spreading of the turbulent jet, it is advantageous to introduce a similarity transformation first. The following transformation is used.

Let

$$
\begin{cases}
\eta = r/z \\
\xi = z
\end{cases} \qquad (4.7)
$$

and

$$\left\{\begin{array}{rcl} U & = & (s/\xi)U_a(\eta,\xi) \\ W & = & (s/\xi)W_a(\eta,\xi) \\ \overline{u'^2} & = & (s^2/\xi^2)T_{11}(\eta,\xi) \\ \overline{v'^2} & = & (s^2/\xi^2)T_{22}(\eta,\xi) \\ \overline{w'^2} & = & (s^2/\xi^2)T_{33}(\eta,\xi) \\ \overline{u'w'} & = & (s^2/\xi^2)T_{13}(\eta,\xi) \\ F_a(\eta,\xi) & = & U_a - \eta W_a \\ q_a & = & \sqrt{T_{11}+T_{22}+T_{33}} \\ \Lambda & = & \Lambda_a \xi \\ M_a & = & q_a \Lambda_a \\ f_a & = & -M_a v_c \\ a_a & = & a/\Lambda_a^2 \\ b_a & = & b q_a/\Lambda_a \\ c_a & = & -M_a p_c \\ d_a & = & -q_a/\Lambda_a \\ Re_a & = & sRe \end{array}\right\} \tag{4.8}$$

where s is a constant. The transformed governing equations are:

Continuity:

$$-\xi\frac{\partial W_a}{\partial \xi} = \frac{\partial F_a}{\partial \eta} + \frac{F_a}{\eta} + W_a \tag{4.9}$$

z-momentum:

$$-\xi W_a\frac{\partial W_a}{\partial \xi} = F_a\frac{\partial W_a}{\partial \eta} - {W_a}^2 - \frac{1}{Re_a}\left(\frac{\partial^2 W_a}{\partial \eta^2} + \frac{1}{\eta}\frac{\partial W_a}{\partial \eta}\right) + \left(\frac{\partial T_{13}}{\partial \eta} + \frac{T_{13}}{\eta}\right) \tag{4.10}$$

Reynolds-stresses transport equations:

$$
\begin{aligned}
-\xi\frac{\partial T_{11}}{\partial \xi} &= F_a\frac{\partial T_{11}}{\partial \eta} + 2\frac{\partial F_a}{\partial \eta}T_{11} + 2\eta\frac{\partial W_a}{\partial \eta}T_{11} + (3v_c + 2p_c)\frac{\partial T_{11}}{\partial \eta}\frac{\partial M_a}{\partial \eta} \\
&+ \frac{\partial^2 T_{11}}{\partial \eta^2}\left(3f_a + 2c_a - \frac{1}{Re_a}\right) + \frac{1}{\eta}\frac{\partial T_{11}}{\partial \eta}\left(3f_a + 2c_a - \frac{1}{Re_a}\right) \\
&- 2\frac{T_{11}}{\eta^2}\left(2f_a + c_a - \frac{1}{Re_a}\right) + 2T_{11}\left[\frac{-d_a + b_a(2\beta+1)}{3} + \frac{a_a}{Re_a}\right] \\
&- \frac{2}{\eta}\frac{\partial T_{22}}{\partial \eta}(f_a + c_a) + \frac{2T_{22}}{\eta^2}\left(2f_a + c - \frac{1}{Re_a}\right) \\
&+ T_{22}\frac{d_a - 2b_a(\beta-1)}{3} + T_{33}\frac{d_a - 2b_a(\beta-1)}{3}
\end{aligned} \tag{4.11}
$$

$$
\begin{aligned}
-\xi\frac{\partial T_{22}}{\partial \xi} &= F_a\frac{\partial T_{22}}{\partial \eta} + \frac{2}{\eta}F_a T_{22} + v_c\frac{\partial T_{22}}{\partial \eta}\frac{\partial M_a}{\partial \eta} + \frac{\partial^2 T_{22}}{\partial \eta^2}\left(f_a - \frac{1}{Re_a}\right) \\
&+ \frac{1}{\eta}\frac{\partial T_{22}}{\partial \eta}\left(f_a - \frac{1}{Re_a}\right) - 2\frac{T_{22}}{\eta^2}\left(2f_a + c_a - \frac{1}{Re_a}\right) \\
&+ 2T_{22}\left[\frac{-d_a + b_a(2\beta+1)}{3} + \frac{a_a}{Re_a}\right] + \frac{2T_{11}}{\eta^2}\left(2f_a + c - \frac{1}{Re_a}\right) \\
&+ \frac{2}{\eta}\frac{\partial T_{11}}{\partial \eta}(f_a + c_a) + T_{11}\frac{d_a - 2b_a(\beta-1)}{3} + T_{33}\frac{d_a - 2b_a(\beta-1)}{3}
\end{aligned} \tag{4.12}
$$

$$
\begin{aligned}
-\xi\frac{\partial T_{33}}{\partial \xi} &= F_a\frac{\partial T_{33}}{\partial \eta} - 2W_a T_{33} + 2\frac{\partial W_a}{\partial \eta}T_{13} + v_c\frac{\partial M_a}{\partial \eta}\frac{\partial T_{33}}{\partial \eta} \\
&+ \frac{\partial^2 T_{33}}{\partial \eta^2}\left(f_a - \frac{1}{Re_a}\right) + \frac{1}{\eta}\frac{\partial T_{33}}{\partial \eta}\left(f_a - \frac{1}{Re_a}\right) \\
&+ 2T_{33}\left[\frac{-d_a + b_a(2\beta+1)}{3} + \frac{a_a}{Re_a}\right] + T_{11}\frac{d_a - 2b_a(\beta-1)}{3} \\
&+ T_{22}\frac{d_a - 2b_a(\beta-1)}{3}
\end{aligned} \tag{4.13}
$$

$$
\begin{aligned}
-\xi\frac{\partial T_{13}}{\partial \xi} &= F_a\frac{\partial T_{13}}{\partial \eta} - W_a T_{13} + \frac{\partial F_a}{\partial \eta}T_{13} + \eta\frac{\partial W_a}{\partial \eta}T_{13} + \frac{\partial W_a}{\partial \eta}T_{11} \\
&+ (2v_c + p_c)\frac{\partial M_a}{\partial \eta}\frac{\partial T_{13}}{\partial \eta} + \frac{\partial^2 T_{13}}{\partial \eta^2}\left(2f_a + c_a - \frac{1}{Re_a}\right) \\
&+ \frac{1}{\eta}\frac{\partial T_{13}}{\partial \eta}\left(2f_a + c_a - \frac{1}{Re_a}\right) - \frac{T_{13}}{\eta^2}\left(2f_a + c_a - \frac{1}{Re_a}\right) \\
&+ T_{13}\left[2b_a\beta - d_a + 2\frac{a_a}{Re_a}\right] \qquad (4.14)
\end{aligned}
$$

The boundary conditions on these equations are:

At $\eta = 0$:

$$
\begin{cases}
F_a &= 0 \\
\frac{\partial W_a}{\partial \eta} &= 0 \\
T_{11} &= T_{22} \\
T_{13} &= 0 \\
\frac{\partial T_{22}}{\partial \eta} &= \frac{\partial T_{33}}{\partial \eta}
\end{cases} \qquad (4.15)
$$

At $\eta = \infty$:

$$
\begin{cases}
F_a = W_a = 0 \\
T_{11} = T_{22} = T_{33} = T_{13} = 0
\end{cases} \qquad (4.16)
$$

In the computation, the inner boundary conditions are applied at $\eta = 0$ but the outer boundary condition (for $\eta = \infty$) are applied at $\eta = \eta_n$, where η_n is 0.4, which is found to be large enough for the satisfaction of the asymptotic condition (4.16)

Note that explicit reference to ξ appears only on the left-hand-side of the equations (4.9) through (4.14). These equations with the boundary conditions (4.15) and (4.16) admit a self-similar solution in which U_a, W_a, T_{11}, T_{22}, T_{33} and T_{13} are functions only of the similarity variable η. To determine such a solution, one may set the partial derivatives w.r.t. ξ to zero and solve a set of ordinary differential equations in η. Unfortunately, the present effort using a finite-difference method failed to provide a converged solution to the

ODE's. However, an alternative procedure has been found to be successful in providing a self-similar solution.

A pseudo marching technique is used to obtain a self-similar solution to equations (4.9) through (4.14). The coefficients of the partial derivatives w.r.t. ξ are set to unity. With ξ and η playing the role of t and r, the finite-difference method described in chapter three for the unsteady vortex problem is used to advance the solution in ξ until the magnitudes of the partial derivatives w.r.t. ξ are all reduced below a small number.

Several different forms of the distributions of W_a, T_{11}, T_{22}, T_{33} and T_{13} were tried, as the initial conditions. The results presented in this chapter are obtained using the following distributions:

$$W_a(\eta, \xi_0) = \sum_{k=0}^{N} w_k \eta^k e^{-W_{10}\eta^2} \tag{4.17}$$

$$T_{ii}(\eta, \xi_0) = \sum_{k=0}^{N} (t_i)_k \eta^k e^{-T_{i0}\eta^2} \tag{4.18}$$

$$T_{13}(\eta, \xi_0) = \sum_{k=0}^{N} (t_4)_k \eta^k e^{-T_{40}\eta^2} \tag{4.19}$$

where w_k, $(T_i)_k$, $(t_4)_k$, W_{10}, T_{i0} and T_{40} are constants, $i = 1, 2, 3$. Taken from the curve fit of HCG[32], these constants are as following:

$N = 7$, $W_{10} = 111$, $T_{10} = 79$, $T_{20} = 73$, $T_{30} = 156$, $T_{40} = 78$

k	0	1	2	3	4	5	6	7
w_k	1.00	0	12.12	0	2815	0	0	0
$(t_1)_k$	0.04723	0	2.222	0	0.5174	0	0	0
$(t_2)_k$	0.049	0	2.316	0	0.5745	0	0	0
$(t_3)_k$	0.07468	0	17.29	0	−484.5	0	58640	0
$(t_4)_k$	0	0.55	0	−29.62	0	1282	0	−18980

4.3 Results and discussion

For the two-dimensional vortex case, the model constants a, b, β, p_c, v_c, etc. were taken to reproduce the model applied by Donaldson and Sullivan[16]. However, these values produce totally incorrect behavior of the jet case. For the axisymmetric jets, recent experimental results such as those of PL[48, 49] and HCG[32] make it possible to determine more reliable values for the model constants. After many tests of different sets, we found that the following combination gives the best comparison with the experimental data.

$$\begin{cases} a_a &= 3.25 \\ b_a &= 0.1 \\ p_c &= 0.05 \\ v_c &= 0.05 \\ \beta &= 0 \\ \Lambda_a/r_{05} &= 0.8 \end{cases} \tag{4.20}$$

where r_{05} is the half-width of the jet.

Figure 4.1 shows the radial distribution of the self-similar solution of the mean axial velocity. The measurements of air jet presented by PL[48], and HCG[32] are also plotted. It is clear that the current computation agree very well with the experiments by HCG[32]. Also it can be seen in figure 4.2 that the self-similar profile for the radial velocity, which is related to the axial velocity by the continuity equation, fits the experimental data of HCG[32].

Figure 4.3 compares the computed and the measured turbulent shear stress profile, in the self-similar variables. In the inner region ($r/z \leq 0.1$), the current computation agrees with PL[48], while in the outer region it predicts HCG[32].

Figure 4.4 presents the radial distributions of the turbulent intensity in the axial direc-

tion. In this plot the computed results are still in good agreement with the experiments in most of the area except near the centerline. The results from different measurements also vary more in this area than in the outer region. Hence, it is likely that the actual difference between the computation and the experiment at the centerline is less than what appears in this plot.

Similar differences appear in figure 4.5 and figure 4.6, which show the mean magnitudes of turbulent fluctuations in the radial and tangential directions. However, while the quantitative differences obviously exist, the calculated curves still qualitatively agree with the measurements.

Chapter 5

CONCLUSIONS

The Reynolds-stress transport equations have been derived in cylindrical coordinates without the assumption of axisymmetry. The second-order closure model developed by Donaldson[13] has been applied to these equations so that a closed system at the second-order level is obtained. Some simplified governing equations corresponding to the specific applications of axisymmetric vortices and jets have been shown as well. Finite-difference codes have been developed to solve the simplified equations.

The decay of an axisymmetric vortex has been computed. In this study, the self-similar solution to the problem has been found numerically. The Reynolds number effects on the self-similar solution have also been considered.

The results have shown that the self-similar solution obtained is independent of the initial conditions, but it is sensitive to the Reynolds number.

It has been found that the slopes of radius and velocity curves asymptotically approach $1/2$ and $-1/2$ with time, respectively. This is true at all Reynolds numbers.

It has been shown that the kinetic energy as well as all the turbulent intensities have a local minimum at the centerline and attain their maxima around a radius of 2.2 times the core radius. As the Reynolds number is increased, the maximum of the turbulent energy normalized by the square of the core velocity deceases but the region with significant turbulent energy extends farther out.

The computed results have also shown that the core region is practically free from turbulent shear stresses. Only the viscous shear stresses prevail in the core.

It has been found that the overshoot of the circulation is 5% of the circulation at infinity. Although the magnitude of the overshoot is almost independent of the Reynolds number, its location is very sensitive to the Reynolds number. The location of overshoot increases rapidly with the Reynolds number. Furthermore, the core circulation decreases with the increase in Reynolds number.

The second-order closure model has also been applied to the case of axisymmetric jets. A suitable set of model coefficients has been found. With these coefficients, a self-similar solution has been obtained. The numerical results are in excellent agreement with the experimental data of Panchapakesan and Lumley[48] and Hussein, Capp and George[32] for the mean velocity profiles and turbulent shear stress, but only fair agreement is obtained for the turbulent intensities.

REFERENCES

[1] ABID, R. AND SPEZIALE, C. G. (1992) Predicting Equilibrium States with Reynolds Stress Closures in Channel Flow and Homogeneous Shear Flow., *ICASE Report No.92-28*, NASA Langley Research Center.

[2] BALDWIN, B. S., CHIGIER, N. A. AND SHEAFFER, Y. S. (1972) Predicting of Far Flow Field in Trailing Vortices., *AIAA Paper 72-989.*

[3] BANDYOPADHYAY, P., STEAD, D AND ASH, R. (1990) The Organized Nature of a Turbulent Trailing Vortex., *AIAA paper 90-1625*, AIAA 21st Fluid Dynamics, Plasma Dynamics and Laser Conference, June, 1990, Seattle, WA.

[4] BILANIN, A. J., TESKE, M. E., HIRSCH, J. E. (1978) Neutral atmospheric effects on the dissipation of aircraft vortex wakes. *AIAA J.*, **16** , No. 9, pp. 956-961.

[5] CHOU, P. Y. (1945) On Velocity correlation and the Solution of the Equations of Turbulent Fluctuation., *Q. Appl. Math.*, **3**, pp.38-54.

[6] CHOU, P. Y. (1945) Pressure Flow of a Turbulent Fluid Between Parallel Planes., *Q. Appl. Math.*, **3**, pp.198-209.

[7] CHOU, P. Y. (1947) Turbulent Flow Along a Semi-infinite Plane., *Q. Appl. Math.*, **5**, pp.346-353.

[8] CORSIGLIA, V. R., SCHWIND, R. G., CHIGIER, N. A. (1973) Rapid scanning, Three-Dimensional hot-wire anemometer surveys of wing-tip vortices. *J. Aircraft.* **10**, No. 12., pp.752-757

[9] DAVIDOV, B. I. (1960) On the Statistical Dynamics of an Incompressible Turbulent Fluid., (English Translated from Soviet Phy. -Doklady),*Am. Int. Phys.*, **4**, No. 4, pp.769-772.

[10] DAVIDOV, B. I. (1960) On the Statistical Theory of Turbulence., (English Translated from Soviet Phy. -Doklady),*Am. Int. Phys.*, **4**, No. 4, pp.779-781.

[11] DEVENPORT, SHARMA, G. AND GLEGG, S. A. L.(1992) Turbulence measurements in trailing vortices for BWI noise prediction. *VPI-AOE* **192**, VPISU, Balcksburg, Va.

[12] DEVENPORT, W. J., RIFE, M. C., LIAPIS, S. I. AND MIRANDA, J. (1994) Turbulent Trailing Vortices *32nd Aerospace Science Meeting & Exhibit*, January 1994, Reno, Nevada. *AIAA 94-0404*

[13] DONALDSON C. DUP. (1972) Calculation of Turbulent Shear Flows for Atmospheric and Vortex Motions., *AIAA Journal* , **10** , pp.4-12.

[14] DONALDSON C. DUP. AND BILANIN, A. J. (1975) Vortex Wakes of Conventional Aircraft., *AGARDograph* AGARD-AG-204 , (ed. KORKEGI, R. H.).

[15] DOSANJH, D. S., GASPAREK, E. P., ESKINAZI, S. (1962) The decay of a viscous trailing vortex., *Aeronautical Quaterly* **13** , May , pp 167-188.

[16] DONALDSON C. DUP.AND SULLIVAN, R. D. (1971) Decay of an Isolated Vortex., *Aircraft Wake Turbulence and Its Detection* , (ed. OLSEN, J. H., GOLDBURG, A. AND ROGERS, M.) Plenum Press, pp.389-411.

[17] GARODZ, L. J. (1971) Federal Aviation Administration Full-scale Aircraft Vortex Wake Turbulence Flight Test Investigations: Past, Present, Future., *AIAA paper 71-97*, AIAA 9th Aerospace Science Meeting

[18] GOVINDARAJU, S. P. (1970) A Study of Some Turbulent Flows using a Model for Inhomogeneous Turbulence., (PhD Dissertation, California Institute of Technology).

[19] GOVINGARAJU, S. P. AND SAFFMAN, P. G. (1971) Flow in a Trubulent Trailing Vortex., *The Physics of Fluids* , **14** , pp.2074-2080

[20] GRANGER(1986) Turbulent vortices. *Intr. to Vortex Dynamics. (Von Karman Institute Lecture Series).*

[21] HA, M. H. (1992) The Impact of Turbulence Modeling on the Numerical Predictions of Flows., *Lecture Notes on Physiscs (Vol. 414): Thirteen International Conference on Nemerical Methods in Fluid Mechanics* July 6-10, 1992 pp.27-46

[22] HALL, M. G. (1961) A Theory of the Core of a Leading-edge Vortex,. *J. Fluid Mech.*, **11** , pp.209-228

[23] HALL, M. G. (1965) A Numerical method for Solving the Equations for a Vortex Core., *Royal Aircraft Establishment Technical Report*, **65106**

[24] HANJALIC, K. AND LAUNDER, B. E. (1972) A Reynolds Stress Model of Turbulence and Its Application to Thin Shear Flow., *J. Fluid Mech.* , **52** , pp.609-638.

[25] HASEN, G. A.(1982) Navier-Stokes Solutions for an Axisymmetric Nozzle., *AIAA Journal* , **20** , pp.1219-1227.

[26] HECHT, A. M., BILANIN, A. J., HIRSCH, J. E., SNEDEKER, R. S. (1980) Turbulent vortices in stratified fluids. *AIAA J.*, **18** , No. 7.

[27] HECHT, A. M., BILANIN, A. J. AND HIRSCH, J. E. (1981) Turbulent trailing vortices in stratified fluids. *AIAA J.*, **19** , No. 6.

[28] HINZE, J. O. (1975) *Turbulence* , (2nd ed.), McGraw-Hill, Inc.

[29] HIRSCH, C. (1988) *Numerical Computation of Internal and External Flows*, John Wiley & Sons Ltd.

[30] HOFFMANN, E.R. AND JOUBERT, P. N. (1963) Turbulent Line Vortices., *J. Fluid Mech.* , **16** , pp.395-411.

[31] HOGG, S., LESCHZINER, M. A. (1989) Computation of Highly Swirling Confined Flow with a Reynolds Stress Turbulence Model., *AIAA J.* , **27** , No. 1, pp. 57-63.

[32] HUSSEIN, H. J., CAPP, S. T. AND GEORGE, W. K. (1994) Velocity Measurements in a High-Reynolds Number, Momentum Conserving, Axisymmetric Turbulent Jet., *J. Fluid Mech.* , **258** , pp.31-75.

[33] KIM, J., MOIN, P., AND MOSER, R. D. (1987) Turbulence statistics in fully-developed channel flow at low Reynolds number. *J. Fluid Mech.* **177** , pp. 133-166.

[34] LAMB, H. (1945) *Hydrodynamics.*, Dover. New York.

[35] LAUNDER, B. E., REECE, G. J. AND RODI, W. (1975) Progress in the Development of a Reynolds-stress Turbulene Closure., *J. Fluid Mech.* , **68** , pp.537-566.

[36] LAUNDER, B. E. AND TSELEPIDAKIS, D. P. (1991) Directions in Second-Moment Modelling of near-Wall Turbulence., *29th Aerospace Science Meeting*, January 1991, Reno, Nevada.

[37] LESIEUR, M. (1990) *Turbulence in Fluids*, (2nd rev. ed.), Kluwer Academic Publishers.

[38] LUMLEY, J. L. (1978) Computational Modeling of Turbulenct Flows., *Advances in Applied Mechnics*, **18** ,(ed. Yih, C. S.), Academic Press, NY, pp.123-176

[39] LUMLEY, J. L. AND KHAJE-NOURI, B. (1974) Computational Modeling of Turbulenct Transport., *Advances in Geographics*, **18** , (ed. Landsberg, H. E. and Van Miegham, J.), Academic Press, NY, pp.186-192

[40] LIU, C. H., KRAUSE, E. AND MENNE, S. (1986) Admissible Upstream Conditions for Slender Compressible Vortices., *AIAA/ASME 4th Fluid Mechanics, Plasma Dynamics and Laser Conference*, May 1986, Atlanta, GA.

[41] MAYER, E. W. AND POWELL, K. G. (1992) Similarity Solutions for Viscous Vortex Cores., *J. Fluid Mech.*, **238** , pp.487-507.

[42] NEWMAN, B. G. (1959) Flow in a Viscous Trailing Vortex., *Aeronautical Quaterly* **10** , May , pp 149-162.

[43] OLWI, I. AND GHAZI, M. (1992) Effect of Wing Tip Vortices on a Trailing Aircraft., *AIAA J.*, **30**, No. 9, pp.2186-2187

[44] OWEN, P. R. (1970) The Decay of Turbulent Trailing Vortices., *The Aeronautical Quarterly*, Feb. 1970, pp.69-78

[45] ORSZAG, S. A., AND PATTERSON, G. S. (1972) Numerical simulation of three-dimensional homogeneous isotropic turbulence, *Phys. Rev. Lett.* , **28** , pp. 76-79.

[46] NIELSEN, J. N., SCHWIND, R. G. (1971) Decay of a vortex pair behind an aircraft., *Aircraft Wake Turbulence and Its Detection.* Plenum Press, New York.

[47] PANTON, R. L. (1984) *Incompressible Flow* John Wiley & Sons Ltd.

[48] PANCHAPAKESAN, N. R. AND LUMLEY, J. L. (1993) Turbulent Measurements in Axisymmetric Jets of Air and Helium. Part 1. Air jet., *J. Fluid Mech.* , **246** , pp.197-223.

[49] PANCHAPAKESAN, N. R. AND LUMLEY, J. L. (1993) Turbulent Measurements in Axisymmetric Jets of Air and Helium. Part 2. Helium jet., *J. Fluid Mech.* , **246** , pp.225-247.

[50] PHILLIPS, W. R. C., GRAHAM, J. A. H. (1984) Reynolds-stress measurements in a turbulent trailing vortex. *J. Fluid Mech.* **147** , pp 353-371

[51] RAGAB, S. A. (1993) (unpublished notes)

[52] REYNOLDS, W. C. (1990) The potential and limitations of direct and large eddy simulations, *Whither Turbulence*, (Ed. Lumley, J. L.), Springer-Verlag, NY.

[53] ROGERS, M. M., AND MOIN, P. (1987) The structure of the vorticity field in homogeneous turbulent flow, *J. Fluid Mech* ., **176** , pp. 33-66.

[54] SAFFMAN, P. G. (1973) Structure of turbulent line vortices. *Phys. Fluids A* , **16**, No. 8.,pp 1181-1188.

[55] SCHLICHTING, H. (1979) *Boundary-Layer Theory*, (2nd ed.), McGraw-Hill, Inc.

[56] SINGH, P. I. (1974) Doctoral Dissertation, University of Colorado, Boulder.

[57] SPALART, P. R. (1988) Direct numerical simulation of a turbulent boundary layer up to Re=1410, *J. Fluid Mech.* , **187** , pp. 61-98.

[58] SPEZIALE, C. G. (1989) Discussion of Turbulence Modeling: Past and Future., *ICASE Report No.89-58*, NASA Langley Research Center.

[59] SQUIRES, H. B. (1965), The Growth of a Vortex in Turbulent Flow, *Aeronautical Quaterly* , August 1985., pp. 302-306.

[60] TAUBEE D. B. (1989) Engineering Turbulence Models., *Advances in Turbulence*, (ed. George, W. K. and Arndt, R.), Hemisphere Publishing Corp., pp.75-125.

[61] UBEROI, M. S. (1979) Mechanisms of deacy of laminar and turbulent vortices. *J. Fluid Mech* ., **90** , pp. 241-255.

[62] WYGNANSKI, I. AND FIEDLER, H. (1969) Some measurements in the self-preserving jet., *J. Fluid Mech*, **38** , pp.577-612.

[63] ZHENG, Z. AND ASH, R. L. (1993) Prediction of Turbulent Wake Vortex Motion near the Ground., *ASME*, FED-Vol.**151** , pp.195-207.

[64] ZSOLDOS, J. S. AND DEVENPORT, W. J.(1992) An experimental investigation of interacting trailing vortex pairs. *Proceed. of the 19th Symp. on Naval Hydrodynamics*. Seoul, South Korea, August.

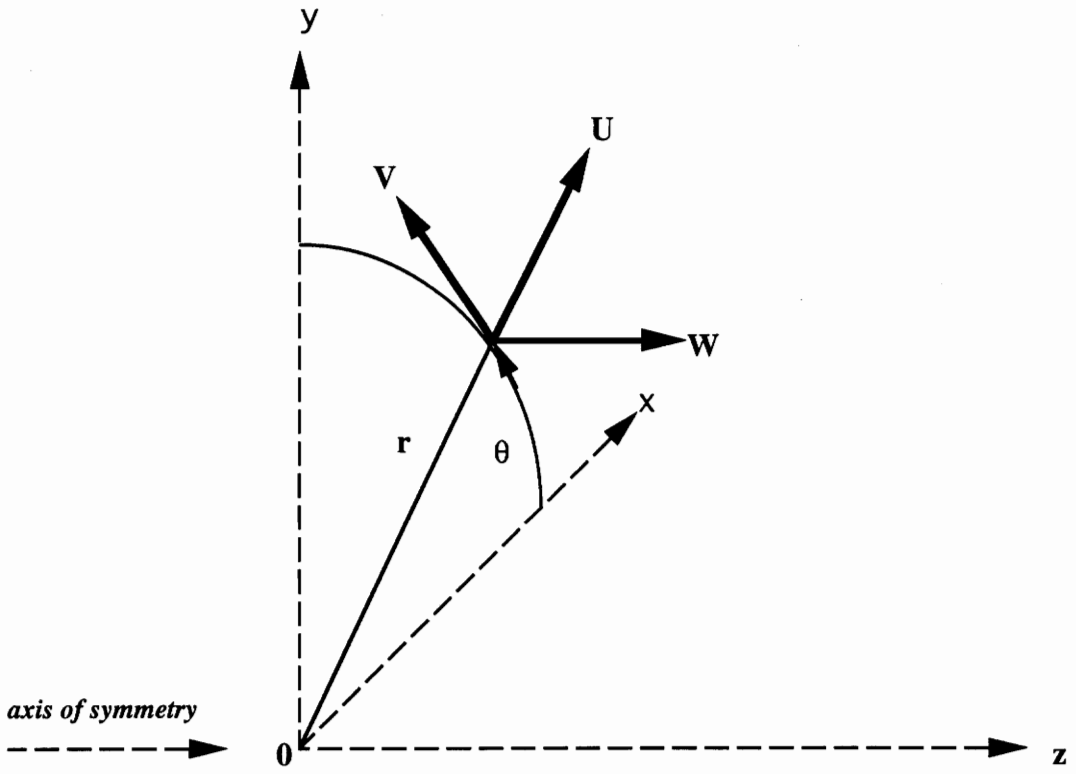

Figure 2.1: The cylindrical coordinate system (r, θ, z)

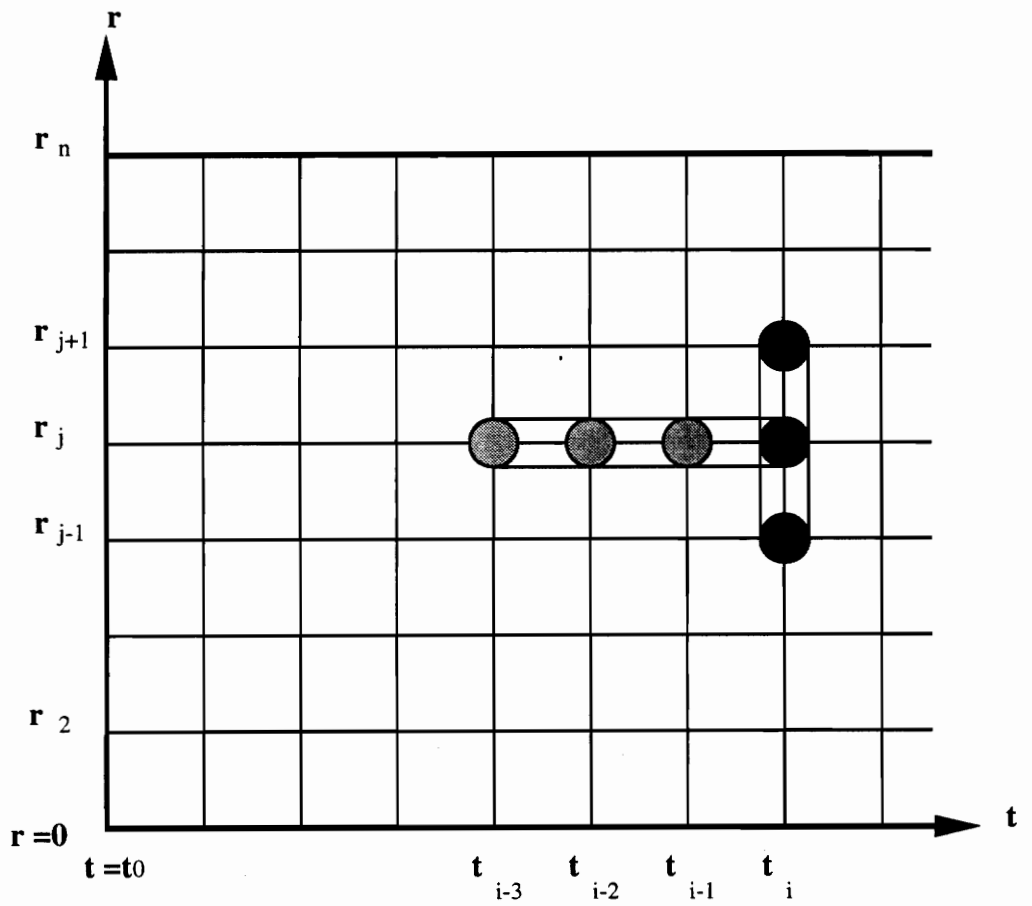

Figure 3.1: The computational grid for 4-point backward differencing in axial direction and 3-point central differencing in Radial Direction

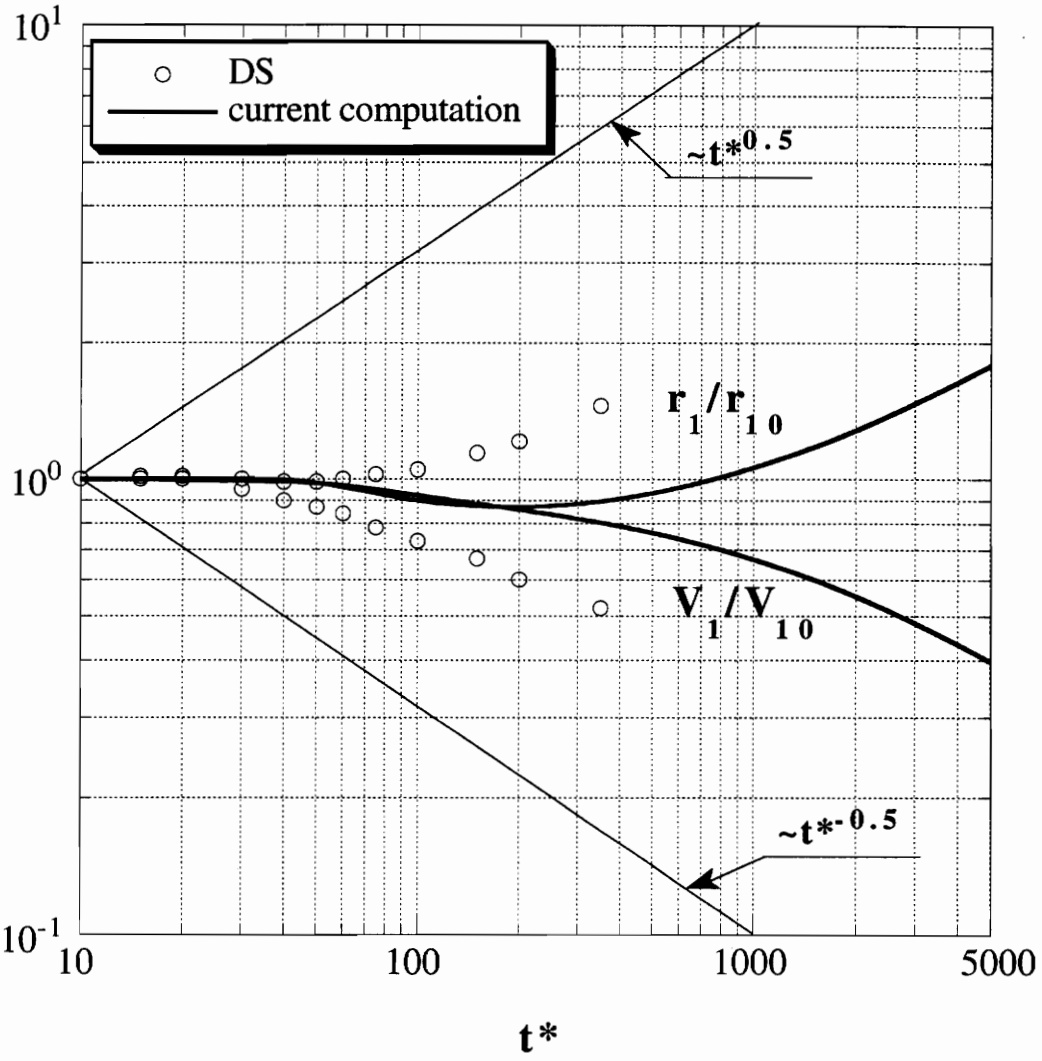

Figure 3.2: Behavior of the core radius and core velocity from the current computation and comparison with Donaldson's results ($Re = 10^4$, $t^* = (\frac{V_{10}}{r_{10}})t$) [DS: Donaldson[8] and Donaldson & Sullivan[11]]

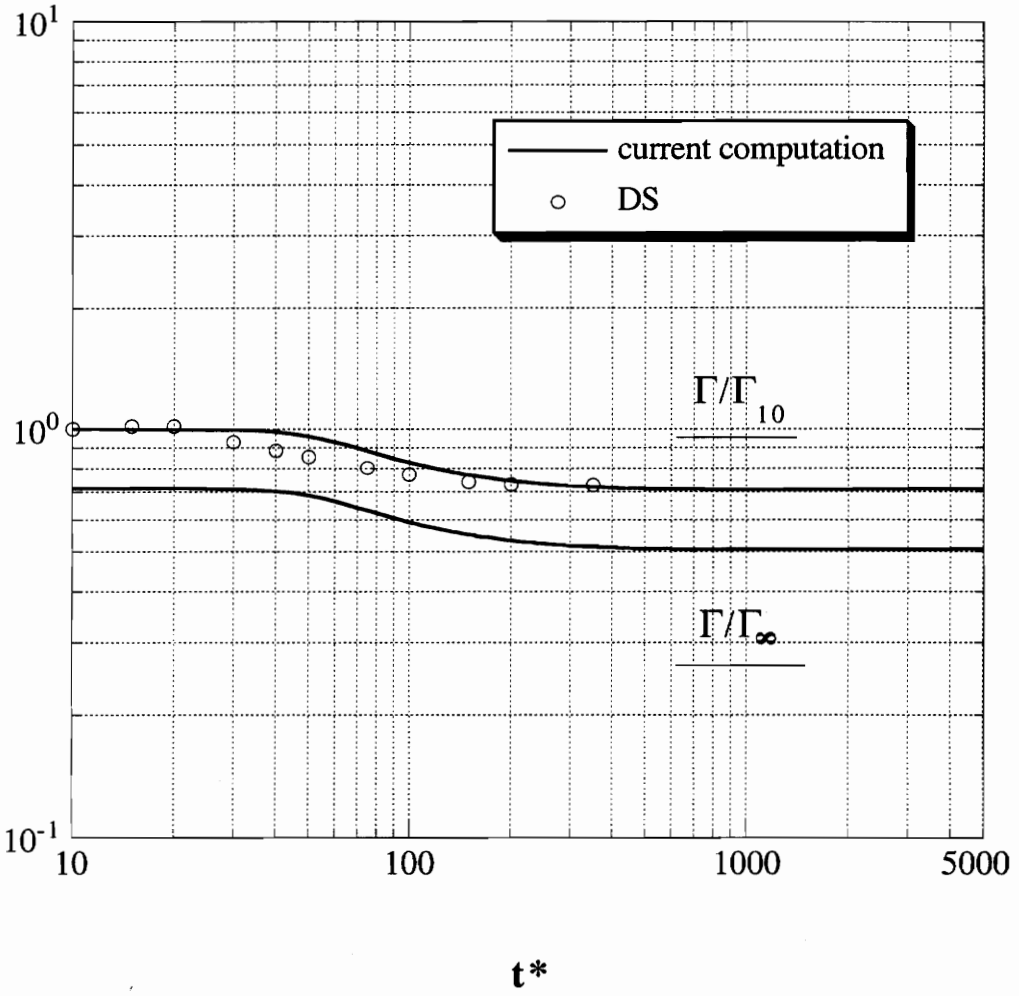

Figure 3.3: Behavior of the circulation at the core radius, in comparison with Donaldson's results ($Re = 10^4$, $t^* = (\frac{V_{10}}{r_{10}})t$) [DS: Donaldson[8] and Donaldson & Sullivan[11]]

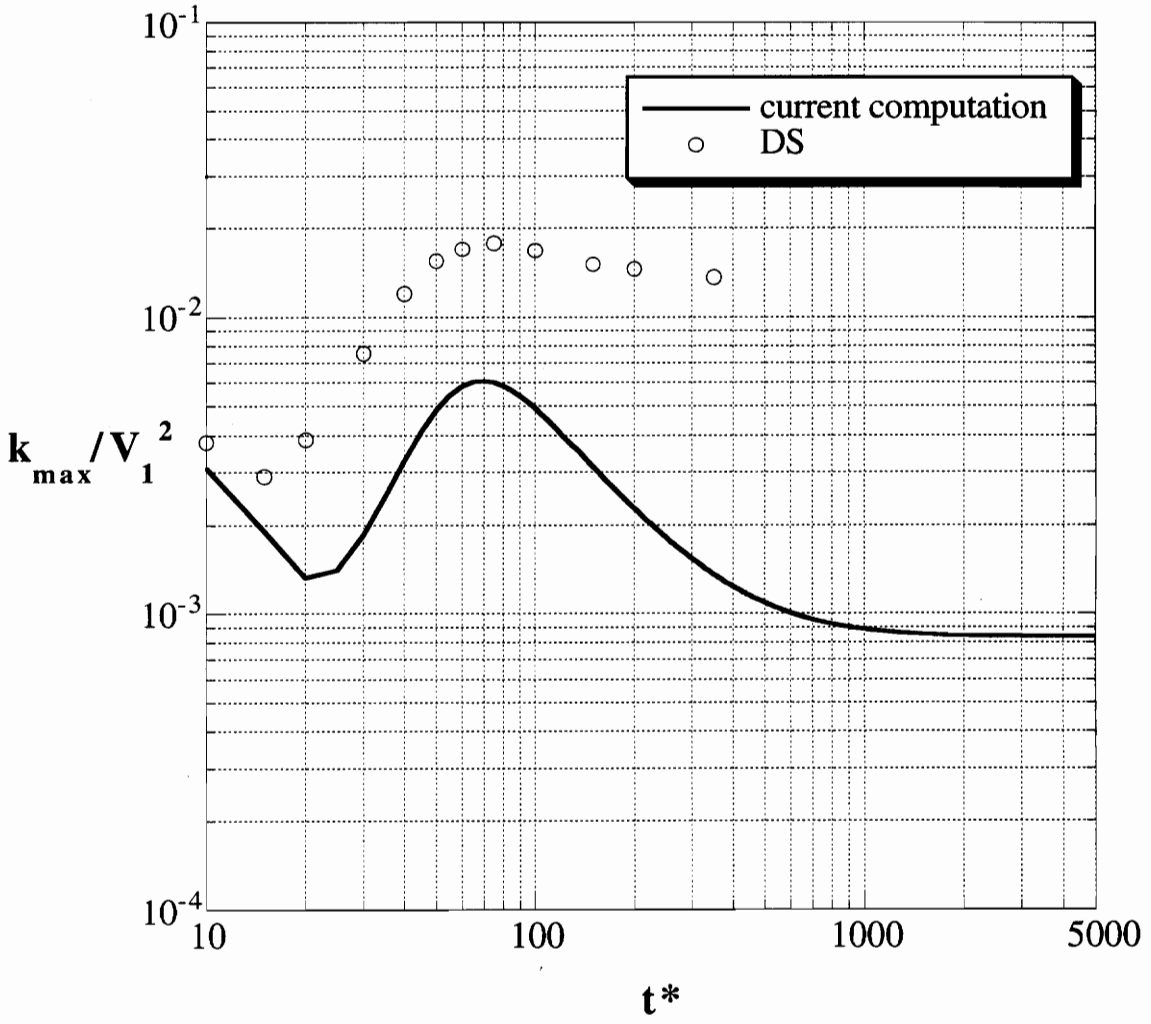

Figure 3.4: Behavior of the maximum turbulent kinetic energy, in comparison with Donaldson's results ($Re = 10^4$, $t^* = (\frac{V_{10}}{r_{10}})t$, $k_{max} = (\overline{u_i' u_i'})_{max}$) [DS: Donaldson[8] and Donaldson & Sullivan[11]]

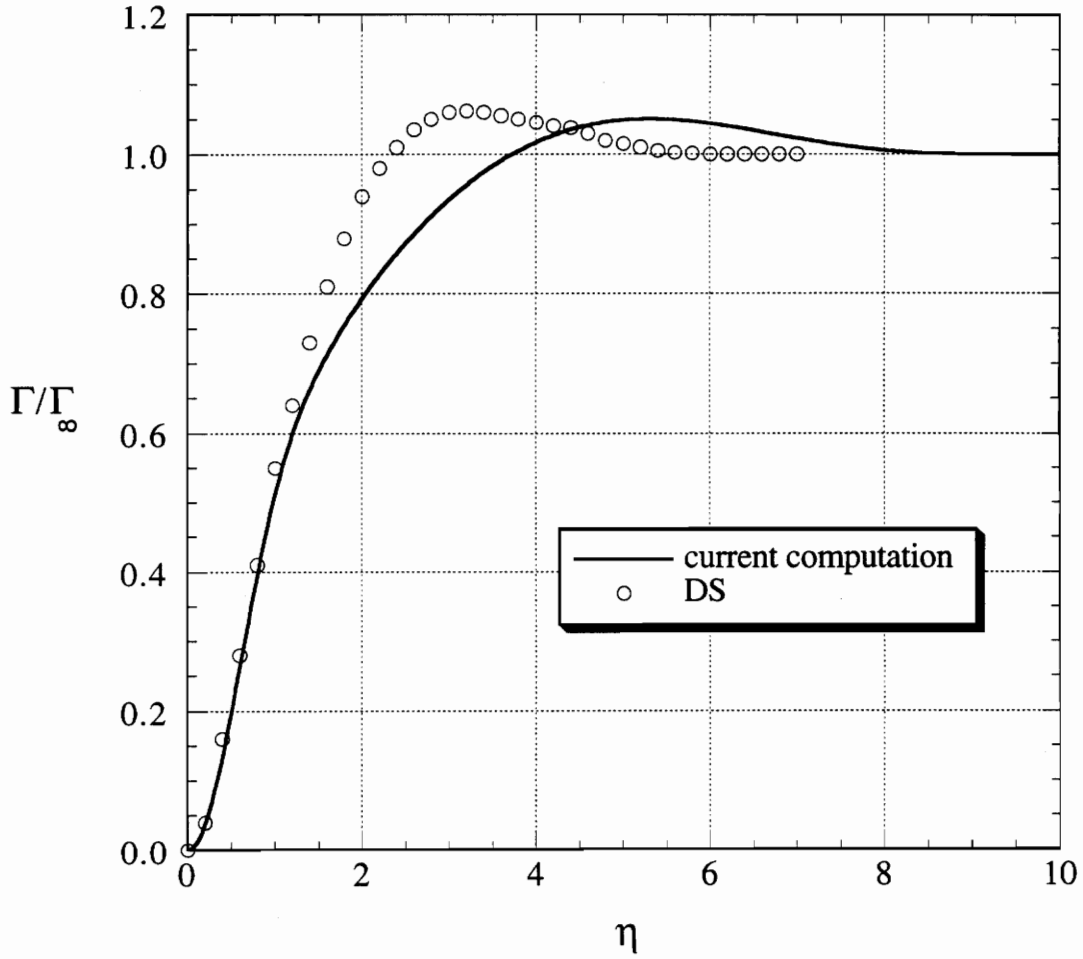

Figure 3.5: Radial distribution of the circulation for the self-similar solution, in comparison with Donaldson's results ($Re = 10^4$) [DS: Donaldson[8] and Donaldson & Sullivan[11]]

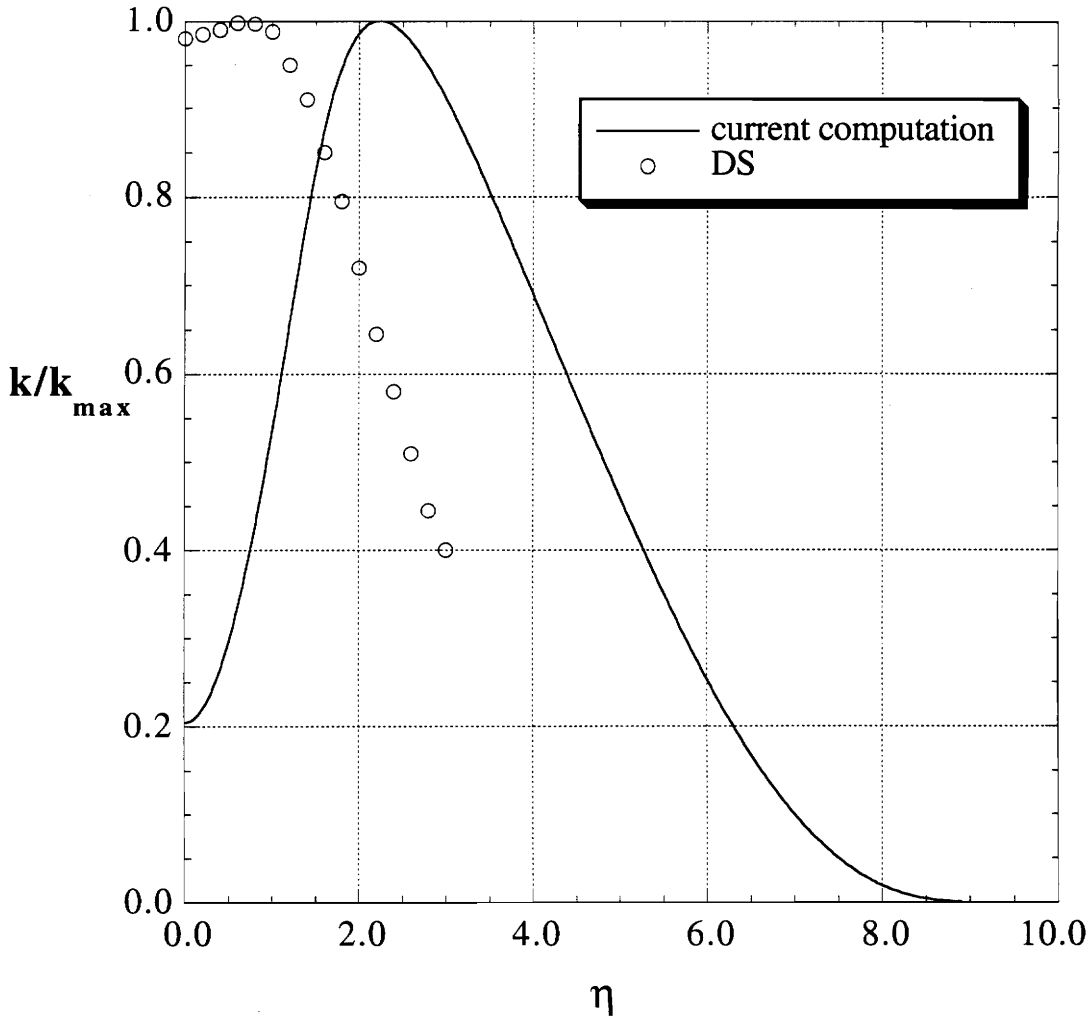

Figure 3.6: Radial distribution of the normalized turbulent kinetic energy for the self-similar solution, in comparison with Donaldson's results ($Re = 10^4$) [DS: Donaldson[8] and Donaldson & Sullivan[11]]

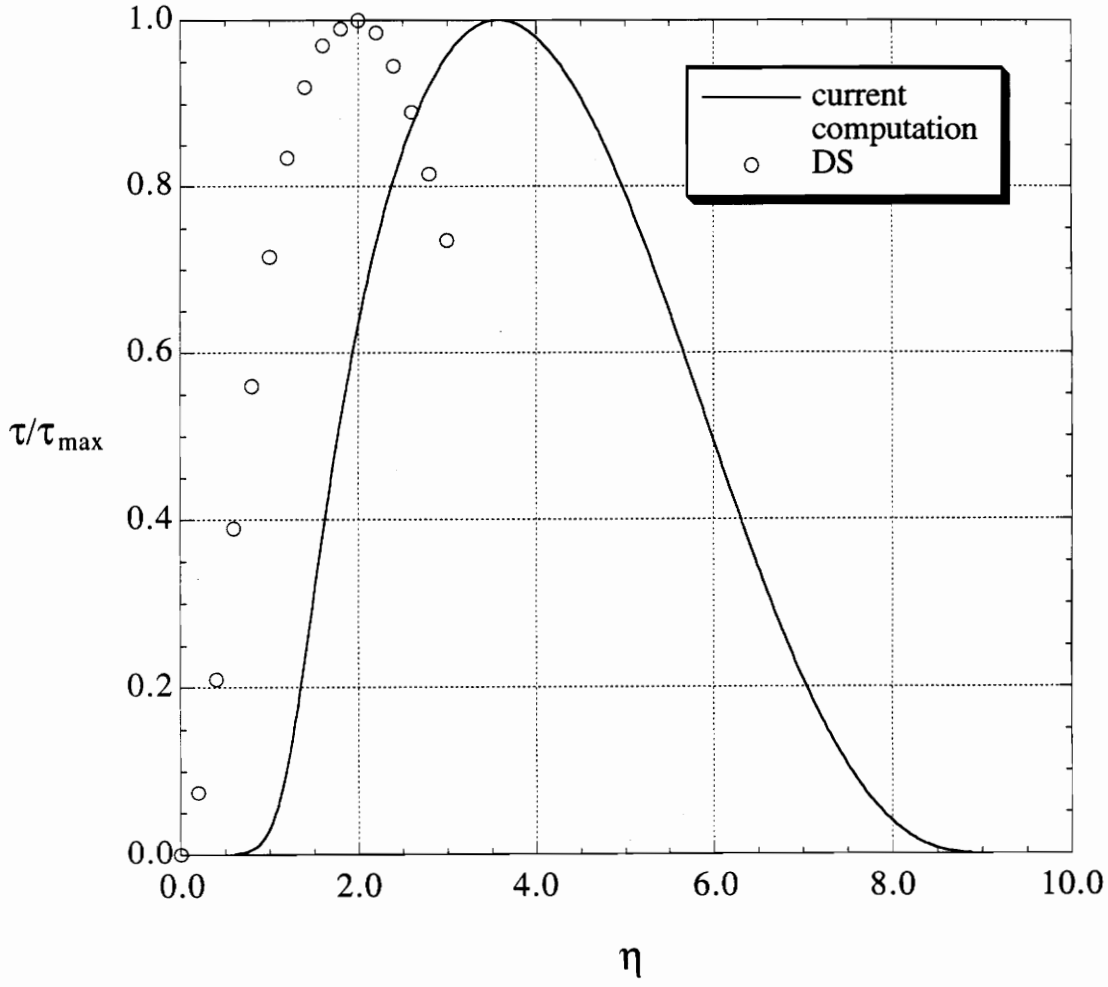

Figure 3.7: Radial distribution of the normalized turbulent shear stress for the self-similar solution, in comparison with Donaldson's results ($Re = 10^4$) [DS: Donaldson[8] and Donaldson & Sullivan[11]]

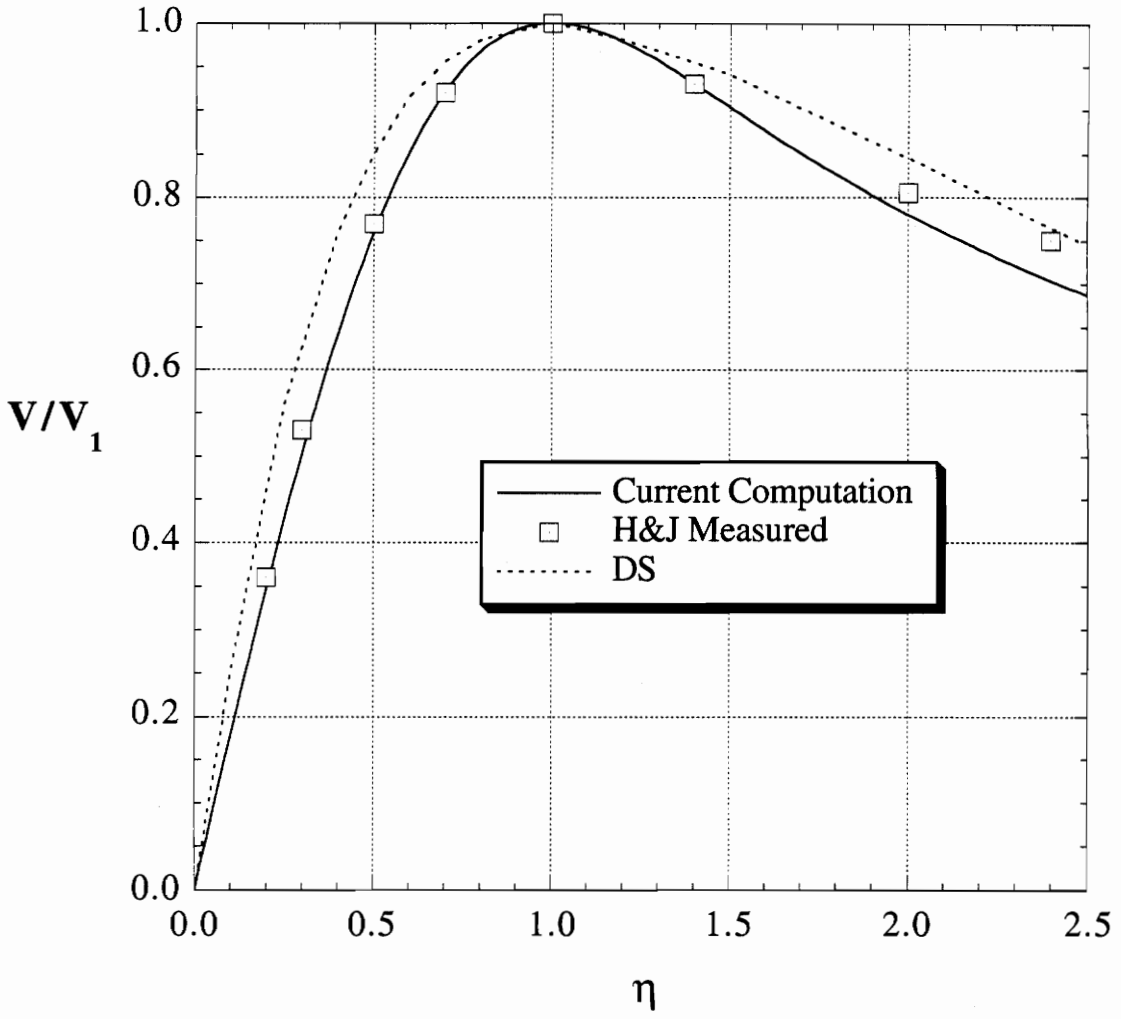

Figure 3.8: Comparison of computations with the measurements for the mean flow velocity in the inner region [DS: Donaldson[8] and Donaldson & Sullivan[11]; H&J measured: Hoffmann and Joubert[23]]

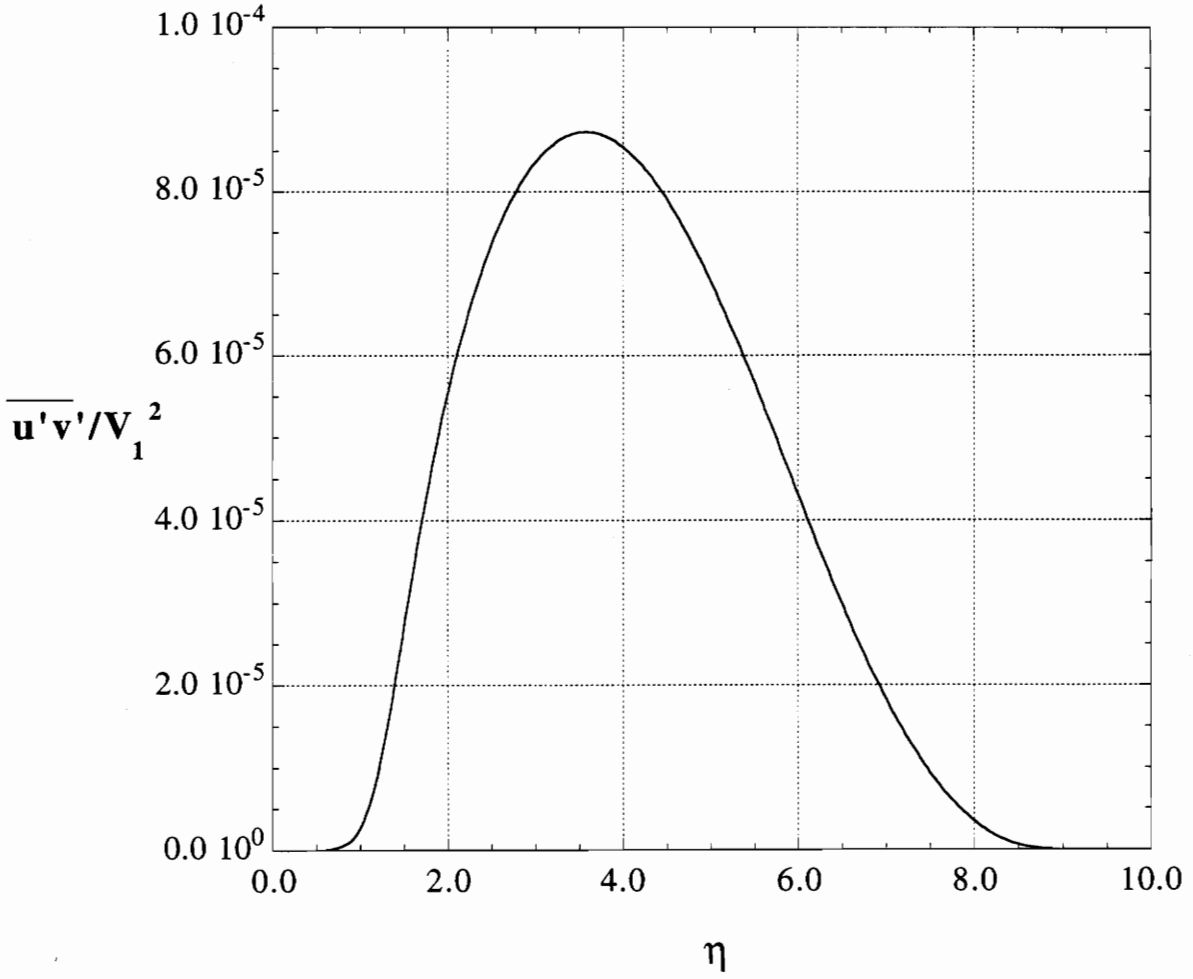

Figure 3.9: Radial distribution of the turbulent shear stress for the self-similar solution ($Re = 10^4$)

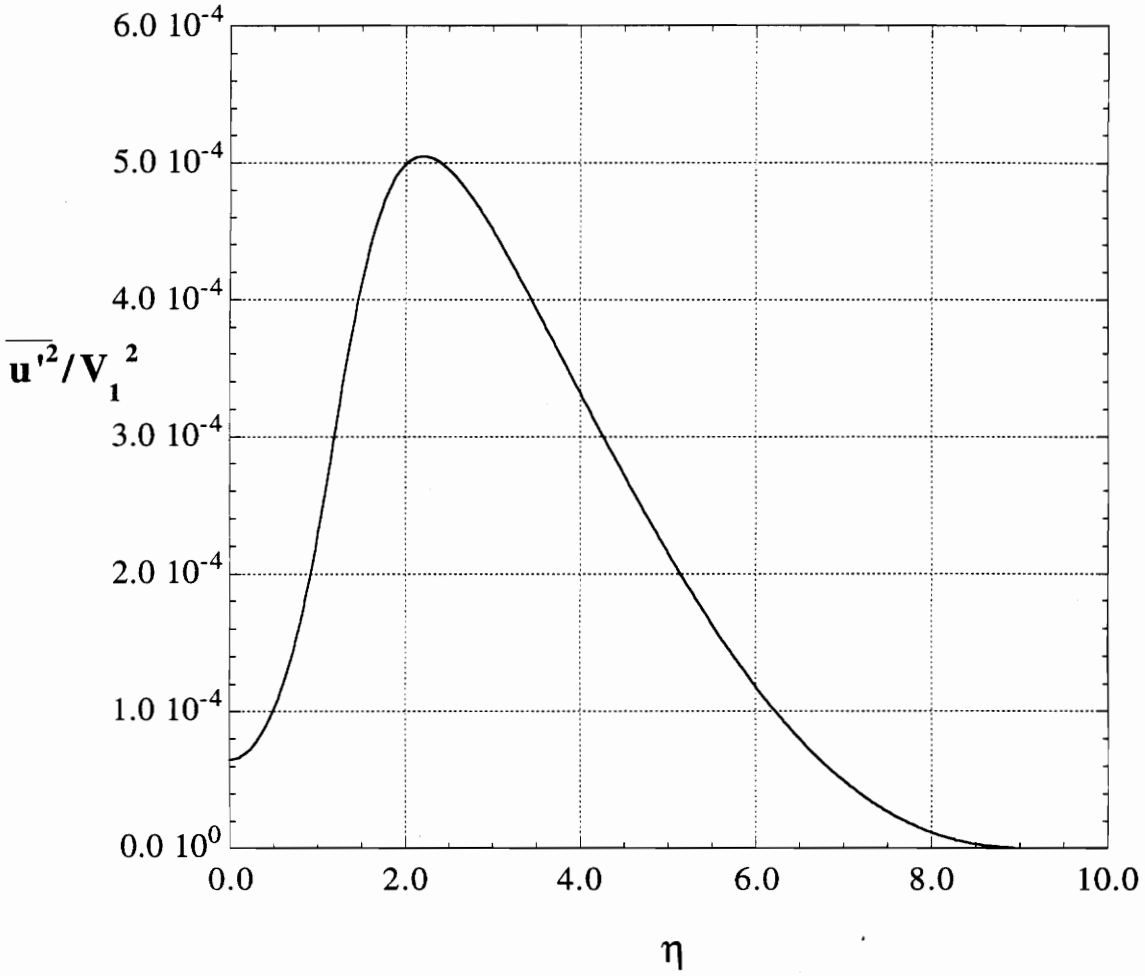

Figure 3.10: Radial distribution of the turbulent radial normal stress component for the self-similar solution ($Re = 10^4$)

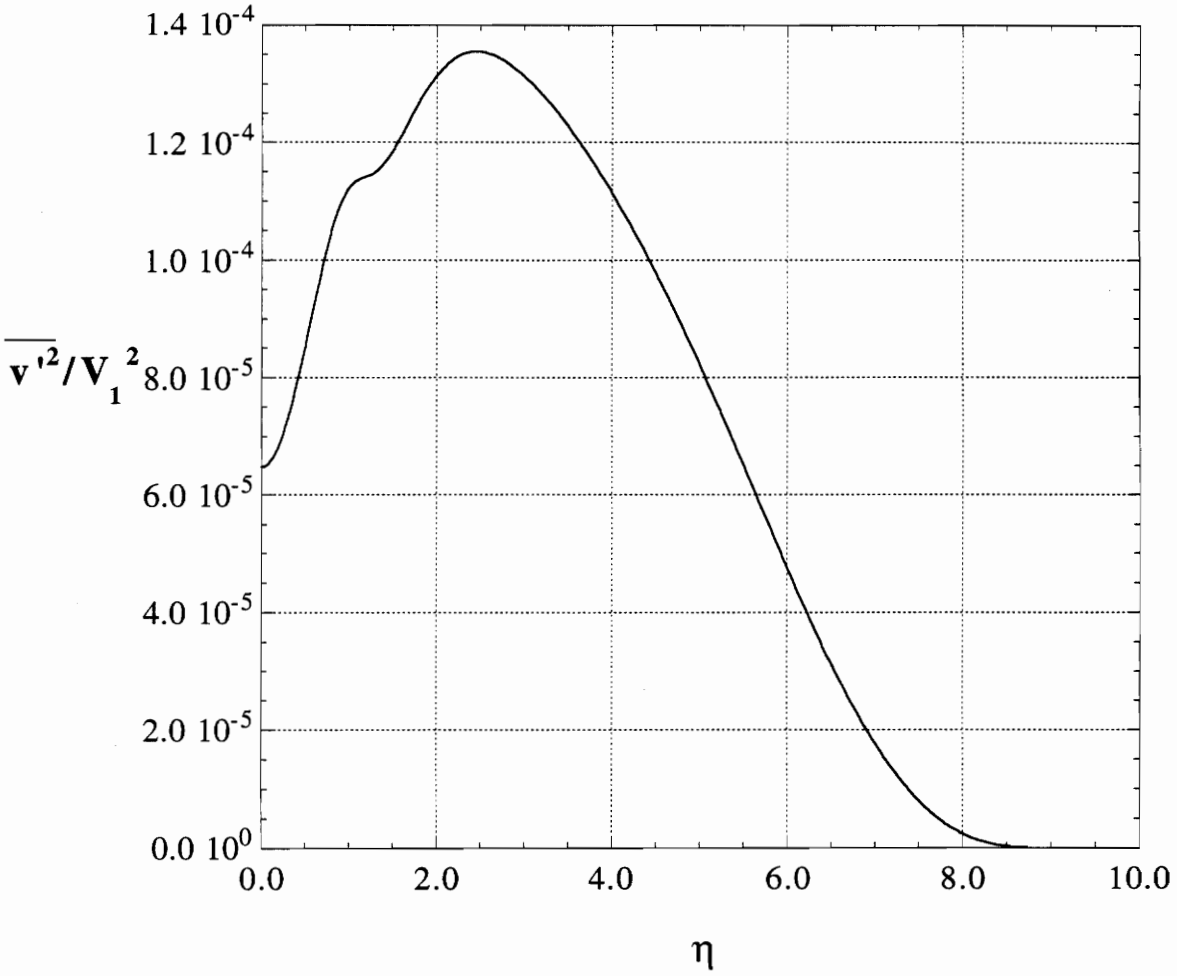

Figure 3.11: Radial distribution of the turbulent circumferential normal stress component for the self-similar solution ($Re = 10^4$)

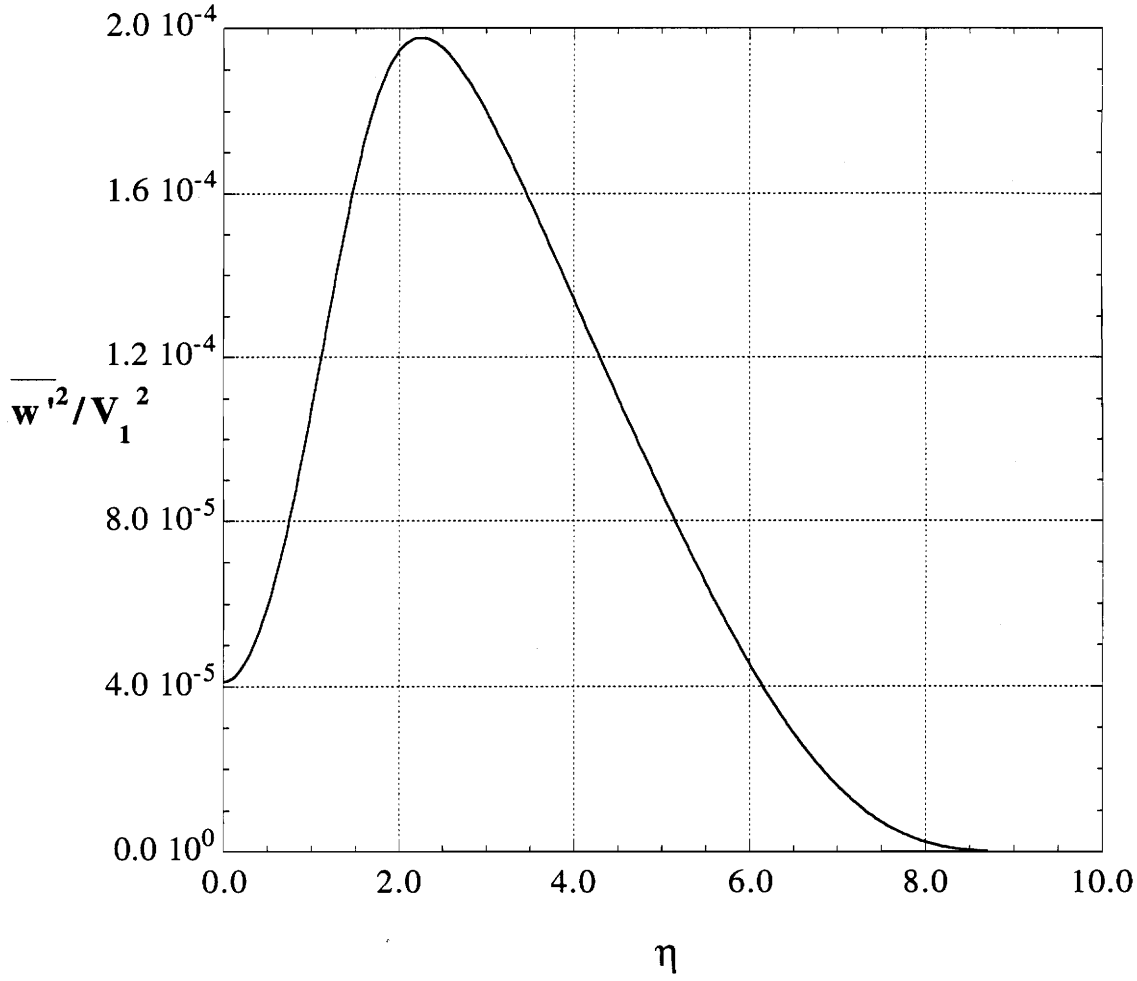

Figure 3.12: Radial distribution of the turbulent axial normal stress component for the self-similar solution ($Re = 10^4$)

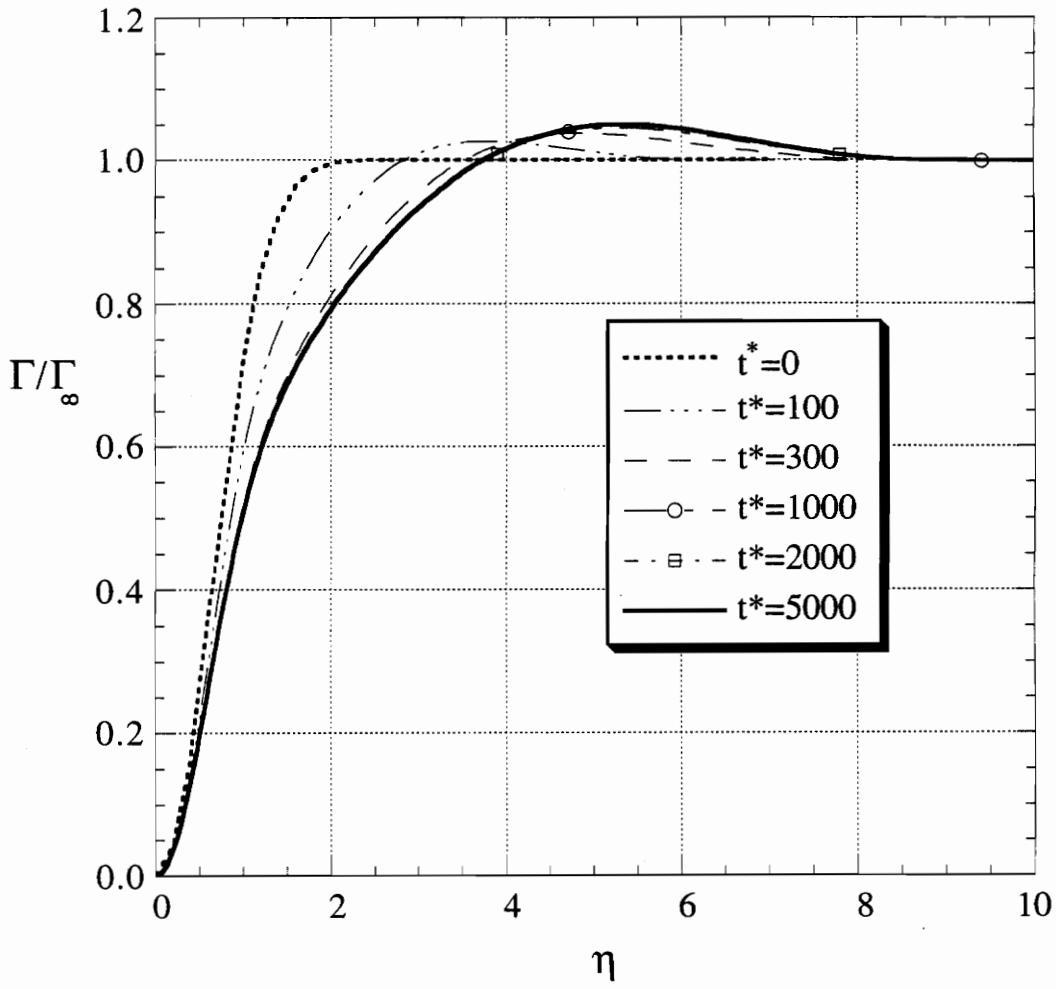

Figure 3.13: Radial profiles of the circulation at different times in comparison with the laminar case ($Re = 10^4$, $t^* = (\frac{V_{10}}{r_{10}})t$)

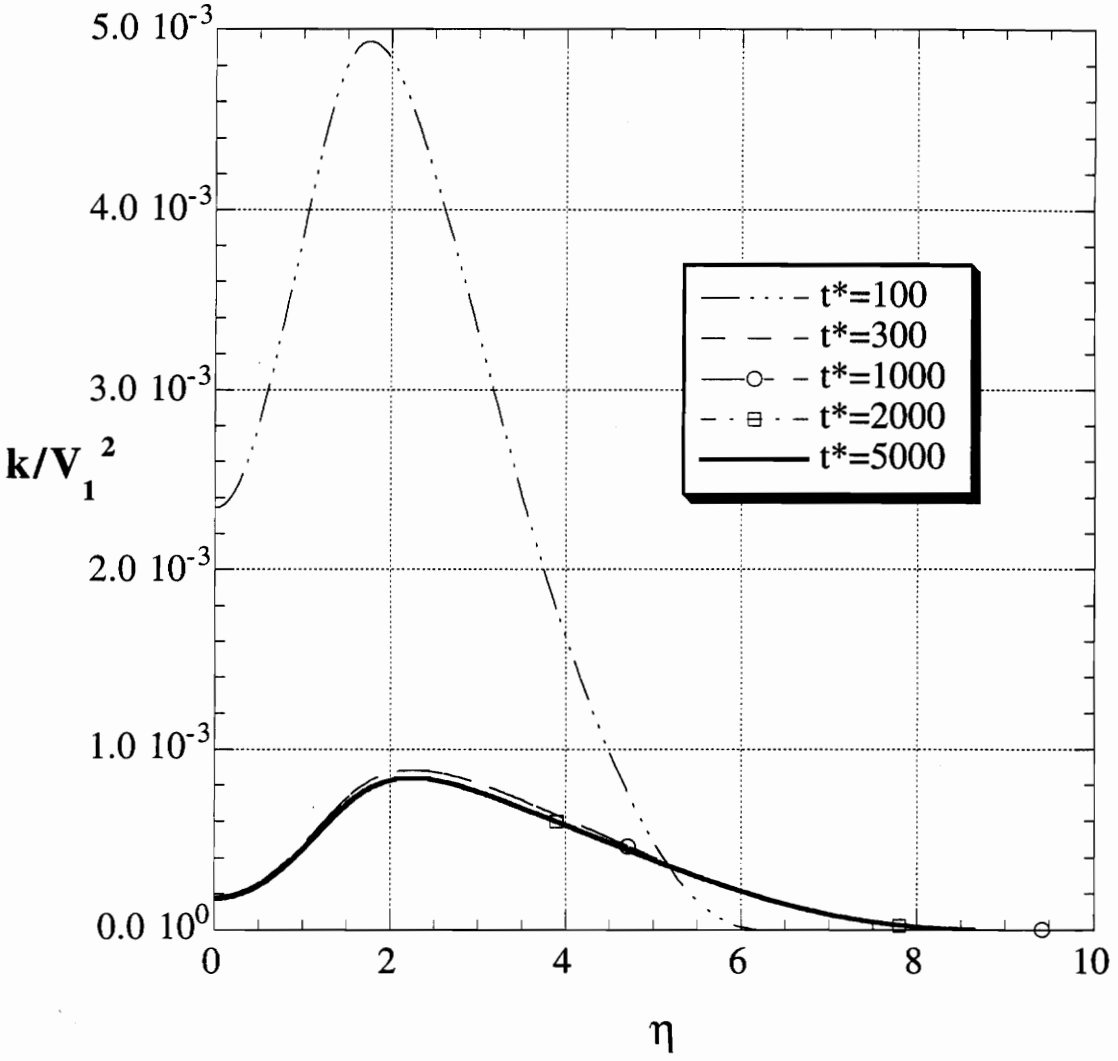

Figure 3.14: Radial profiles of the turbulent kinetic energy at different times ($Re = 10^4$, $t^* = (\frac{V_{10}}{r_{10}})t$)

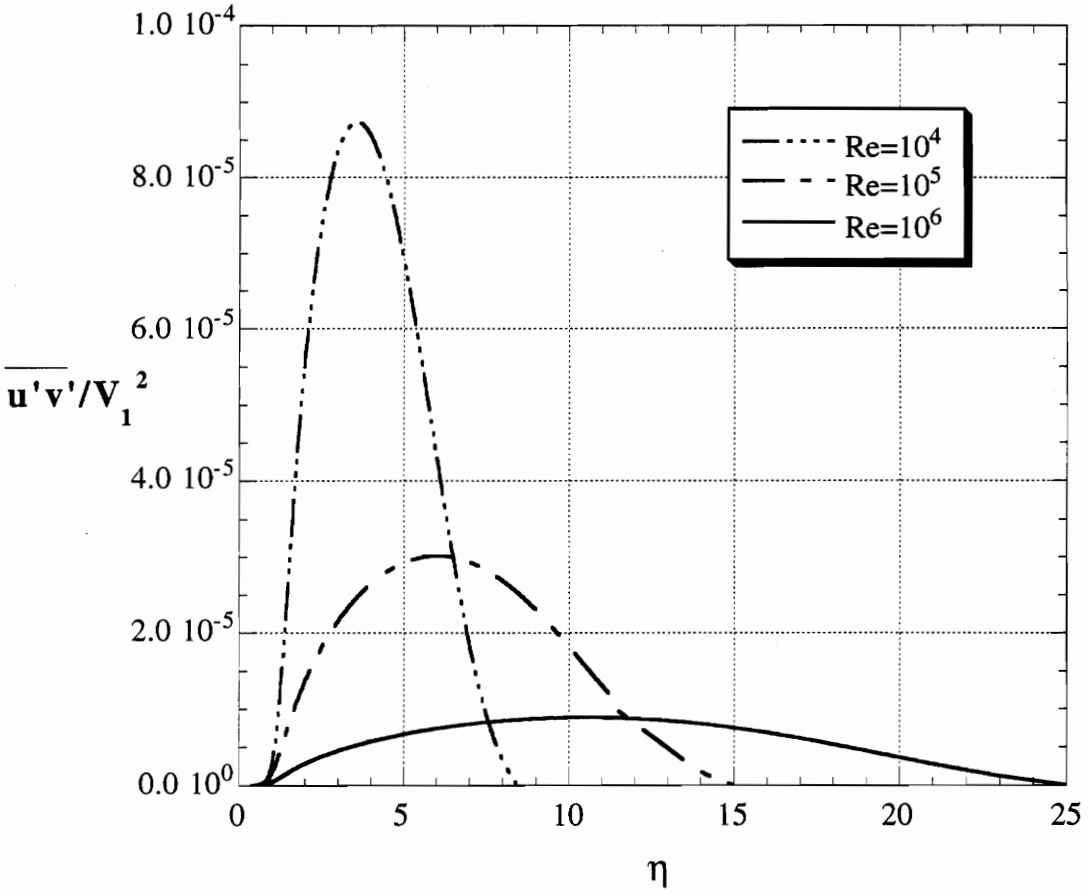

Figure 3.15: Sensitivity of k_{max}/V_1^2 to the initial magnitude of the turbulent fluctuations

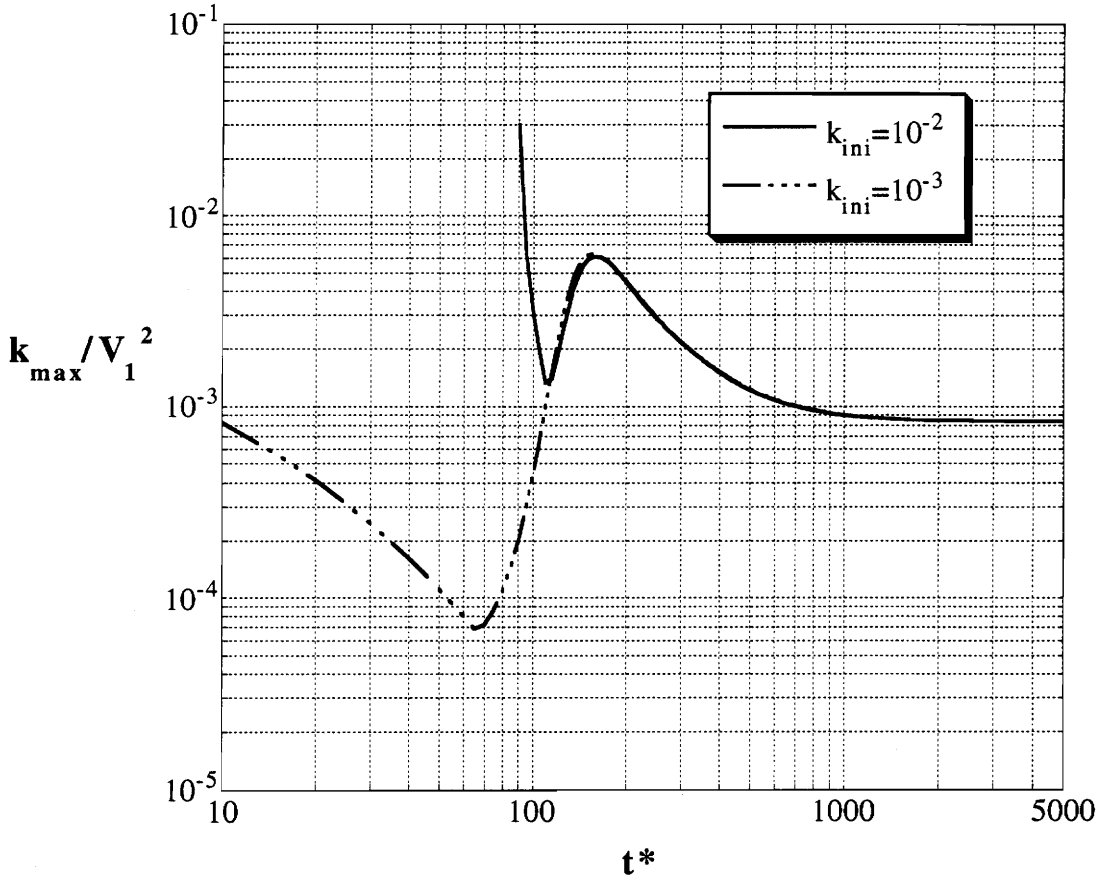

Figure 3.16: Effect of the initial magnitude of fluctuation on the behavior of maximum turbulent kinetic energy ($Re = 10^4$, $t^* = (\frac{V_{10}}{r_{10}})t$)

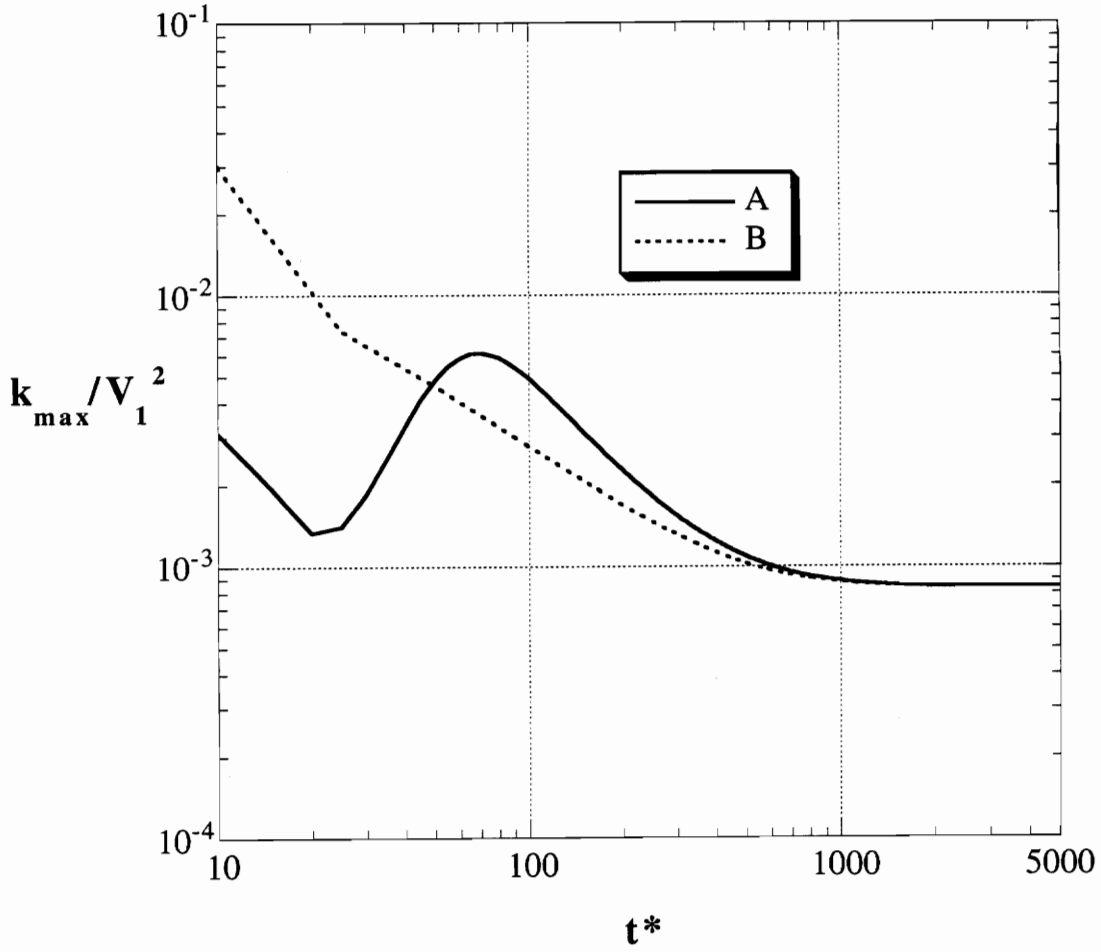

Figure 3.17: Effect of the initial distribution of fluctuation on the behavior of maximum turbulent kinetic energy ($Re = 10^4$, $t^* = (\frac{V_{10}}{r_{10}})t$) [A: initial distributions of turbulent intensities follow Eq(3.8) through (3.10)] [B: initial distributions of turbulent intensities follow Eq(3.26)]

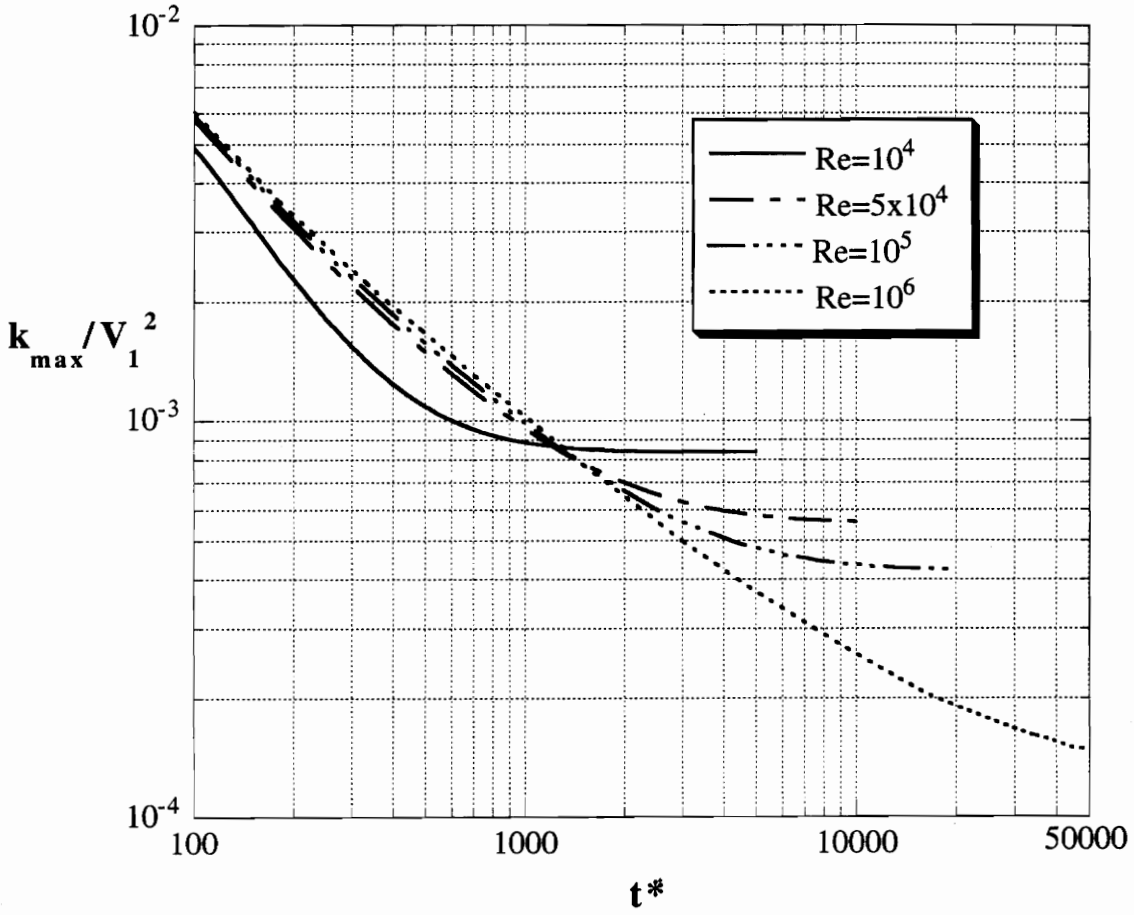

Figure 3.18: Dependence of maximum turbulent kinetic energy on Reynolds number

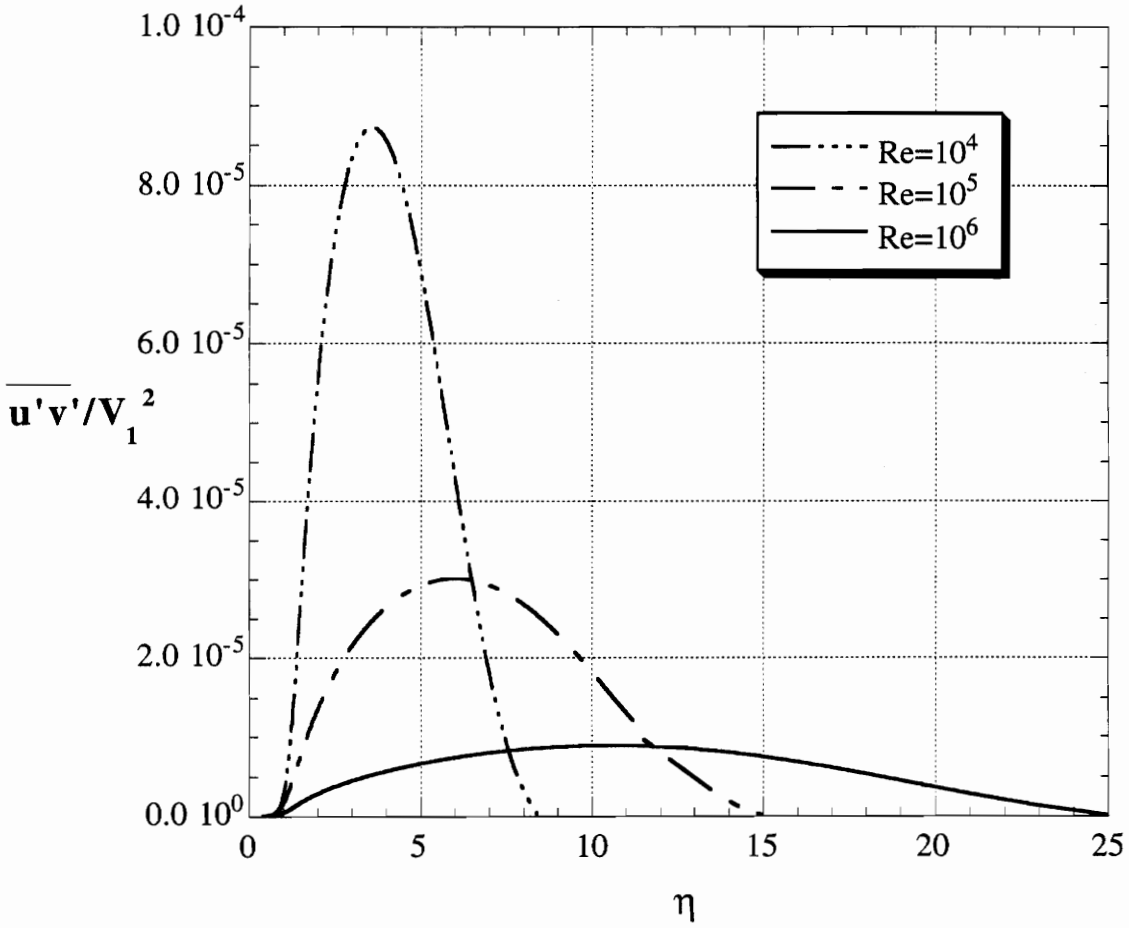

Figure 3.19: Effect of the Reynolds number on the radial profiles of the turbulent shear stress

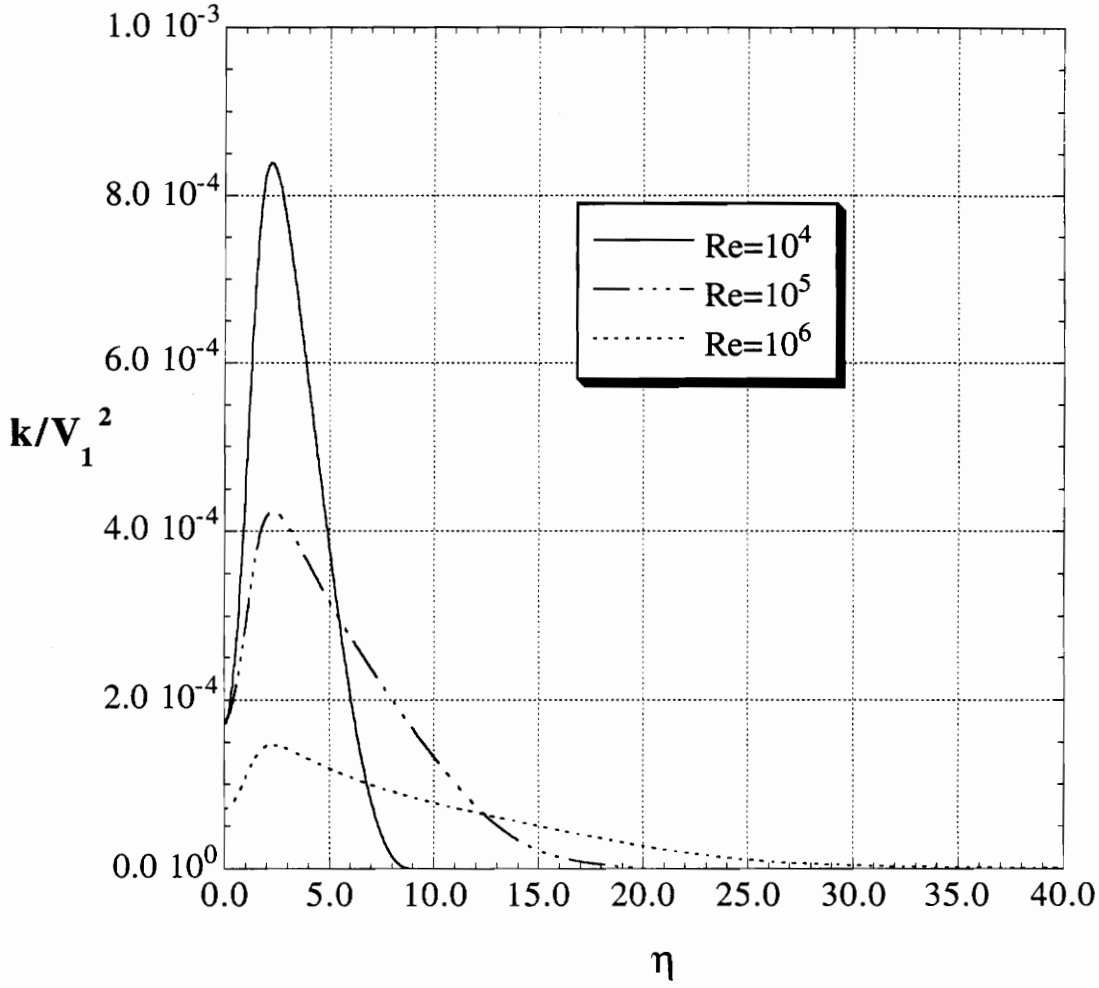

Figure 3.20: Effect of the Reynolds number on the radial profiles of the turbulent kinetic energy

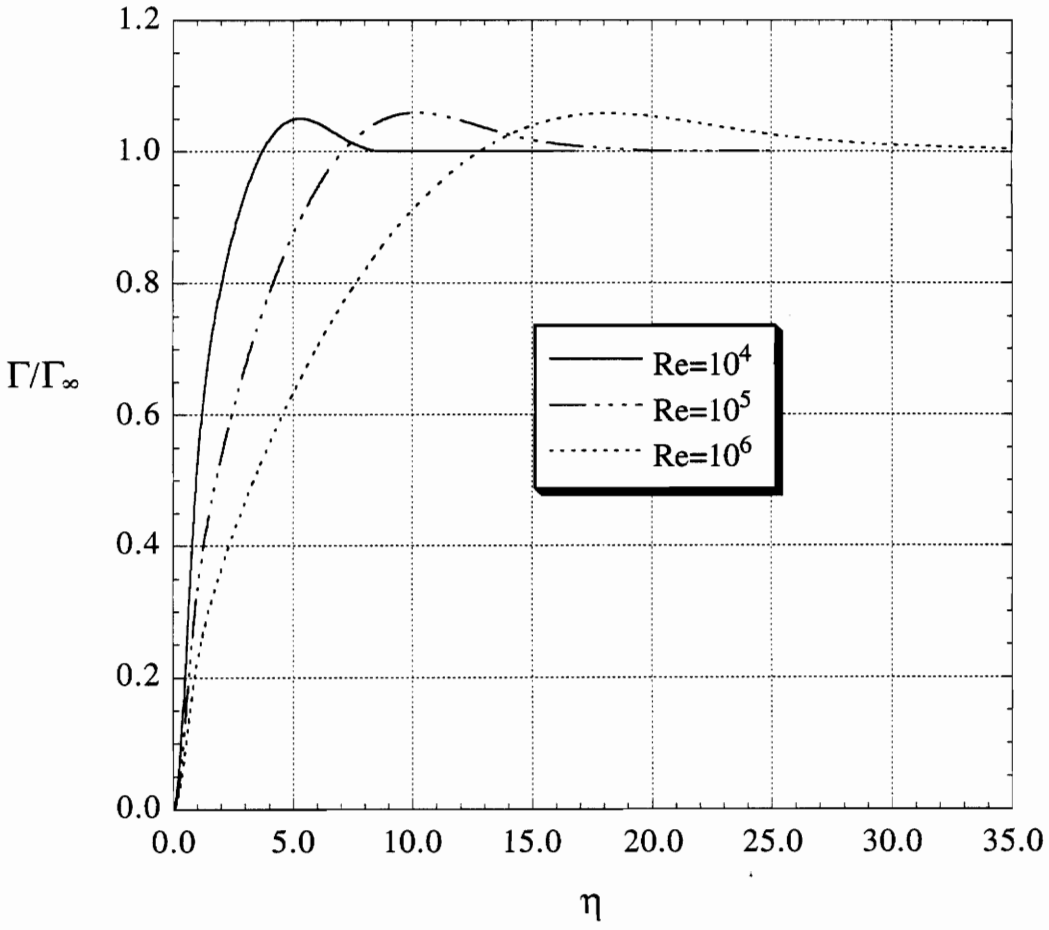

Figure 3.21: Effect of the Reynolds number on the circulation profiles

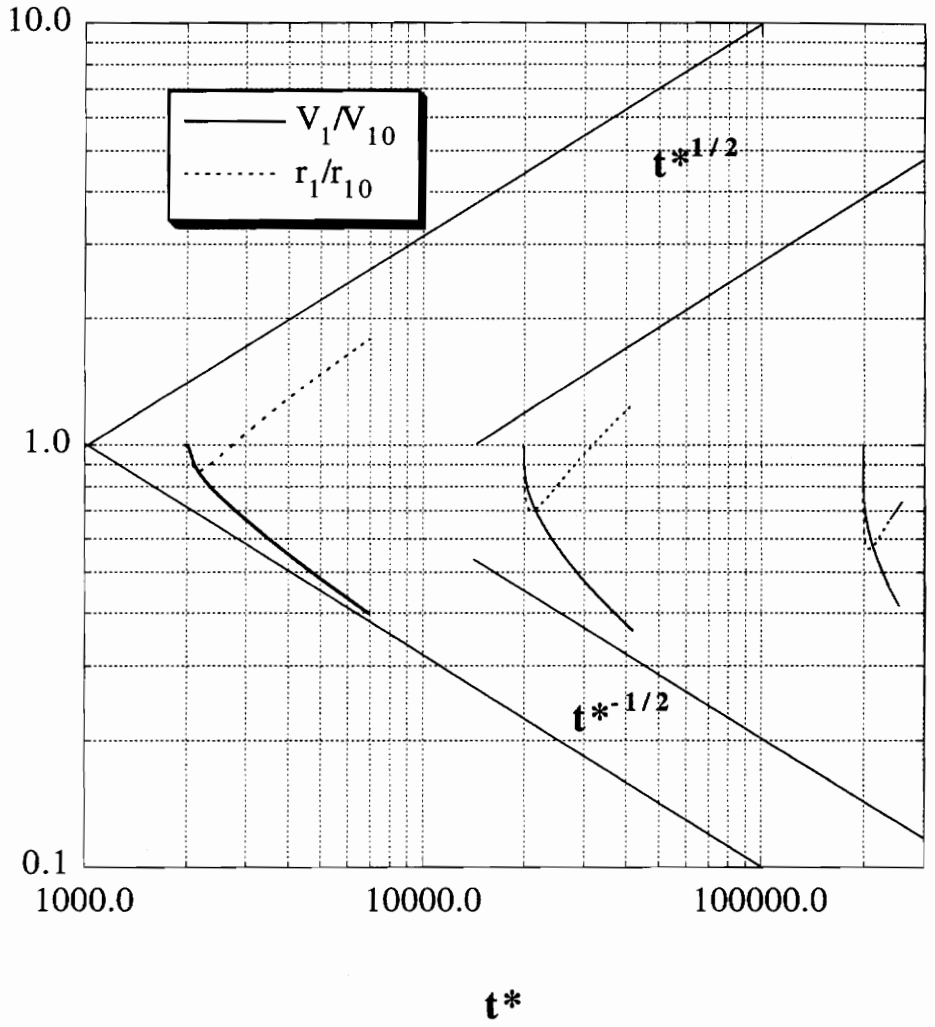

Figure 3.22: Behavior of the core radius and velocity for different Reynolds number after accounting for time origins

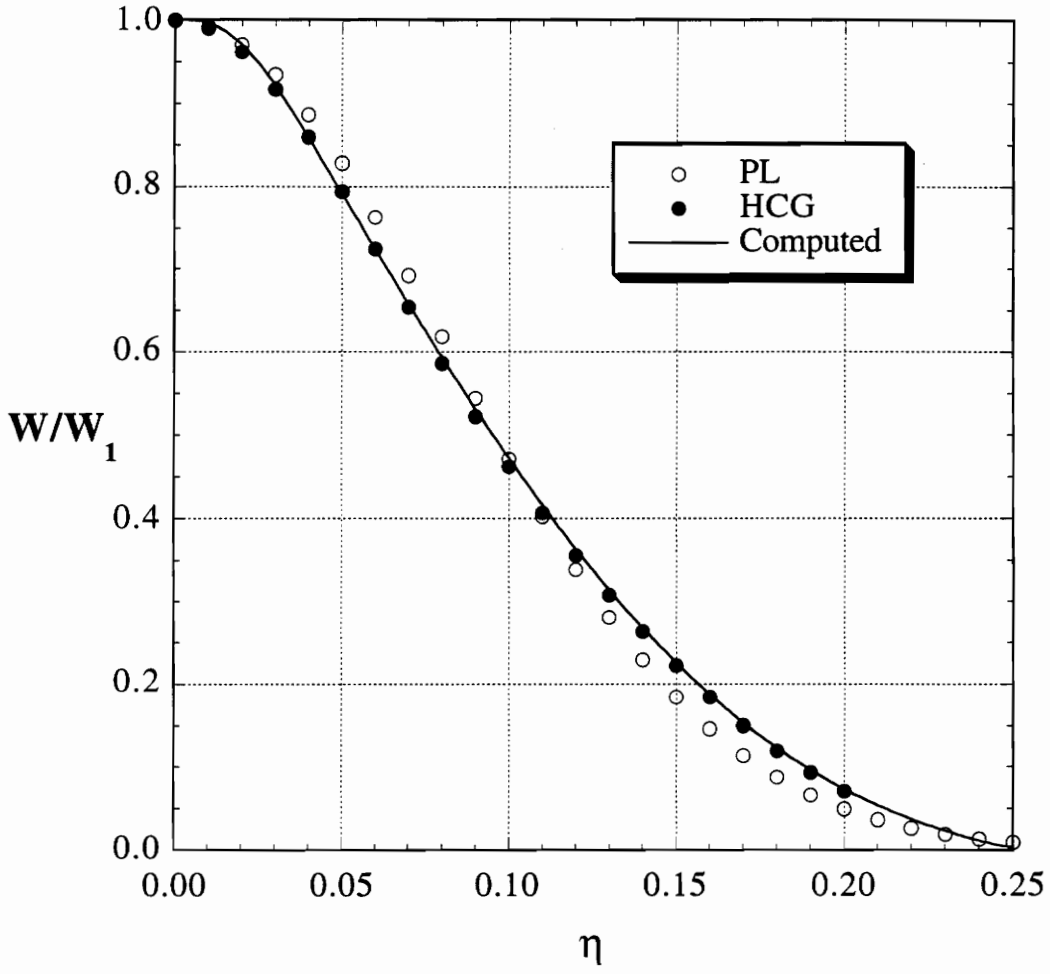

Figure 4.1: Comparison of self-similar solution of computed mean axial velocity with experimental results for an axisymmetric jet
[PL: Panchapakesan and Lumley[48]] [HCG: Hussein et al.[32]]

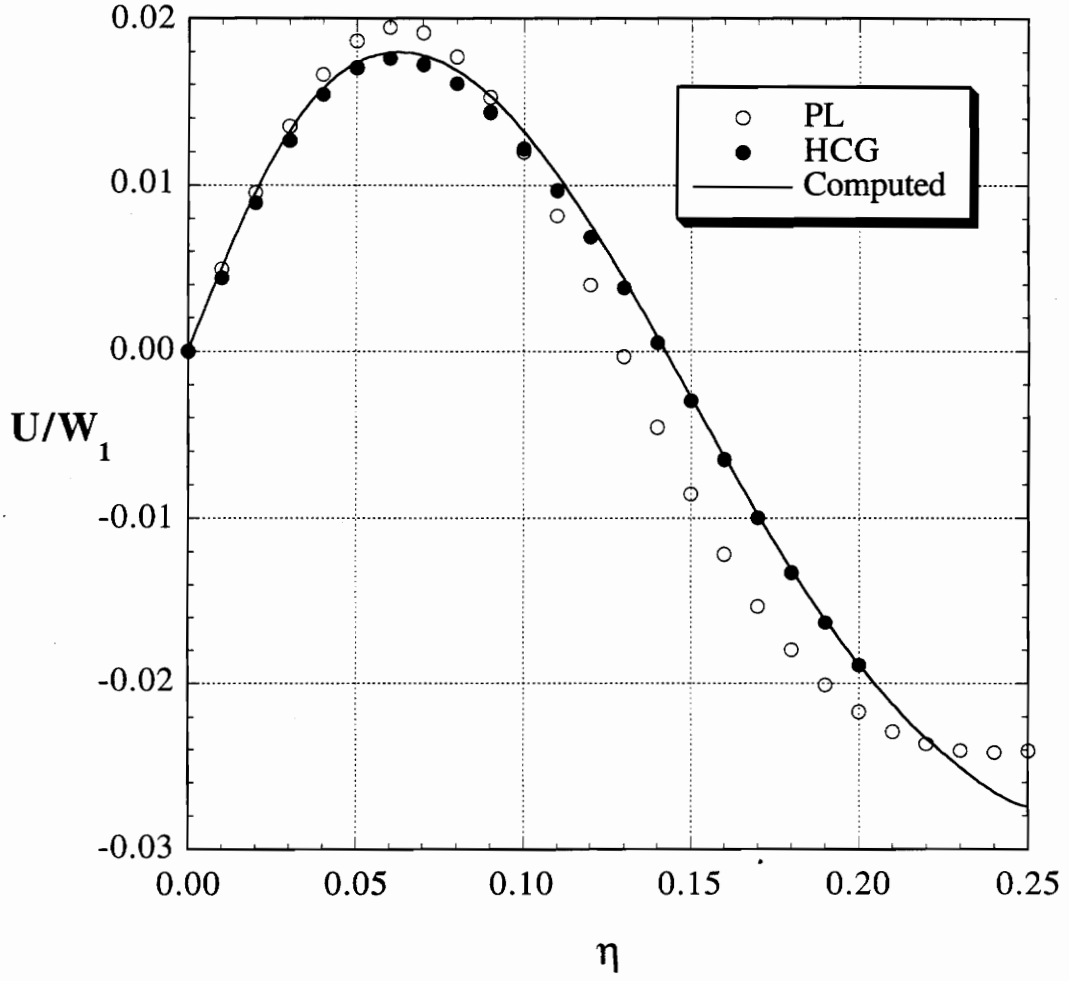

Figure 4.2: Comparison of self-similar solution of computed mean radial velocity with experimental results
[PL: Panchapakesan and Lumley[48]] [HCG: Hussein et al.[32]]

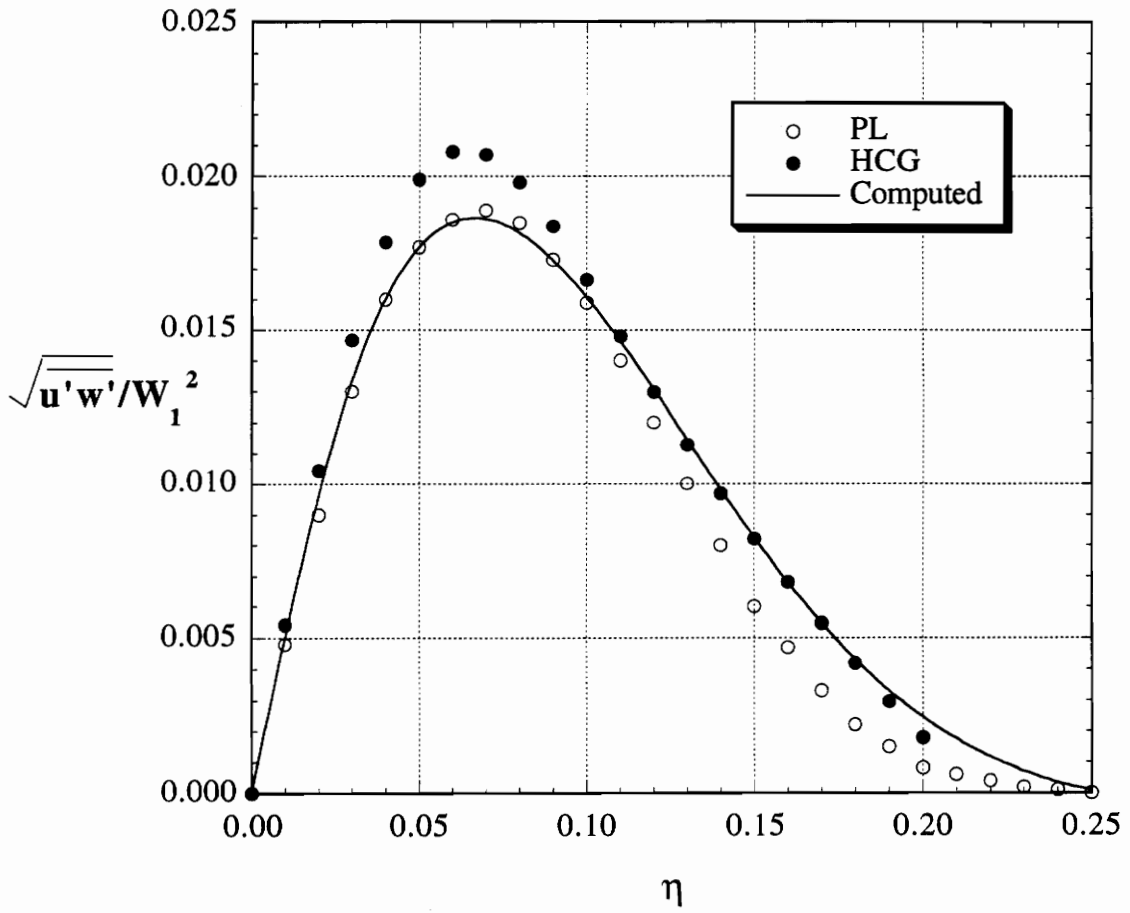

Figure 4.3: Comparison of self-similar solution of computed turbulent shear stress with experimental results
[PL: Panchapakesan and Lumley[48]] [HCG: Hussein et al.[32]]

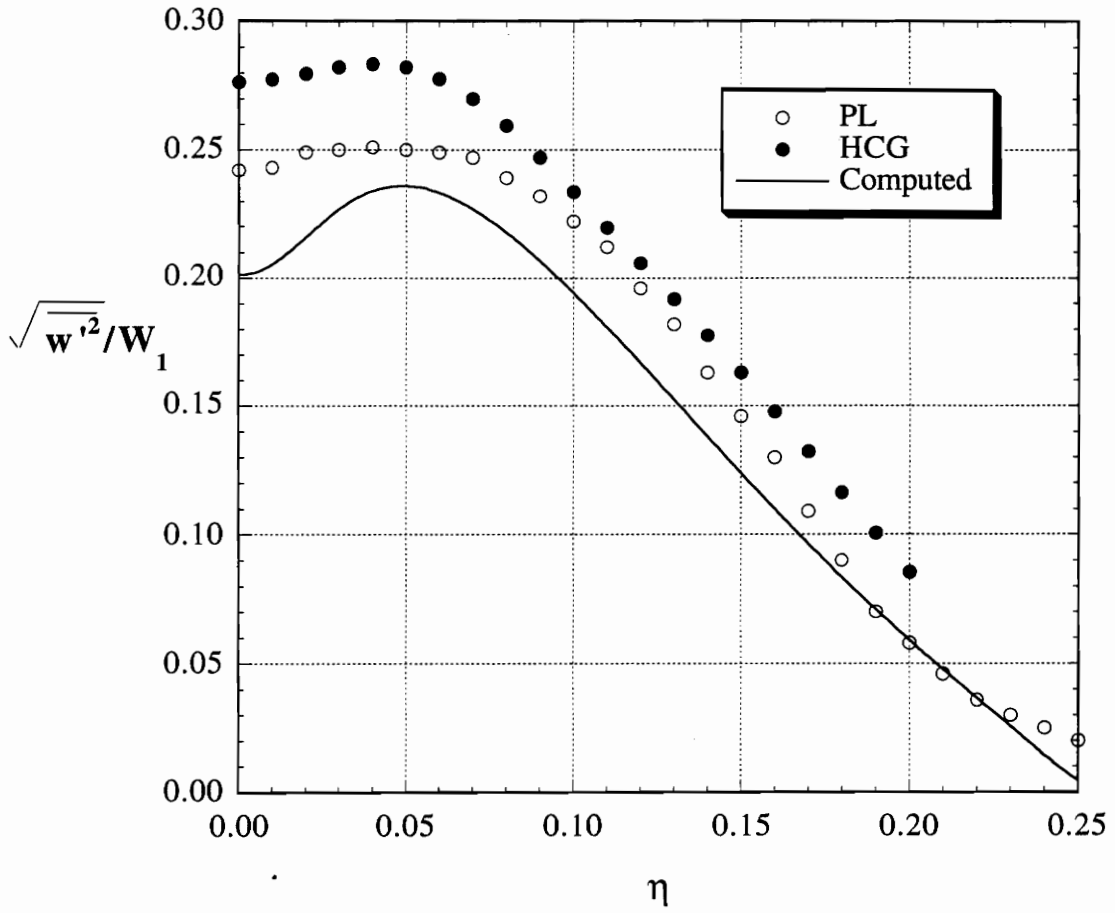

Figure 4.4: Comparison of computational results with experimental data: magnitude of axial velocity fluctuations
[PL: Panchapakesan and Lumley[48]] [HCG: Hussein et al.[32]]

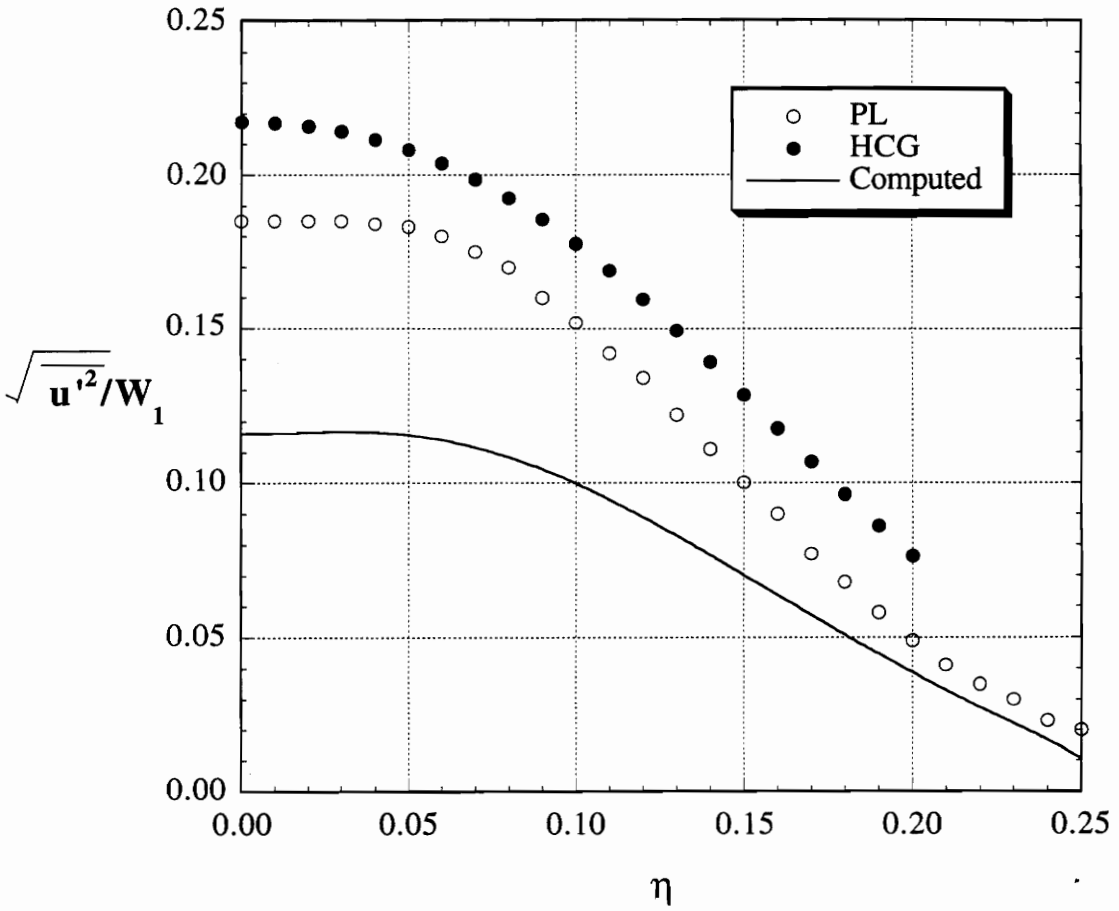

Figure 4.5: Comparison of computational results with experimental data: magnitude of radial velocity fluctuations
[PL: Panchapakesan and Lumley[48]] [HCG: Hussein et al.[32]]

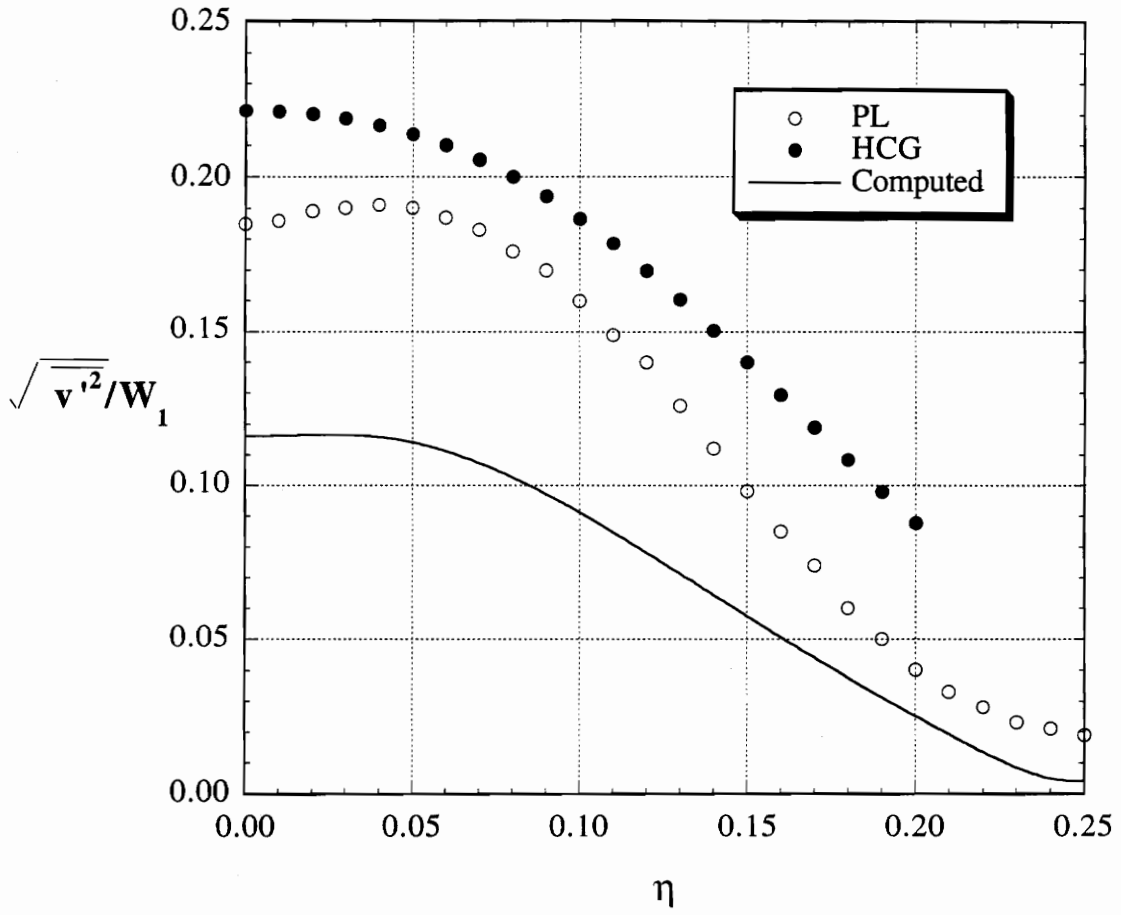

Figure 4.6: Comparison of computational results with experimental data: magnitude of circumferential velocity fluctuations
[PL: Panchapakesan and Lumley[48]] [HCG: Hussein et al.[32]]

Appendix A

RANS AND RST EQUATIONS IN CYLINDRICAL COORDINATES

A.1 Definitions of the variables

In the following equations, (r, θ, z, t) denote the radial, circumferential, axial and time coordinates, respectively. (U, V, W) denote the mean velocity components in radial, circumferential and axial directions, respectively. (u', v', w') denote the turbulent fluctuations of the velocity components in radial, circumferential and axial directions, respectively. P and p' represent the mean value and the turbulent fluctuation of the pressure.

A.2 The Reynolds-averaged Navier-Stokes equations (RANS)

Continuity:

$$\frac{\partial U}{\partial r} + \frac{U}{r} + \frac{1}{r}\frac{\partial V}{\partial \theta} + \frac{\partial W}{\partial z} = 0 \quad . \tag{A.1}$$

θ-momentum:

$$\begin{aligned} &\frac{\partial V}{\partial t} + U\frac{\partial V}{\partial r} + \frac{V}{r}\frac{\partial V}{\partial \theta} + \frac{UV}{r} + W\frac{\partial V}{\partial z} + \frac{1}{r}\frac{\partial P}{\partial \theta} \\ &+\frac{2\overline{u'v'}}{r} + \frac{\partial \overline{u'v'}}{\partial r} + \frac{1}{r}\frac{\partial \overline{v'^2}}{\partial \theta} + \frac{\partial \overline{v'w'}}{\partial z} \\ &-\frac{1}{Re}\left(\frac{\partial^2 V}{\partial r^2} + \frac{1}{r}\frac{\partial V}{\partial r} - \frac{V}{r^2} + \frac{1}{r^2}\frac{\partial^2 V}{\partial \theta^2} + \frac{\partial^2 V}{\partial z^2} + \frac{2}{r^2}\frac{\partial U}{\partial \theta}\right) = 0 \end{aligned} \tag{A.2}$$

z-momentum:

$$\begin{aligned}
&\frac{\partial W}{\partial t} + U\frac{\partial W}{\partial r} + \frac{V}{r}\frac{\partial W}{\partial \theta} + W\frac{\partial W}{\partial z} + \frac{\partial P}{\partial z} \\
&+\frac{\partial \overline{u'w'}}{\partial r} + \frac{\overline{u'w'}}{r} + \frac{1}{r}\frac{\partial \overline{v'w'}}{\partial \theta} + \frac{\partial \overline{w'^2}}{\partial z} \\
&-\frac{1}{Re}\left(\frac{\partial^2 W}{\partial r^2} + \frac{1}{r}\frac{\partial W}{\partial r} + \frac{1}{r^2}\frac{\partial^2 W}{\partial \theta^2} + \frac{\partial^2 W}{\partial z^2}\right) = 0
\end{aligned} \tag{A.3}$$

r-momentum:

$$\begin{aligned}
&\frac{\partial U}{\partial t} + U\frac{\partial U}{\partial r} + \frac{V}{r}\frac{\partial U}{\partial \theta} - \frac{V^2}{r} + W\frac{\partial U}{\partial z} + \frac{\partial P}{\partial r} \\
&+\frac{\partial \overline{u'^2}}{\partial r} + \frac{1}{r}\frac{\partial \overline{u'v'}}{\partial \theta} + \frac{\overline{u'^2} - \overline{v'^2}}{r} + \frac{\partial \overline{u'w'}}{\partial z} \\
&-\frac{1}{Re}\left(\frac{\partial^2 U}{\partial r^2} + \frac{1}{r}\frac{\partial U}{\partial r} - \frac{U}{r^2} + \frac{1}{r^2}\frac{\partial^2 U}{\partial \theta^2} + \frac{\partial^2 U}{\partial z^2} - \frac{2}{r^2}\frac{\partial V}{\partial \theta}\right) = 0
\end{aligned} \tag{A.4}$$

A.3 The Reynolds-stress transport equations (RST)

Equation for $\overline{u'^2}$:

$$\begin{aligned}
&\frac{\partial \overline{u'^2}}{\partial t} + \frac{\overline{u'^3}}{r} + \frac{\partial \overline{u'^3}}{\partial r} + \frac{1}{r}\frac{\partial \overline{u'^2 v'}}{\partial \theta} + \frac{\partial \overline{u'^2 w'}}{\partial z} - \frac{2\overline{u'v'^2}}{r} \\
&+2\overline{u'\frac{\partial p'}{\partial r}} + U\frac{\partial \overline{u'^2}}{\partial r} + \frac{V}{r}\frac{\partial \overline{u'^2}}{\partial \theta} - 4V\frac{\overline{u'v'}}{r^2} + W\frac{\partial \overline{u'^2}}{\partial z} \\
&+2\overline{u'^2}\frac{\partial U}{\partial r} + 2\frac{\overline{u'v'}}{r}\frac{\partial U}{\partial \theta} + 2\overline{u'w'}\frac{\partial U}{\partial z} - \frac{1}{Re}\left\{-2\frac{\overline{u'^2} - \overline{v'^2}}{r^2} - \frac{4}{r^2}\frac{\partial \overline{u'v'}}{\partial \theta}\right. \\
&+\frac{\partial^2 \overline{u'^2}}{\partial r^2} + \frac{1}{r}\frac{\partial \overline{u'^2}}{\partial r} + \frac{1}{r^2}\frac{\partial^2 \overline{u'^2}}{\partial \theta^2} + \frac{\partial^2 \overline{u'^2}}{\partial z^2} \\
&\left.-2\left[\overline{(\frac{\partial u'}{\partial r})^2} + \frac{1}{r^2}\overline{(\frac{\partial u'}{\partial \theta} - v')^2} + \overline{(\frac{\partial u'}{\partial z})^2}\right]\right\} = 0
\end{aligned} \tag{A.5}$$

Equation for $\overline{v'^2}$:

$$\begin{aligned}
&\frac{\partial\overline{v'^2}}{\partial t}+\frac{\partial\overline{u'v'^2}}{\partial r}+\frac{1}{r}\frac{\partial\overline{v'^3}}{\partial\theta}+\frac{\partial\overline{v'^2w}}{\partial z}+3\frac{\overline{u'v'^2}}{r}+\frac{2}{r}\overline{v'\frac{\partial p'}{\partial\theta}}+2\overline{u'v'}\frac{\partial V}{\partial r}\\
&+U\frac{\partial\overline{v'^2}}{\partial r}+\frac{V}{r}\frac{\partial\overline{v'^2}}{\partial\theta}+2\frac{U\overline{v'^2}}{r}+2\overline{v'w'}\frac{\partial V}{\partial z}+2\frac{V\overline{u'v'}}{r}+W\frac{\partial\overline{v'^2}}{\partial z}+2\frac{\overline{v'^2}}{r}\frac{\partial V}{\partial\theta}\\
&-\frac{1}{Re}\left\{\frac{\partial^2\overline{v'^2}}{\partial r^2}+\frac{1}{r}\frac{\partial\overline{v'^2}}{\partial r}+\frac{1}{r^2}\frac{\partial^2\overline{v'^2}}{\partial\theta^2}+\frac{\partial^2\overline{v'^2}}{\partial z^2}+2\frac{\overline{u'^2}-\overline{v'^2}}{r^2}\right.\\
&\left.+\frac{4}{r^2}\frac{\partial\overline{u'v'}}{\partial\theta}-2\left[\overline{(\frac{\partial v'}{\partial r})^2}+\frac{1}{r^2}\overline{(\frac{\partial v'}{\partial\theta}+u')^2}+\overline{(\frac{\partial v'}{\partial z})^2}\right]\right\}=0
\end{aligned}\tag{A.6}$$

Equation for $\overline{w'^2}$:

$$\begin{aligned}
&\frac{\partial\overline{w'^2}}{\partial t}+\frac{\partial\overline{w'^3}}{\partial z}+\frac{\partial\overline{u'w'^2}}{\partial r}+\frac{1}{r}\frac{\partial\overline{v'w'^2}}{\partial\theta}+\frac{\overline{u'w'^2}}{r}+2\overline{w'\frac{\partial p'}{\partial z}}\\
&+U\frac{\partial\overline{w'^2}}{\partial r}+\frac{V}{r}\frac{\partial\overline{w'^2}}{\partial\theta}+W\frac{\partial\overline{w'^2}}{\partial z}+2\overline{u'w'}\frac{\partial W}{\partial r}+2\frac{\overline{v'w'}}{r}\frac{\partial W}{\partial\theta}+2\overline{w'^2}\frac{\partial W}{\partial z}\\
&-\frac{1}{Re}\left\{\frac{\partial^2\overline{w'^2}}{\partial r^2}+\frac{1}{r}\frac{\partial\overline{w'^2}}{\partial r}+\frac{1}{r^2}\frac{\partial^2\overline{w'^2}}{\partial\theta^2}+\frac{\partial^2\overline{w'^2}}{\partial z^2}\right.\\
&\left.-2\left[\overline{(\frac{\partial w'}{\partial r})^2}++\frac{1}{r^2}\overline{(\frac{\partial w'}{\partial\theta})^2}+\overline{(\frac{\partial w'}{\partial z})^2}\right]\right\}=0
\end{aligned}\tag{A.7}$$

Equation for $\overline{u'v'}$:

$$\begin{aligned}
&\frac{\partial\overline{u'v'}}{\partial t}+\frac{\partial\overline{u'^2v'}}{\partial r}+\frac{1}{r}\frac{\partial\overline{u'v'^2}}{\partial\theta}+\frac{\partial\overline{u'v'w'}}{\partial z}+2\frac{\overline{u'^2v'}}{r}-\frac{\overline{v'^3}}{r}\\
&+\frac{1}{r}\overline{u'\frac{\partial p'}{\partial\theta}}+\overline{v'\frac{\partial p'}{\partial r}}+U\frac{\partial\overline{u'v'}}{\partial r}+\frac{V}{r}\frac{\partial\overline{u'v'}}{\partial\theta}+V\frac{\overline{u'^2}-2\overline{v'^2}}{r}+W\frac{\partial\overline{u'v'}}{\partial z}+\frac{U\overline{u'v'}}{r}\\
&+\overline{u'^2}\frac{\partial V}{\partial r}+\frac{\overline{u'v'}}{r}\frac{\partial V}{\partial\theta}+\overline{u'w'}\frac{\partial V}{\partial z}+\overline{u'v'}\frac{\partial U}{\partial r}+\frac{\overline{v'^2}}{r}\frac{\partial U}{\partial\theta}+\overline{v'w'}\frac{\partial U}{\partial z}\\
&-\frac{1}{Re}\left\{\frac{\partial^2\overline{u'v'}}{\partial r^2}+\frac{1}{r}\frac{\partial\overline{u'v'}}{\partial r}+\frac{1}{r^2}\frac{\partial^2\overline{u'v'}}{\partial\theta^2}+\frac{\partial^2\overline{u'v'}}{\partial z^2}+\frac{2}{r^2}\frac{\partial}{\partial\theta}(\overline{u'^2}-\overline{v'^2})-4\frac{\overline{u'v'}}{r^2}\right.\\
&\left.-2\left[\overline{\frac{\partial u'}{\partial r}\frac{\partial v'}{\partial r}}+\frac{1}{r^2}\overline{(\frac{\partial u'}{\partial\theta}-v')(\frac{\partial v'}{\partial\theta}+u')}+\overline{\frac{\partial u'}{\partial z}\frac{\partial v'}{\partial z}}\right]\right\}=0
\end{aligned}\tag{A.8}$$

Equation for $\overline{u'w'}$:

$$\begin{aligned}
&\frac{\partial \overline{u'w'}}{\partial t} + \frac{\partial \overline{u'^2 w'}}{\partial r} + \frac{\partial \overline{u'w'^2}}{\partial z} + \frac{1}{r}\frac{\partial \overline{u'v'w'}}{\partial \theta} + \frac{\overline{u'^2 w'}}{r} - \frac{\overline{v'^2 w}}{r} \\
&\overline{w'\frac{\partial p'}{\partial r}} + \overline{u'\frac{\partial p'}{\partial z}} + U\frac{\partial \overline{u'w'}}{\partial r} + \frac{V}{r}\frac{\partial \overline{u'w'}}{\partial \theta} + W\frac{\partial \overline{u'w'}}{\partial z} - 2V\frac{\overline{v'w'}}{r} \\
&+\overline{u'w'}\frac{\partial U}{\partial r} + \frac{\overline{v'w'}}{r}\frac{\partial U}{\partial \theta} + \overline{w'^2}\frac{\partial U}{\partial z} + \overline{u'^2}\frac{\partial W}{\partial r} + \frac{\overline{u'v'}}{r}\frac{\partial W}{\partial \theta} + \overline{u'w'}\frac{\partial W}{\partial z} \\
&-\frac{1}{Re}\left\{\frac{\partial^2 \overline{u'w'}}{\partial r^2} + \frac{1}{r}\frac{\partial \overline{u'w'}}{\partial r} + \frac{1}{r^2}\frac{\partial^2 \overline{u'w'}}{\partial \theta^2} + \frac{\partial^2 \overline{u'w'}}{\partial z^2} - \frac{\overline{u'w'}}{r^2} - \frac{2}{r^2}\frac{\partial \overline{v'w'}}{\partial \theta}\right. \\
&\left.-2\left[\frac{\partial u'}{\partial r}\frac{\partial w'}{\partial r} + +\frac{1}{r^2}\overline{(\frac{\partial u'}{\partial \theta} - v')\frac{\partial w'}{\partial \theta}} + \frac{\partial u'}{\partial z}\frac{\partial w'}{\partial z}\right]\right\} = 0
\end{aligned} \tag{A.9}$$

Equation for $\overline{v'w'}$:

$$\begin{aligned}
&\frac{\partial \overline{v'w'}}{\partial t} + \frac{\partial \overline{u'v'w'}}{\partial r} + \frac{1}{r}\frac{\partial \overline{v'^2 w}}{\partial \theta} + \frac{\partial \overline{v'w'^2}}{\partial z} + 2\frac{\overline{u'v'w'}}{r} + \frac{1}{r}\overline{w'\frac{\partial p'}{\partial \theta}} + \overline{v'\frac{\partial p'}{\partial z}} \\
&+U\frac{\partial \overline{v'w'}}{\partial r} + \frac{V}{r}\frac{\partial \overline{v'w'}}{\partial \theta} + W\frac{\partial \overline{v'w'}}{\partial z} + \frac{U}{r}\overline{v'w'} + V\frac{\overline{u'w'}}{r} \\
&\overline{u'w'}\frac{\partial V}{\partial r} + \frac{\overline{v'w'}}{r}\frac{\partial V}{\partial \theta} + \overline{w'^2}\frac{\partial V}{\partial z} + \overline{u'v'}\frac{\partial W}{\partial r} + \frac{\overline{v'^2}}{r}\frac{\partial W}{\partial \theta} + \overline{v'w'}\frac{\partial W}{\partial z} \\
&-\frac{1}{Re}\left\{\frac{\partial^2 \overline{v'w'}}{\partial r^2} + \frac{1}{r}\frac{\partial \overline{v'w'}}{\partial r} + \frac{1}{r^2}\frac{\partial^2 \overline{v'w'}}{\partial \theta^2} + \frac{\partial^2 \overline{v'w'}}{\partial z^2} - \frac{2}{r^2}\frac{\partial \overline{u'w'}}{\partial \theta} - \frac{\overline{v'w'}}{r^2}\right. \\
&\left.-2\left[\frac{\partial v'}{\partial r}\frac{\partial w'}{\partial r} + +\frac{1}{r^2}\overline{(\frac{\partial v'}{\partial \theta} + u')\frac{\partial w'}{\partial \theta}} + \frac{\partial v'}{\partial z}\frac{\partial w'}{\partial z}\right]\right\} = 0
\end{aligned} \tag{A.10}$$

The equation for the turbulent kinetic energy, $k_t = \frac{1}{2}(\overline{u'^2} + \overline{v'^2} + \overline{w'^2})$, can be obtained by summing up the equations (A.5), (A.6) and (A.7).

VITA
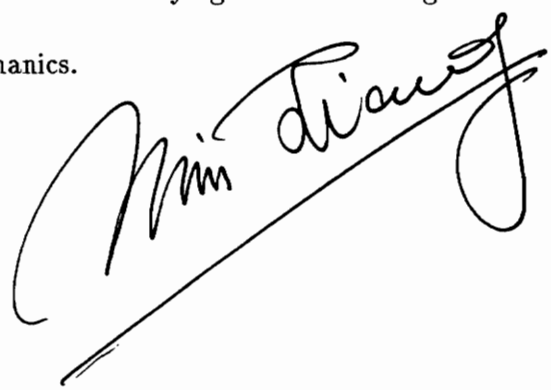
Min Jiang was born on December 26, 1961, in Shanghai, China. He graduated from Yanan High School, Shanghai, in July 1980, and then joined the University of Science and Technology of China, Hefei, Anhui, China, with a major in Engineering Mechanics. In July 1985 he was awarded the degree of Bachelor of Science. Later that month, he joined Shanghai Aircraft Design and Research Institute, Shanghai, as an Aerodynamic Load Analyst and Software Engineer. In April 1991 he came to the United States to join his wife, Lan Xu, at the University of Connecticut. And then in August 1992, he joined the Engineering Science and Mechanics Department at Virginia Polytechnic Institute and State University, Blacksburg, Virginia, where, he has been studying towards his degree of Master of Science in Engineering Science and Mechanics.